

**CHARACTERIZATION OF PROTOCADHERIN-21 IN PHOTORECEPTOR DISK  
SYNTHESIS**

by

Lee Ling Yang

B.Sc. (Hons.), The University of British Columbia, 2010

A THESIS SUBMITTED IN PARTIAL FULFILLMENT OF  
THE REQUIREMENTS FOR THE DEGREE OF

MASTER OF SCIENCE

in

The Faculty of Graduate Studies

(Cell and Developmental Biology)

THE UNIVERSITY OF BRITISH COLUMBIA

(Vancouver)

November 2012

© Lee Ling Yang, 2012

## Abstract

Protocadherin-21 (pcdh-21) is a transmembrane protein concentrated at nascent disks in mouse photoreceptors and thought to regulate disk synthesis. *PCDH-21* mutations are associated with retinal degenerative diseases. Pcdh-21 undergoes proteolytic cleavage that may be essential for disk synthesis. In mice, Pcdh-21 interacts with prominin-1 (prom-1) and their interaction may be required for their localization and function in disk synthesis.

To compare pcdh-21 localization across species, we performed immunofluorescence microscopy using an antibody raised against the N-terminus of *X.laevis* pcdh-21 (xpcdh-21). In rods and cones of all species, pcdh-21 was localized to nascent disks at the base of the outer segment, suggesting a conserved role in disk assembly. However, in contrast with the idea that pcdh-21 localizes only to the basal outer segment, pcdh-21 was localized to other outer segment regions, and this localization was different across cell types and species, suggesting that pcdh-21 has cell type- and species- specific structural roles. Pcdh-21 was restricted to open disk rims in *X.laevis* cones. Prom-1, an interacting partner of pcdh-21 in mice, shows identical labeling at the open disk rims. Pcdh-21 and prom-1 may therefore interact to maintain open disk structure. Immunoblots showed that proteolytic cleavage of pcdh-21 may be unique to mice. In *X.laevis* rods, pcdh-21 labeling in the nascent disks did not vary with disk synthesis rate.

We attempted to inhibit pcdh-21 function using a dominant negative approach. Full length pcdh-21 (FL) and deletion constructs consists of mouse (mpcdh-21) and xpcdh-21 were overexpressed in *X.laevis* rods. Retinal degeneration and disk defects were only observed in retinas overexpressing mpcdh-21 FL. Mpcdh-21 FL was retained in the ER,

caused abnormal ER structure, and was not cleaved in *X. laevis* retinas. Xpcdh-21 variants were correctly localized and did not cause retinal degeneration.

This study illustrated that pcdh-21 localization, processing and properties may not be conserved across species. Differences in pcdh-21 localization may reflect differences in disk synthesis mechanisms or disk ultrastructure. However, the conserved association of pcdh-21 and prom-1 with open disk rims and nascent disks suggests that they may form a complex involved in regulating disk synthesis and/ or in maintaining disk structure.

## **Preface**

This research was approved by UBC Animal Care Committee (Certificate Number: A10-0109, A10-0102) and UBC Clinical Research Ethics Board (Certificate Number: H11-02050).

## Table of Contents

<b>Abstract.....</b>	<b>ii</b>
<b>Preface.....</b>	<b>iv</b>
<b>Table of Contents .....</b>	<b>v</b>
<b>List of Tables .....</b>	<b>ix</b>
<b>List of Figures.....</b>	<b>x</b>
<b>List of Symbols and Abbreviations .....</b>	<b>xiv</b>
<b>Acknowledgements .....</b>	<b>xvii</b>
<b>Dedication .....</b>	<b>xviii</b>
<b>Chapter 1: Introduction .....</b>	<b>1</b>
1.1    The eye.....	1
1.1.1    The retina .....	1
1.1.2. Rod and cone photoreceptors.....	1
1.1.3    Retinas and photoreceptors across species .....	3
1.1.4    Phototransduction .....	4
1.1.5    Disk morphogenesis and shedding.....	6
1.2    Pcdh-21 and prom-1.....	7
1.2.1    Initial characterization of pcdh-21 .....	8
1.2.2    Pcdh-21 expression in developing mouse retinas .....	9
1.2.3    Pcdh-21 cleavage may be required for disk synthesis in mice .....	10
1.2.4    Initial characterization of prom-1 .....	11
1.2.5    Molecular evidence supporting the “membrane evagination model”.....	13
1.3    Mutations in <i>PCDH-21</i> and <i>PROM-1</i> cause inherited photoreceptor degeneration	15

1.3.1	<i>PCDH-21</i> mutations.....	16
1.3.2	<i>Pcdh-21</i> <sup>-/-</sup> mice .....	16
1.3.3	<i>PROM-1</i> mutations .....	17
1.3.4	<i>Prom-1</i> transgenic mice .....	17
1.4	Significance.....	18
1.5	Rationale and objectives .....	19
<b>Chapter 2: Subcellular localization of pcdh-21.....</b>		<b>37</b>
2.1	Introduction.....	37
2.2	Materials and methods .....	38
2.2.1	Generation of pcdh-21 polyclonal antibody .....	38
2.2.2	Peptide competition assays on Western blots and immunohistochemistry .....	38
2.2.3	Preparation of frozen retinal sections from multiple species.....	39
2.2.4	Immunofluorescence labeling of frozen retinal sections .....	40
2.2.5	Expression and purification of mouse and <i>X.laevis</i> pcdh-21 from COS-7 cells.	41
2.2.6	Immunofluorescence labeling of COS-7 cells .....	42
2.2.7	Retinal extracts from multiple species .....	42
2.2.8	SDS page and western blotting.....	43
2.3	Results.....	43
2.3.1	Characterization of anti-pcdh-21 antibodies and proteolytic cleavage of pcdh-21 across species .....	43
2.3.2	Distribution of pcdh-21 in <i>X.laevis</i> rods .....	46
2.3.3	Distribution of pcdh-21 in <i>X.laevis</i> cones.....	48
2.3.4	Peptide competition assays for testing antibody specificities.....	49

2.3.5	Variation in pcdh-21 labeling intensity in <i>X.laevis</i> retinas during disk synthesis	49
2.3.6	Distribution of pcdh-21 in non-mammalian retinas.....	51
2.3.7	Distribution of pcdh-21 in mammalian retinas.....	52
2.3.8	Distribution of pcdh-21 in human photoreceptors.....	54
2.3.9	Localization of pcdh-21 in COS-7 cells.....	55
2.4	Discussion.....	57
2.4.1	Differential pcdh-21 localization in rods and cones of the same species.....	57
2.4.2	Pcdh-21 may be involved in maintaining open disk structure in <i>X.laevis</i> .....	58
2.4.3	Conserved localization of pcdh-21 in basal OS support its role in disk synthesis	59
2.4.4	Pcdh-21 likely performs species- and cell type-specific structural roles.....	61
2.4.5	Pcdh-21 abundance at the basal ROS does not increase with disk synthesis or open disks.....	62
2.4.6	Xpcdh-21 and mpcdh-21 have different localizations and effects.....	63
2.4.7	Pcdh-21 cleavage is not conserved across species.....	64
<b>Chapter 3: Generation of pcdh-21 mutants to study pcdh-21 function in disk synthesis.</b>		<b>86</b>
.....		
3.1	Introduction.....	86
3.2	Materials and methods.....	87
3.2.1	Generation of constructs.....	87
3.2.2	Generation and rearing of transgenic <i>X.laevis</i> .....	88
3.2.3	Dot blot.....	89

3.2.4	SDS page and Western blot .....	89
3.2.5	Immunohistochemistry and confocal microscopy .....	90
3.2.6	Transmission electron microscopy .....	90
3.3	Results.....	91
3.3.1	Retinal degeneration in transgenic <i>X.laevis</i> expressing mpcdh-21 variants .....	91
3.3.2	Subcellular localization of mpcdh-21 variants .....	92
3.3.3	Mpcdh-21 cleavage in transgenic <i>X.laevis</i> .....	93
3.3.4	Disk ultrastructure in rods overexpressing mpcdh-21 FL.....	93
3.3.5	Retinal morphology in transgenic <i>X.laevis</i> overexpressing xpcdh-21 variants ..	94
3.4	Discussion.....	94
3.4.1	Pcdh-21 deletion constructs did not generate dominant negative mutations .....	94
3.4.2	Mpcdh-21 FL, but not xpcdh-21, caused retinal degeneration and abnormal disk synthesis .....	96
3.4.3	Mechanisms by which mpcdh-21 FL causes retinal degeneration .....	97
3.4.4	Mpcdh-21 FL results in overgrown disks .....	98
	<b>Bibliography .....</b>	<b>109</b>
	<b>Appendix A .....</b>	<b>116</b>

## List of Tables

<b>Table 1-1. <i>PCDH-21</i> and <i>PROM-1</i> mutations associated with inherited photoreceptor degeneration. ....</b>	<b>36</b>
---	-----------

## List of Figures

Figure 1-1. The human eye (A) and retina (B). .....	21
Figure 1-2. Overview of <i>X.laevis</i> rod and cone morphology.....	22
Figure 1-3. Ultrastructural differences between <i>X.laevis</i> rods and cones.....	23
Figure 1-4. Structural diversity between photoreceptors of different species. ....	24
Figure 1-5. Phototransduction cascade activation and inactivation.....	25
Figure 1-6. The membrane evagination model is separated into two steps: the formation of disk surface (A) and disk rims (B-C).....	27
Figure 1-7. Two contradicting models of rod disk synthesis.....	28
Figure 1-8. Schematic diagram of pcdh-21 structure.....	29
Figure 1-9. Phylogenetic tree generated by comparing first cadherin domain of pcdh-21 and other cadherin family members. ....	30
Figure 1-10. Pcdh-21 localization in mouse rods. ....	31
Figure 1-11. Pcdh-21 localization in mouse cones. ....	32
Figure 1-12. Pcdh-21 cleavage in mouse and bovine retinas.....	33
Figure 1-13. Localization of OS proteins involved in disk synthesis in rodent rods.....	34
Figure 1-14. <i>X.laevis</i> with defects in actin polymerization (A) and transgenic mice containing a prom-1 R373C mutation (B) have abnormally large disks. ....	35
Figure 2-1. Epitopes recognized by the anti-N and anti-C-pcdh-21 antibodies. ....	67
Figure 2-2. Immunoblot of extracts from transfected cells and non-mammalian retinas probed with anti-N-and anti-C-pcdh-21 antibodies (left). Peptide competition assays for testing antibody specificities (right). ....	68

Figure 2-3. Immunoblot of extracts from transfected cells and mammalian retinas, probed with anti-N-pcdh-21 antibody (left) or antibody incubated with peptide (right).....	69
Figure 2-4. Pcdh-21 localization in longitudinal sections of <i>X.laevis</i> photoreceptors labeled with anti-N-pcdh-21 antibody.....	70
Figure 2-5. Pcdh-21 localization in cross sections of <i>X.laevis</i> photoreceptors.....	71
Figure 2-6. Pcdh-21 localization in longitudinal (A) and cross sections (B-C) of <i>X.laevis</i> photoreceptors.....	72
Figure 2-7. Peptide competition confirmed the specificities of anti-N (A-B) and anti-C-pcdh-21 antibodies (C-D).....	73
Figure 2-8. Analysis of pcdh-21 expression at the basal ROS over a diurnal cycle.....	74
Figure 2-9. Pcdh-21 localization in <i>X. tropicalis</i> and zebrafish retinas.....	75
Figure 2-10. Mouse retinal sections immunolabeled with antibodies against mouse pcdh-21 (A-B) and <i>X.laevis</i> pcdh-21(C).....	76
Figure 2-11. Verification of anti-N xpcdh-21 antibody labeling specificity in mouse retinal sections.....	77
Figure 2-12. Pcdh-21 localization is conserved between mouse and pig. ....	78
Figure 2-13. Mouse retinal sections labeled with anti-N-pcdh-21, anti-acetylated tubulin antibody and wheat germ agglutinin.....	79
Figure 2-14. Longitudinal sections of human retinas were double labeled with anti-N-pcdh-21 and WGA (A-B) or anti-acetylated- $\alpha$ -tubulin (C) or anti-cone arrestin 7G6 (D). ....	80
Figure 2-15. Verification of pcdh-21 antibody labeling specificity in human retinal sections. ....	81

Figure 2-16. Localization of rhodospin, xpcdh-21 and mpcdh-21 in permeabilized (left) and non-permeabilized (right) COS-7 cells.....	82
Figure 2-17. Localization of rhodopsin, xpcdh-21 and mpcdh-21 in the ER of COS-7 cells.	83
Figure 2-18. ER morphologies of non-transfected cells (A) and cells expressing rhodopsin (B), xpcdh-21 (C) or mpcdh-21 (D).....	84
Figure 2-19. Pcdh-21 distribution in rods and cones of different species. ....	85
Figure 3-1. (a) Pcdh-21 cleavage in mice. ....	100
Figure 3-2. Strategies used to generate the pcdh-21 $\Delta$ N constructs. ....	101
Figure 3-3. Analysis of transgenic <i>X.laevis</i> expressing mpcdh-21 variants by confocal microscopy (A-D) and dot blot (E).....	102
Figure 3-4. Localization of mpcdh-21 variants in transgenic <i>X.laevis</i> rods. ....	103
Figure 3-5. Pcdh-21 localization in the inner segments of transgenic (A-B) and non-transgenic (C) <i>X.laevis</i> retinas. ....	104
Figure 3-6. ER ultrastructure of non-transgenic (A) and mpcdh-21 FL expressing <i>X.laevis</i> rods (B). ....	105
Figure 3-7. Western blot analysis of mpcdh-21 FL cleavage in transgenic <i>X.laevis</i> eyes....	106
Figure 3-8. Disk ultrastructure of non-transgenic (A, D) and transgenic <i>X.laevis</i> expressing mpcdh-21 FL (B,C,E,F).....	107
Figure 3-9. Analysis of transgenic <i>X.laevis</i> expressing xpcdh-21 variants by confocal microscopy (A-D) and dot blot (E).....	108
Figure A-1. Prom-1 localization in non-transgenic (A) and transgenic <i>X.laevis</i> retinas expressing mpcdh-21 FL (B-C)..	117
Figure A-2. Prom-1 localization in non-transgenic <i>X.laevis</i> retinas.....	119

Figure A-3. Protein sequence alignment of human (hpcdh-21), pig (ppcdh-21), mouse (mpcdh-21), *X.laevis* (xpcdh-21) and zebrafish (zpcdh-21).....120

## List of Symbols and Abbreviations

AD	autosomal dominant
AR	autosomal recessive
ABCA-4	ATP-binding cassette transporter
bp	base pair
cDNA	complementary DNA
COS	cone outer segment
cGMP	guanosine 3', 5'-cyclic monophosphate
CNGC	Cyclic nucleotide gated channel
CORD	cone-rod dystrophy
del	deletion
DMEM	Dulbecco's modified Eagle medium
dup	duplication
EDTA	Ethylaminodiamine tetraacetic acid
eGFP	Enhanced green fluorescence protein
ER	endoplasmic reticulum
FL	full length
GC	Guanylate cyclase
GDP	Guanosine 3'-diphosphate
GFP	green fluorescence protein
GTP	guanosine 3'-triphosphate
GPCR	G protein coupled receptor

ins	insertion
KLH	keyhole limpet hemocyanin.
MD	Macular dystrophy
Mpcdh-21	mouse protocadherin-21
PAGE	polyacrylamide gel electrophoresis
PCR	polymerase chain reaction
PBS	phosphate buffered saline
PMSF	phenyl methyl sulfonyl fluoride
PDE	phosphodiesterase
PI3P	phosphatidylinositol 3-phosphate
Pcdh-21	Protocadherin-21
Prph-2	Peripherin-2
Prom-1	Prominin-1
<i>rds</i>	retinal degeneration slow
PR	photoreceptor
Rom -1	rod outer segment membrane protein-1
ROS	rod outer segment
RP	Retinitis Pigmentosa
RT	room temperature
SARA	Smad anchor for receptor activation
SDS	sodium dodecyl sulfate
T- $\alpha$ cP	transducin cone promoter
Tris	Tris [hydroxymethyl] aminomethane

UPR	unfolded protein response
WGA	wheat germ agglutinin
<i>X. laevis</i>	<i>Xenopus laevis</i>
XOP	<i>X.laevis</i> Rod Opsin
Xpcdh-21	<i>X.laevis</i> protocadherin-21
<i>X. tropicalis</i>	<i>Xenopus tropicalis</i>

## **Acknowledgements**

I would like to give my sincerest gratitude to my supervisor, Dr. Orson Moritz, for his guidance and for making his lab such an enjoyable place to work. He has always been supportive, patient and encouraging. I had grown tremendously over the past two years, both as a scientist and as a person. It has been a truly great experience.

My thanks go to both previous and current members of the Moritz lab, for enlarging my vision of science and being there whenever I needed help. It has been a pleasure working with all of you: Damian Lee, Tami Bogéa, Beatrice Tam, Colette Chiu and Ruanne Lai.

I would like to thank my committee members, Dr. Cheryl Gregory-Evans and Dr. Chris Loewen, who had taken the responsibility to guide me through my graduate study.

I would also like to thank members of the Eye Care Centre, particularly members of Dr. Cheryl Gregory-Evans's lab, Jing Cui, Howard Meadows, for providing the animal samples. This project would not have been possible without their help.

To my friends and family, thank you for your unconditional love and support.

## **Dedication**

*To my parents*

## **Chapter 1: Introduction**

### **1.1 The eye**

#### **1.1.1 The retina**

Vision begins when light passes through the cornea and is focused by the lens. An image is formed on the retina at the posterior of the eye (Fig.1-1A). The retina is organized into layers of cells, forming synapses with each other (Fig.1-1B). Light entering the eye is captured by the light sensing cells, rods and cones. They convert light to electrical signals and communicate them to the bipolar, horizontal and amacrine cells. These cells integrate and transmit the signal to the ganglion cells, whose axons comprise the optic nerve connection to the brain (reviewed by Sung, 2010).

#### **1.1.2. Rod and cone photoreceptors**

Rods and cones, named after their shapes, are the two major types of photoreceptors (PR) in the retina. Rods mediate night and peripheral vision, whereas cones are responsible for color, day and central vision (reviewed by Sung, 2010).

Both rods and cones possess outer segments (OS), specialized compartments for light detection (Fig.1-2A). The OS is a membranous structure filled with thousands of disks stacked on top of each other. The large surface area can accommodate numerous phototransduction proteins to maximize its visual sensitivity (reviewed by Sung, 2010). The inner segment (IS) contains the machinery for protein synthesis and mitochondria for energy production. The OS proteins synthesized in the IS are delivered to the OS through the connecting cilium, a narrow pathway linking the IS and OS. The connecting cilium is the basal part of an axoneme that extends distally to about half the length of the OS. The cell

body contains the nucleus. The synaptic terminal is responsible for releasing neurotransmitters needed for signal transmission (reviewed by Sung, 2010).

Current understanding of the OS structure is mostly derived from studies of frogs. This section will provide an overview of OS structure based on these studies. Their variation among species will be discussed in section 1.1.3.

Several structural differences are observed between rods and cones. Rods have cylindrical OS with uniform disk size; whereas cones have disks that decrease in size from basal to distal OS (Fig.1-2A). Rods possess multiple disk invaginations, called incisures (Fig.1-2B). At each incisure, a corresponding calycal process is present. Calycal processes are protrusions of the IS plasma membrane surrounding the basal third of the OS (Rodieck, 1973) (Fig.1-2B). In cones, only a single incisure is present in most species (reviewed by Anderson, 2010). The functions of calycal processes and incisures are not clear. Calycal processes may provide structural support for ROS and control disk size (Rodieck, 1973; reviewed by Sung, 2010). Incisures are hypothesized to increase disk rim area (Rodieck, 1973).

Each disk in the OS is divided into distinct membrane domains: surfaces and rims. In rods, the upper and lower surfaces are connected by rims at both edges of the disks (Fig.1-3A). These disks are termed "closed disks" since they are surrounded by the plasma membrane (Steinberg, 1980). The rims of "closed disks" possess a characteristic hairpin shape at all edges. (Fetter, 1987).

On the other hand, cones have open disks that are not enclosed by the plasma membrane (Fig.1-3B). Cone disk membranes are therefore continuous with each other. A feature of open disks is that the rims opposite to the axoneme are not fully developed and are

accessible to extracellular matrix (Fig.1-3C) (Cohen, 1968). Similar open disks are observed at the base of the rod outer segments (ROS), where nascent disks are synthesized (Besharse, 1977). In cones, the rims adjacent to the axoneme are structurally analogous to those of rods and exhibit a similar hairpin structure (Fig.1-3B) (Fetter, 1987).

### **1.1.3 Retinas and photoreceptors across species**

The rod and cone density of vertebrate retinas are organized to adapt to their habitats. Rods and cones are responsible for night and day vision, respectively. Popular mammalian research subjects, such as rats and mice, are nocturnal and therefore have rod dominant retinas. Humans and lower vertebrates, including *X.laevis* and zebrafish (*Danio rerio*), are diurnal species with higher concentration of cones (reviewed by Anderson, 2010). Because rod-dominant retinas limit the study of cones that mediate daylight vision in humans, some researchers have turned to lower vertebrates with numerous cones, and also developed cone-rich transgenic mice (Mears 2001; Daniele, 2005).

Rods and cones are distributed unevenly in humans. Rods are concentrated at the peripheral retina where cones are almost absent. In the central retina, called the macula, cones are much more concentrated. The center of the macula, called the "fovea centralis", consists entirely of cones (reviewed by Sung, 2010). A similar cone-rich region is only present in higher mammals, making it difficult to study macular diseases in the most widely used vertebrate animal models (Wikler, 1990; Chandler, 1999). For this reason, larger animals, such as monkeys and pigs, have become increasingly popular models because their rod and cone distribution are more similar to humans (Petters, 1997; Petters, 2000).

The structure of rod outer segments (ROS) differs across species. The most obvious

difference is the diameter and length of the ROS. Amphibians have ROS that are much larger than those of mammals (Fig.1-4A) (Rodieck, 1973). The number and depth of incisures also vary across species. Compared to rodent rods, primates and *X. laevis* have more prominent incisures and calycal processes (Cohen, 1960; Cohen, 1965; Papermaster, 1978) (Fig.1-4B).

The distribution of open disks varies across species. Amphibian cones are composed entirely of open disks whereas mammalian cones possess both open and closed disks (Cohen, 1968). Open disks are mostly observed at the basal third of the cone outer segment (COS) (Cohen 1961; Anderson, 1978). The distribution of open disks in rods is more controversial across species. In *X. laevis* and monkey rods, the most basal OS have open disks (Besharse, 1977; Steinberg, 1980). It is unclear whether similar open disks are present at the base of rodent ROS (Obata, 1992; Chuang, 2007). These discrepancies have led to contradicting models of disk synthesis, which will be further discussed in section 1.1.5.

#### **1.1.4 Phototransduction**

Phototransduction is the process by which a single photon of light is converted to an electrical signal (Fig.1-5, middle disk). The signal generated from a single photon is amplified through the G-protein signaling pathway. The G-protein coupled receptor, rhodopsin, contains the light-capturing chromophore, 11-cis retinal. It isomerizes to *all-trans* retinal following absorption of a photon. The activated rhodopsin (metarhodopsin II, or R\*), recruits the heterotrimeric G protein, transducin. Once it interacts with R\*, transducin exchanges GDP for GTP, causing the alpha subunit ( $G\alpha$ ) to dissociate from  $G\beta,\gamma$  and bind phosphodiesterase (PDE) (reviewed by Burns, 2005; Fu, 2010).

The activated PDE hydrolyzes cGMP to 5'GMP. A decrease in cytoplasmic cGMP causes the cyclic nucleotide gated channel (CNGC) to close, reducing the entrance of cations. This hyperpolarizes the cell and reduces neurotransmitter release at the synaptic terminal. The response initiated by a single photon is amplified at two major steps. Each R\* can activate 100-500 molecules of transducin and each transducin-activated PDE can hydrolyze up to 100 molecules of cGMP (reviewed by Burns, 2005).

Rapid inactivation of the phototransduction cascade is required to respond to subsequently absorbed photons. This is achieved by efficient termination of the cascade components at two amplification steps (Fig.1-5, lower disk). First, R\* is phosphorylated by rhodopsin kinase, facilitating the binding of R\* to arrestin. Second,  $G_{\alpha}$  converts GTP to GDP, leading to reassembly of the heterotrimeric G protein complex and subsequently inactivation of PDE (reviewed by Burns, 2005).

Restoring cGMP levels to the dark state is essential for reopening of the CNGC. This is accomplished by guanylate cyclase (GC), the enzyme that synthesizes cGMP from GMP. Low  $Ca^{2+}$  levels increase the activity of GC. During a light response,  $Ca^{2+}$  entry is inhibited due to CNGC closure, while  $Ca^{2+}$  continues to leave the cell through the  $Na^{+} Ca^{2+}$  exchanger. The fall in  $Ca^{2+}$  level stimulates cGMP synthesis through GC. Increased cGMP levels then cause CNGC to reopen and the cell returns to its resting depolarized state (reviewed by Burns, 2005).

Similar reactions and homologous phototransduction proteins are found in cones. However, to suit their roles in mediating vision under bright light, their kinetics and properties differ from those of rods (Kefalov, 2010). The specific differences will not be reviewed in detail here.

### 1.1.5 Disk morphogenesis and shedding

PR disks are renewed continuously to replace highly active rhodopsin. In rods, disks are synthesized at the base of the OS, displaced distally by disks added at the basal OS, and shed at the tip of the OS. The shed disks are subsequently engulfed and degraded by the neighboring retinal pigment epithelial cells (Young, 1967). A balance of disk synthesis and loss is essential for maintaining OS length and PR survival.

Two controversial models have been proposed to describe disk synthesis in rods. The predominant model, the "membrane evagination model", proposes that disk surfaces and rims are developed in two separate, sequential processes. First, the inner face of the plasma membrane at the distal connecting cilium evaginates and grows away from the connecting cilium (Fig.1-6A). As the evagination expands in size, it is remodeled into a disk shape. Second, rim formation begins at the connecting cilium (Fig.1-6B). It proceeds as the proximal and distal surface of two adjacent evaginations grow bilaterally along the edge of the disk. The two ends meet opposite to the connecting cilium and separate from the plasma membrane (Steinberg, 1980). Based on this model, nascent and mature disks can be distinguished according to their positions in the OS and the formation of rims opposite to connecting cilium, as illustrated in Fig. 1-6C.

An alternative model, the "vesicular targeting model", suggests that disks assemble by fusion between nascent disks and vesicles transported from the IS or the base of the OS (Fig.1-7A) (Chuang, 2007). These vesicles are enriched with rhodopsin, syntaxin3 and Smad anchor for receptor activation (SARA), which interacts with the C-terminus of rhodopsin and syntaxin 3 to fuse with nascent disks through interaction with phosphatidylinositol 3-phosphate (PI3P) (Fig.1-7B). Inhibition of SARA function and interaction with PI3P disrupts

rhodopsin trafficking and disk synthesis. In contrast to the membrane evagination model, the authors observed plasma membrane surrounding all basal disks and did not observe any membrane evaginations (ie. open disks) (compare Fig.1-7A and 1-7C).

Proponents of the vesicular targeting model argued that the observation of open disks is due to disruption of the fragile nascent disk plasma membrane during tissue processing (Obata, 1992; Chuang, 2007). However, there is evidence suggesting that these open disks are not likely to be artifacts. First, significant numbers of open disks are observed in cones (Cohen, 1968). Second, the dye Lucifer yellow, when introduced extracellularly, labels the basal ROS as a thin band in *X.laevis* retinas. This band is displaced towards the distal OS over time. The labeling pattern is thought to result from dye penetration into the nascent open disks. After the open disks develop rims, the dye is trapped in closed disks (Matsumoto, 1985). This labeling pattern was not reported when a similar experiment was performed in some mammals (dog and rat), suggesting that the mechanism of disk synthesis may vary between species (Laties, 1976). Furthermore, studies supporting the vesicular targeting model were conducted in rodents whereas the membrane evagination model is based on experiments using monkeys, squirrels and amphibians (Nilsson, 1964; Steinberg, 1980; Besharse, 1977).

## **1.2 Pcdh-21 and prom-1**

Evidence illustrating the mechanisms of disk synthesis is mainly based on morphological and immunohistochemical analysis. The molecular players involved in this process are not well defined. In mice, protocadherin-21 (pcdh-21) and prominin-1 (prom-1)

are the only two proteins with exclusive localization in nascent disks, suggesting indispensable roles in disk synthesis (Maw, 2000; Rattner, 2001).

### **1.2.1 Initial characterization of pcdh-21**

Pcdh-21 is a type 1 single pass transmembrane protein, containing a signal peptide, an N-terminal extracellular domain and a C-terminal cytoplasmic domain (Fig.1-8) (Rattner, 2001). The N-terminus consists of six cadherin repeats, a characteristic domain found in cadherin superfamily members. These repeats act as  $\text{Ca}^{2+}$  binding sites and are best known for their function in cell-cell adhesion (reviewed by Angst, 2001).

Cadherin superfamily members are divided into six sub-branches. Despite its name, pcdh-21 is actually grouped into cadherin-related subbranch 2, rather than the protocadherin subbranch (Fig.1-9). Pcdh-21 differs from the well-studied, classical cadherins (eg. E-cadherin, N-cadherin). First, pcdh-21 did not demonstrate homotypic adhesive interaction *in vitro* (Rattner, 2004). Second, pcdh-21 is not likely to bind to cytoskeleton or  $\beta$ -catenin in the cytoplasm like most classical cadherins because pcdh-21 orthologues have divergent cytoplasmic domains (Rattner, 2004; reviewed by Hulpiau, 2009).

Pcdh-21 orthologues have been identified in diverse vertebrate species, including mammal, chicken, fish and amphibian (GenBank database). The N-terminal cadherin domains are highly conserved whereas sequences in the cytoplasmic domain are more divergent (Rattner, 2004).

In mice, *pcdh-21* transcripts are most prominent in the retina (Rattner, 2001). *In situ* hybridization using retinal sections of *X. laevis* and zebrafish demonstrates that *pcdh-21*

transcripts are exclusively found in the PR nuclei layer (Rattner, 2001; 2004). Because of its exclusive localization to PR, pcdh-21 is also named “photoreceptor cadherin”.

In mouse PR, pcdh-21 is localized to the base of the OS, where disk synthesis occurs. Ultrastructural analysis of mouse rods showed that it is particularly localized to the nascent disk rims opposite to the axoneme, and is not expressed in the mature disk rims at the tip of the OS (Fig.1-10) (Rattner, 2001). In mouse cones, pcdh-21 localization is confined to the connecting cilium, as demonstrated at the light microscopic level (Fig.1-11) (Rattner, 2001). Its ultrastructural localization in cones has not been studied.

### **1.2.2 Pcdh-21 expression in developing mouse retinas**

Pcdh-21 expression pattern in developing mouse retinas also confirmed its role in disk synthesis. It is detected as soon as rods begin to differentiate, and its expression increases as rods become more numerous (Rattner, 2004). Pcdh-21 is detected at the site of developing OS before other OS structural proteins, including the  $\alpha$  subunit of cyclic nucleotide gated channel and ROM-1 (Bascom, 1992; Cook, 1989). Two essential phototransduction proteins, rhodopsin and arrestin, are expressed at the same time as pcdh-21. In contrast to pcdh-21, they accumulate in the IS and are not targeted to the OS until later in development (Rattner, 2001). It is thought that OS proteins that are involved in phototransduction or structural maintenance will only be expressed after the OS is synthesized.

### 1.2.3 Pcdh-21 cleavage may be required for disk synthesis in mice

In mouse and bovine retinas, pcdh-21 is cleaved in the last cadherin domain, producing a soluble N-terminal fragment and a C-terminal fragment that remains associated with disk membrane (Fig.1-12) (Rattner, 2004). The cleavage site was predicted by matching the electrophoretic mobility of a series of *in vitro* translated fragments with the C-terminal cleaved fragments obtained from mouse retinas (Rattner, 2004). Enzymatic treatments excluded the possibility that the C-terminal fragments were phosphorylated and glycosylated (Rattner, 2004). However, other post translational modifications may affect electrophoretic mobility of the cleaved fragments, so the accuracy of this cleavage site is uncertain. In addition, the cleavage site predicted from mice is conserved across species, but pcdh-21 cleavage has only been demonstrated in rodent and bovine retinas (Rattner, 2004).

Proteolysis is a thermodynamically favourable irreversible reaction that initiates many processes, for example blood clotting and apoptosis (Davie, 1991; Hengartner, 2000). The function of pcdh-21 cleavage is unclear but has been proposed to ensure that OS assembly proceeds in a unidirectional manner (Rattner, 2004).

*In vivo* studies of mouse retinas showed that only a portion of pcdh-21 is cleaved (Rattner, 2004). This implies that irreversible proteolysis of pcdh-21 may be tightly regulated. In transgenic mouse models with abnormal disks, this regulation is disrupted and the full length, uncleaved pcdh-21 accumulates (Rattner, 2004; Yang, 2008). It should be noted that the evidence supporting the role of pcdh-21 in disk synthesis was solely based on data obtained using mice.

*Rds*<sup>-/-</sup> mice, which do not express peripherin-2 (prph-2), a critical OS protein, fail to develop OS. Instead, disorganized and abnormal vesicles derived from PR accumulate

between PR and retinal pigment epithelial cells (Jansen, 1984). In *rds*<sup>-/-</sup> mice, full length pcdh-21 increased by four fold relative to levels seen in wild type mice, while the ratio of full length to cleaved fragments increased by two fold. This suggested that mice are capable of cleaving a portion of the abnormally high levels of pcdh-21 (Rattner, 2004). The full length pcdh-21 is mislocalized to PR-derived vesicles, lending evidence that pcdh-21 is cleaved at the base of the OS (Rattner, 2004). If the OS, the proposed site of pcdh-21 cleavage, is not formed, it is expected that its cleavage is disrupted and the full length protein accumulates at the site where the protein should be cleaved (Rattner, 2004).

The fate of the cleaved fragments and the site of cleavage in PR are unclear. Labeling with both antibodies against the N- and C-terminus produced identical labeling pattern that is exclusively at the base of the OS (Rattner, 2004). It is possible that pcdh-21 is cleaved at the base of the OS and the soluble N-terminal fragments diffuse away from the basal OS, as evidenced by the detection of the N-terminal fragments in the medium used to lyse the mouse retinas (Rattner, 2004). Alternatively, the N-terminal fragments may be retained at the basal OS by binding to other membrane proteins (Rattner, 2004).

#### **1.2.4 Initial characterization of prom-1**

Prom-1 is a pentaspan transmembrane glycoprotein best characterized for its role as a stem cell marker. Prom-1 is often referred to as CD133 or AC133 (Weigmann, 1997; Miraglia, 1997; Fargeas, 2003). Evidence suggests that prom-1 is implicated in disk synthesis. In mouse PR, it is exclusively at the base of the ROS where it binds and colocalizes with pcdh-21 (Maw, 2000; Yang, 2008). Transgenic mice that lack *prom-1* or carry *prom-1* mutations had abnormal disks and exhibited retinal degeneration (see section 1.3.4).

Mutations in *PROM-1* have been found to cause several retinal diseases in humans (see section 1.3.1).

*Prom-1* homologues have been identified in diverse species. In flies, axolotl (salamander), zebrafish, chicken, *X. laevis* and mice, *prom-1* transcripts are detected in the PR layers, suggesting a critical role in PR (Jaszai, 2011). *Prom-1* homologues exhibit 40-70% similarity at the amino acid level and share several conserved domains, including an intracellular cysteine rich domain, and several extracellular leucine residues (Weigmann, 1997; Corbeil, 2000).

Prom-1 is specifically localized to plasma membrane protrusions of various cell types (Corbeil, 2001). In epithelial cells, *prom-1* is exclusively localized to the microvilli. In transfected cells, *prom-1* is localized to filopodia and lamellipodia (Weigmann, 1997; Corbeil, 2000; Yang, 2008). Its function may be linked to the formation of membrane protrusions since expression of a mutant *prom-1* in transfected HEK cells abolishes the formation of protrusions (Yang, 2008). The presence of *prom-1*, a protein with high preference for membrane protrusions, in basal disks lends support to the “evagination model”, which predicts that plasma membrane outgrowth is a critical step in disk synthesis (Steinberg, 1978).

Prom-1 function has been studied in flies with compound eyes. Insect eyes consist of many subunits called ommatidia. Each of these has multiple rhabdomeres consisting of hundreds of rhodopsin-containing microvilli. To keep rhabdomeres separated from each other, *prom-1* binds to spacemaker to create spacing between rhabdomeres. In the absence of spacemaker, the rhabdomeres became closely opposed to each other (Zelhof, 2006). The

human homolog of spacemaker, *EYS*, when mutated, caused autosomal recessive RP (Abd El-Aziz, 2008). However, its function in the human retina is unknown.

### **1.2.5 Molecular evidence supporting the “membrane evagination model”**

The “membrane evagination model” predicts that disk synthesis is a kind of cell motility involving membrane protrusion and expansion (Steinberg, 1980; Williams, 1988). The observation that similar components are involved in these two processes may lend support to the model.

At the base of the ROS, a complex consisting of pcdh-21, prom-1 and actin is hypothesized to initiate the formation of membrane evagination, the first step of the membrane evagination model (Yang, 2008). Actin regulates the formation of membrane protrusions through membrane remodeling in diverse cell types. In vertebrate rods and cones, actin is enriched at the distal connecting cilium where the evagination forms (Fig.1-13.) (Steinberg, 1980; Chaitin, 1986; Hale, 1996). The addition of an actin-depolymerizing drug to frog and rabbit retinas results in overgrown disks (Williams, 1988; Vaughan, 1989). The underlying mechanism of this abnormality can be explained using the membrane evagination model. It has been hypothesized that actin plays a role in initiating membrane outgrowth by pushing the membrane away from the connecting cilium. When this step is inhibited, membrane that is normally added to the newly formed evaginations is channeled to disks that have already reached their mature sizes (Williams, 1988).

Prom-1 is specifically localized to membrane protrusions in diverse cell types (Corbeil, 2001). Prom-1 binds to actin in PR and transfected cells. *In vitro*, the interaction of prom-1 and actin mediates membrane protrusion formation. Cells transfected with mutant

prom-1 bind actin less efficiently, and fail to form membrane protrusions. When prom-1 is mutated *in vivo*, abnormally large disks are observed, possibly through inhibiting the ability to generate new membrane evaginations, a mechanism similar to that used to explain the phenotype in actin-defective retinas (Yang, 2008).

The second step of the model, rim formation, is thought to be regulated by prph-2 (Arikawa, 1992). In nascent disks of rods, prph-2 is localized to rims near the connecting cilium, where rim formation begins (Fig.1-13). It is not localized to nascent disk edges opposite to the connecting cilium where rim formation is not completed. In mature disks at the distal ROS, rims opposite to the connecting cilium are formed and prph-2 is observed. In rodent rods, pcdh-21 and prph-2 show complementary localization (Rattner, 2004). Pcdh-21 is concentrated in nascent disk edges opposite to connecting cilium where rims are not developed (Fig.1-13).

The membrane evagination model implies that immature and mature disks can be distinguished morphologically based on the completion of rim development. Nascent disks are membrane evaginations that have not yet developed rims, giving rise to the appearance of “open disks”. Once disk rims are formed, mature disks become “closed disks”. The vesicular targeting model, on the other hand, suggests that both nascent and mature disks are closed disks. The distinct molecular compositions of nascent and mature disk rims may reflect their ultrastructural differences, indirectly supporting the evagination model (Fig.1-13).

### **1.3 Mutations in *PCDH-21* and *PROM-1* cause inherited photoreceptor degeneration**

Inherited photoreceptor (PR) degeneration is defined by the progressive loss of PR function and viability, due to inheritance of a defective gene. To date, mutations in over 180 genes are associated with PR degeneration (Wright, 2010) (See RetNet for a summary of these genes is maintained by Stephen P. Daiger at [www.sph.uth.tmc.edu/Retnet/](http://www.sph.uth.tmc.edu/Retnet/)). Mutations in *PCDH-21* and *PROM-1* are associated with common inherited diseases, including RP, macular degeneration and cone-rod dystrophy (Table 1.1). The onset of these diseases is usually in childhood or early adulthood. The defects continue to progress, causing the patients to become completely blind at later stages of the diseases (Wright, 2010).

Retinitis pigmentosa (RP) is the most common cause of PR degeneration with a world prevalence of 1:3000 to 1:4000 (Wright, 2010). It is characterized by initial defects in rods, leading to the loss of peripheral and night vision. The disease often progresses to secondary defects in cones. (Wright, 2010). In contrast to RP, cone-rod dystrophy (CORD), affects cones before rods. In some forms of CORD, both rods and cones are affected simultaneously but cones may suffer from more severe defects (Wright, 2010), or cone deficits are perceived as more debilitating by patients. Another common disease, macular dystrophy (MD) affects all cell types in the macula, including rods, cones and retinal pigment epithelial cells (Wright, 2010).

To understand the pathogenic mechanisms of *PCDH-21* and *PROM-1* mutations, researchers have modeled PR degeneration caused by these mutations in mice. However, mice have few cones and lack a macula, which hinders the study of macular dystrophies and CORD (Jeon, 1998).

### 1.3.1 *PCDH-21* mutations

Three mutations that occur in the conserved cadherin domains of Pcdh-21 are linked to autosomal recessive retinal degeneration (Table 1-1). These mutations all cause premature termination and, likely non-functional proteins. A single base insertion in the second cadherin domain causes *CORD*, the only disease linked to *PCDH-21* mutation (Ostergaard, 2010). The precise diseases caused by the other two mutations, which occur in the first and fifth cadherin domains, have not been identified (Henderson, 2010).

### 1.3.2 *Pcdh-21*<sup>-/-</sup> mice

The inheritance pattern and clinical features observed in patients with *PCDH-21* mutations resemble those observed in transgenic mice (Rattner, 2001; Ostergaard, 2010; Henderson, 2010). *Pcdh-21* heterozygous knockout mice are unaffected, whereas homozygous knockout mice undergo progressive retinal degeneration. They develop normal retinas but PR cell death is observed as early as one month old, shortly after retinal development is completed. PR continue to degenerate progressively and only 50% of their PR remain after five months.

The phenotype of *pcdh-21*<sup>-/-</sup> mice confirms a link between disk synthesis and *pcdh-21*. At the onset of retinal degeneration, these mice develop shorter OS and misaligned disks (Rattner, 2001). They have impaired vision, as determined by a reduction in rod and cone electroretinography response by two to three fold (Rattner, 2001). However, considering the severe OS abnormalities, the visual dysfunction is not as severe as expected, possibly due to the correct targeting of the phototransduction proteins (Rattner, 2001).

*Pcdh-21* is not likely to play a role in phototransduction because vision is only modestly

compromised in *pcdh-21*<sup>-/-</sup> mice. Furthermore, it is not likely to be involved in OS protein trafficking since phototransduction (eg. rhodopsin, S-cone opsin) and structural proteins (eg. ROM-1) are correctly targeted in *pcdh-21*<sup>-/-</sup> mice.

### 1.3.3 *PROM-1* mutations

Compared to *PCDH-21*, more disease-causing *PROM-1* mutations have been identified (Table 1-1). Of the five known *PROM-1* mutations, only disease associated with the R373C missense mutation is inherited in a dominant pattern. The same R373C mutation is associated with CORD as well as two forms of MD (Stargardt disease 4 and bull's eye macular dystrophy) (Yang, 2008). Two frameshift mutations that result in premature stop codons and likely induce nonsense-mediated decay, are linked to autosomal recessive RP (Permanyer, 2010; Zhang, 2007). Maw *et al.* (2000) also identified a frameshift mutation, but the precise disease has not been identified. Recently, another frameshift mutation in *PROM-1* has been linked to autosomal recessive CORD (Pras, 2009).

### 1.3.4 *Prom-1* transgenic mice

***Prom-1 Knockout*** The absence of *prom-1* causes progressive PR degeneration and disorganized disks in both rods and cones. These defects were first observed two weeks after birth, slightly earlier than observed in *pcdh-21* knockout mice (Rattner, 2001; Zacchigna, 2009). Both rod and cone responses were reduced by ~50% at one month of age and were almost completely absent at six months of age. It is unclear whether loss of *prom-1* causes PR degeneration due to the abnormal distribution of visual pigments and/ or defective disk

ultrastructure. Prom-1 induced defects were inherited in a recessive pattern, since heterozygous knockout mice were unaffected and had normal retinas (Zacchigna, 2009).

***Human R373C Prom-1 transgenic mice*** Transgenic mice expressing the human R373C *PROM-1* mutant exhibit progressive PR degeneration and OS defects two weeks after birth. The mutation is thought to exert a dominant negative effect (Yang, 2008). In transgenic mice, the mutant proteins are mislocalized throughout the OS, affecting the localization of the endogenous prom-1 and pcdh-21. Furthermore, expression of the mutant protein abolishes prom-1 binding with pcdh-21 and actin, two other components that are thought to regulate disk synthesis. Proteolytic cleavage of pcdh-21, a process thought to be essential for normal disk synthesis, is also affected (Yang, 2008). These phenotypes led to the conclusion that the R373C mutation encodes a stable mutant protein that impairs endogenous protein function. This is in direct contrast to another *PROM-1* mutation (c.1878delG), causing truncation of the prom-1 protein. Additionally, *in vitro* study showed that the truncated proteins are degraded in the ER and are not transported efficiently to the plasma membrane (Maw, 2000).

## **1.4 Significance**

PR disks must be synthesized continuously for proper function. Abnormal disk synthesis leading to reduction in OS length and defective disk structures are often associated with PR degeneration (Wright, 2010). This can be caused by the inheritance of defective genes or environmental factors, such as age. Despite the essential role of disk synthesis for PR survival, the components and mechanisms involved in this process are unclear. The results of this study will help define the role of pcdh-21 in disk formation and advance our

understanding of this process, which will in turn help develop therapies for curing blindness caused by defective disk formation.

## **1.5 Rationale and objectives**

Ultrastructural observations from a wide variety of vertebrates have revealed morphological differences between ROS and COS. Comparative studies of ROS from diverse species have also revealed variations in ROS structure. These observations led to several unanswered yet interesting questions regarding to disk synthesis. What is the molecular basis leading to OS structural differences across species and between rods and cones? Is the mechanism of rod disk synthesis evolutionary conserved across species?

Pcdh-21 is one of the two proteins concentrated at the nascent disks of PR, suggesting its role in disk synthesis. Pcdh-21 is expressed in PR of diverse species and its amino acid sequence is evolutionary conserved (Rattner, 2004). Although OS ultrastructure varies across species and between cell types, pcdh-21 localization has only been identified in mice, a species with low abundance of cones. Little is known about pcdh-21 localization in cones and in PR of other species.

*X.laevis* is an ideal organism for studying OS protein functions. It has large OS and high disk turnover rate. Furthermore, its disk synthesis follows a diurnal cycle, making *X.laevis* amenable for determining whether pcdh-21 expression supports its role in disk synthesis. Furthermore, transgenic *X.laevis* are easy to generate, allowing us to study the effect of pcdh-21 deletion mutants on disk morphology, which may be helpful in understanding the role of pcdh-21 in disk synthesis.

To characterize the role of pcdh-21 in PR disk synthesis, this project is divided into three aims:

- To define and compare the subcellular localization of pcdh-21 in PR of different species.
- To examine pcdh-21 abundance in nascent disks of *X.laevis* rods during disk synthesis.
- To investigate pcdh-21 function in *X.laevis* rod disk synthesis.

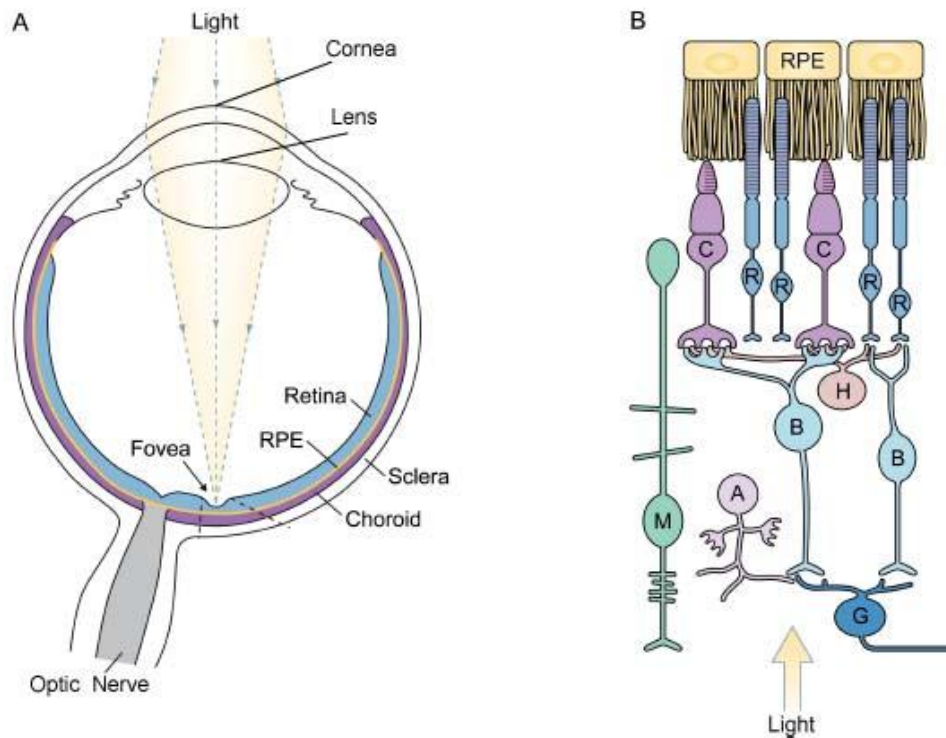


**Figure 1-1. The human eye (A) and retina (B).**

(A) Light passes through the cornea and is focused by the lens. The retina converts light to electrical signals that are sent to the brain through the optic nerve. (B) Diagram illustrating the neural circuitry in the retina. Counter intuitively, the photoreceptors (R=rods; C=cones), the light sensing cells, are located furthest away from the incoming light. Light passes through several cell layers before reaching the photoreceptors. The bipolar cells (B) receive signals from rods and cones that are modulated by the horizontal cells (H). Bipolar cells synapse with the ganglion cells (G). The signals are further modified by the amacrine cells (A). The ganglion cell axons together constitute the optic nerve which is responsible for sending the final signal to the brain. The pigmented neuroepithelial cells (RPE) are adjacent to the rods and cones. They supply nutrients to the photoreceptors and aid in outer segment turnover (Modified from Sung and Chuang, 2010).

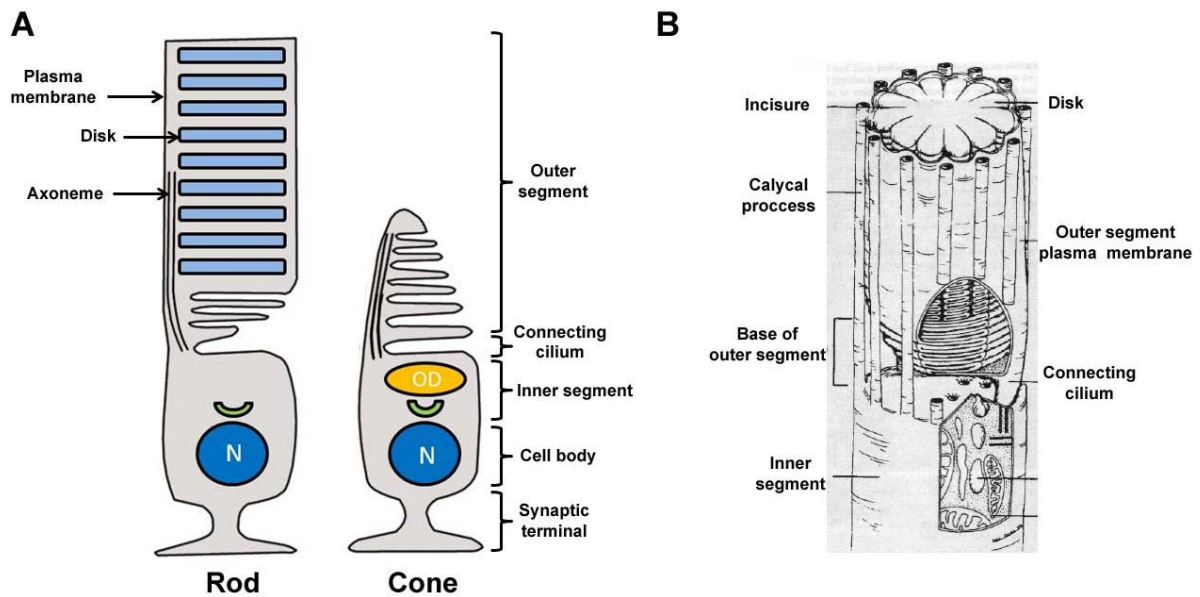


**Figure 1-2. Overview of *X.laevis* rod and cone morphology.**

(A) Rods and cones have four distinct compartments: outer segment, inner segment, cell body and synaptic terminal. The outer segment consists of ~1000 regularly stacked disks. Proteins synthesized in the inner segment are transported to the outer segment through the connecting cilium. In rods, the axoneme extends from the basal outer segment to half of the outer segment. In cones, the axoneme is present along the entire outer segment. N=nucleus; OD=oil droplet (B) 3D view of *X.laevis* rods. Calycal processes are protrusions that extend from the inner segment plasma membrane. They surround the basal outer segment like the calyx of a flower. Rod disks contain multiple incisures, indentations resulting from disk rims penetrating the centre of the disks. (Modified from Besharse & Pfenninger, 1980)

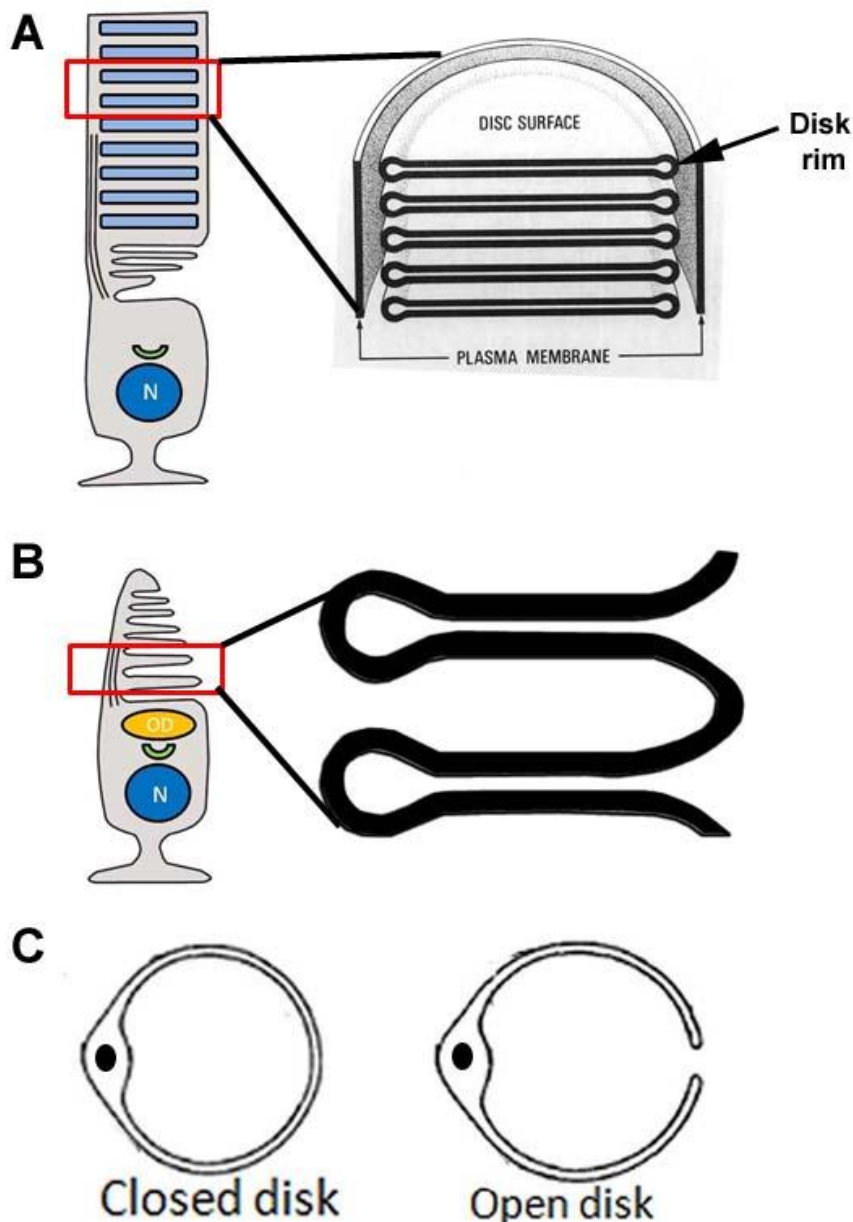


**Figure 1-3. Ultrastructural differences between *X.laevis* rods and cones.**

(A) The distal part of the ROS consists of closed disks surrounded by the plasma membrane. The rims of the rod disks have hairpin shape since the two opposing disk surfaces are closer together (Modified from Steinberg, 1980). (B) Cone outer segments do not have distinct plasma and disk membranes and the disk membranes are continuous with each other. Cone disks are termed “open disks” since the rims opposite to the axoneme are exposed to the extracellular matrix. Note that the rims adjacent to the axoneme adopt a hairpin shape as observed in closed disks of rods. In the basal ROS of *X. laevis*, open disks are observed (A) (modified from Fetter and Corless, 1987). (C) Transverse sections of closed and open disks. In open disks, the rims opposite to the axoneme (circle) are not formed and are accessible to the extracellular matrix (Modified from Steinberg, 1980).

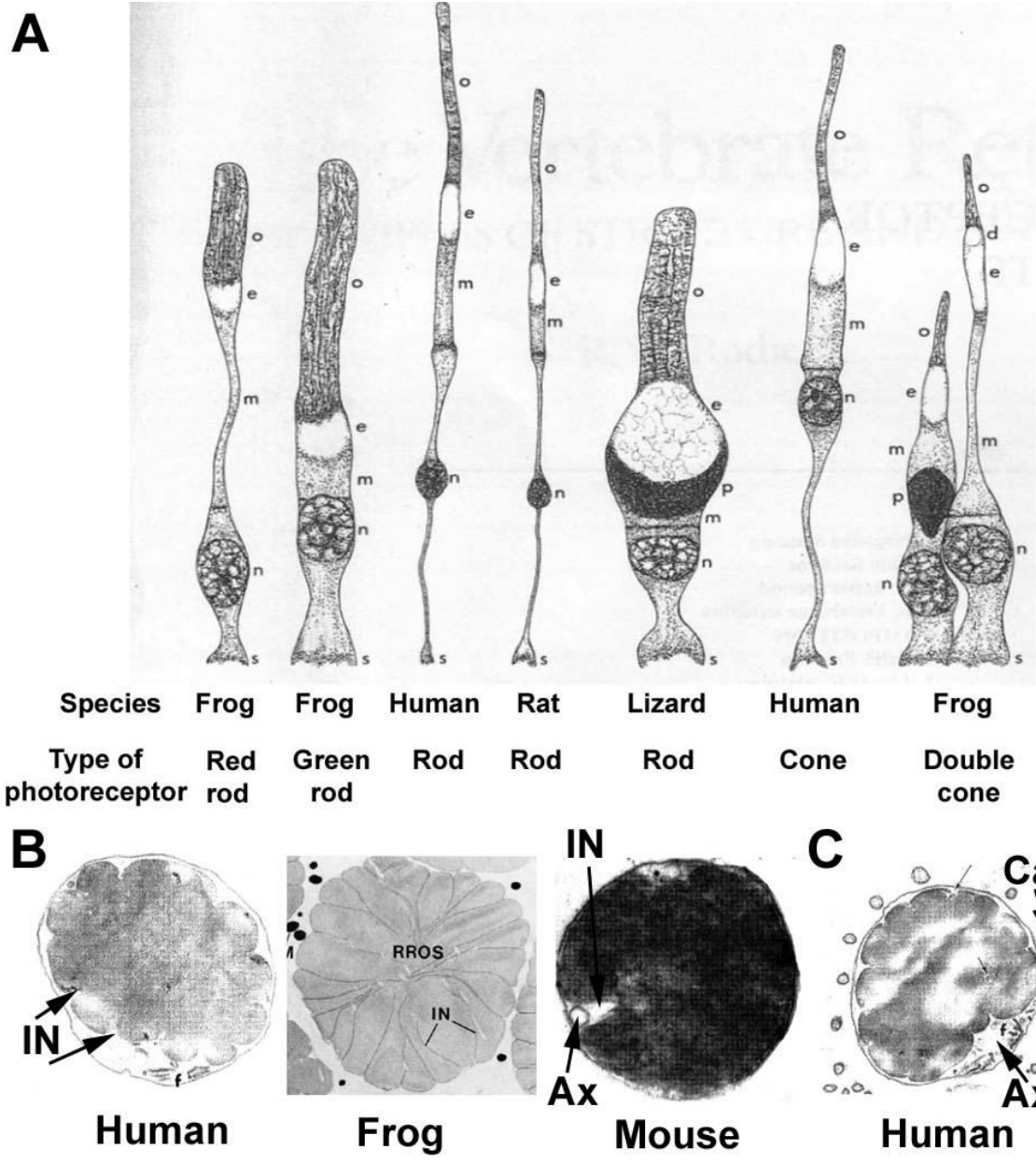


**Figure 1-4. Structural diversity between photoreceptors of different species.**  
 (a) Rods and cones of different species illustrating variation in OS diameter and length. The diameter of frog ROS are almost five times larger than those of humans and rats. The cells are drawn to scale. o=outer segment; e=ellipsoid containing mitochondria m=myoid containing endoplasmic reticulum; n=nucleus; s=synaptic terminal; p=paraboloid containing oil droplet (Modified from Roderick, 1973). (b) Cross sections of human, frog and mouse distal ROS. Humans and frogs have multiple disk incisures, resulting in flower-shaped disks. Mouse rods only have a single incisure and therefore have a circular rod disk. (c) Cross sections of human basal ROS. A calycal process is present at each indentation. One side of the disk is displaced by the axoneme (Modified from Cohen, 1965; 1960; Papermaster, 1982). IN=incisures; Ca=calycal process; Ax=axoneme.

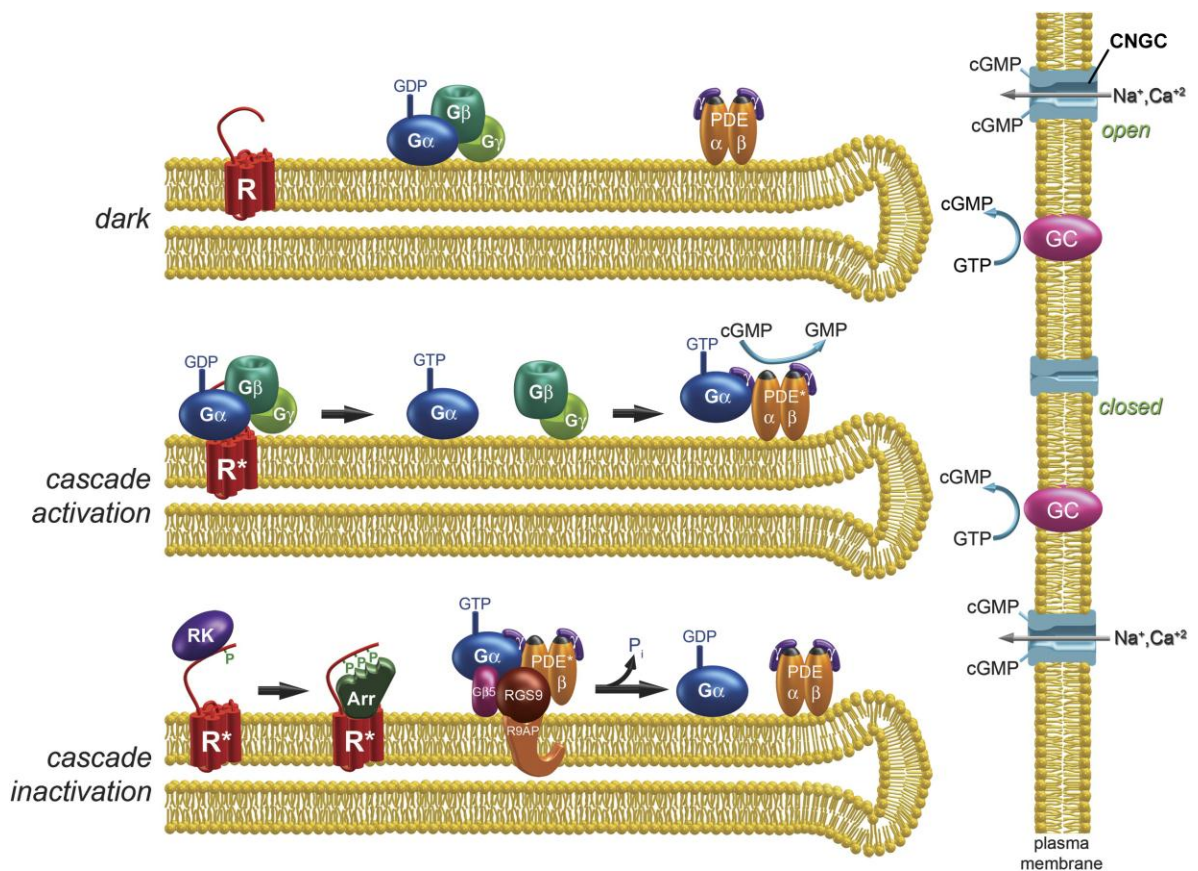


**Figure 1-5. Phototransduction cascade activation and inactivation.**

The upper disk shows that in the dark, rhodopsin (R), transducin ( $G\alpha$ ,  $\beta$ ,  $\gamma$ ) and phosphodiesterase (PDE) are spatially separated from each other. The cGMP gated ion channel in the plasma membrane is open, generating a constant influx of  $\text{Na}^+$  and  $\text{Ca}^{2+}$  into the OS. This flow of ions keeps the cell in its resting, depolarized state. The middle disk depicts cascade activation upon light absorption. Rhodopsin is activated ( $R^*$ ), facilitating binding of heterotrimeric transducin ( $G\alpha$ ,  $\beta$ ,  $\gamma$ ). Once it binds to rhodopsin, it exchanges GDP to GTP. The GTP bound  $G\alpha$  subunit dissociates from the other subunits. It binds and activates PDE, catalyzing the hydrolysis of cGMP to GMP. A decrease in cGMP level leads to the closure of cGMP gated ion channel. The lower disk illustrates steps involved in cascade inactivation. To inactivate rhodopsin, it is phosphorylated by rhodopsin kinase (RK), followed by binding of arrestin (Arr). PDE is inactivated when  $G\alpha$  converts GTP to GDP. (Modified from Burns & Arshavsky, 2005)

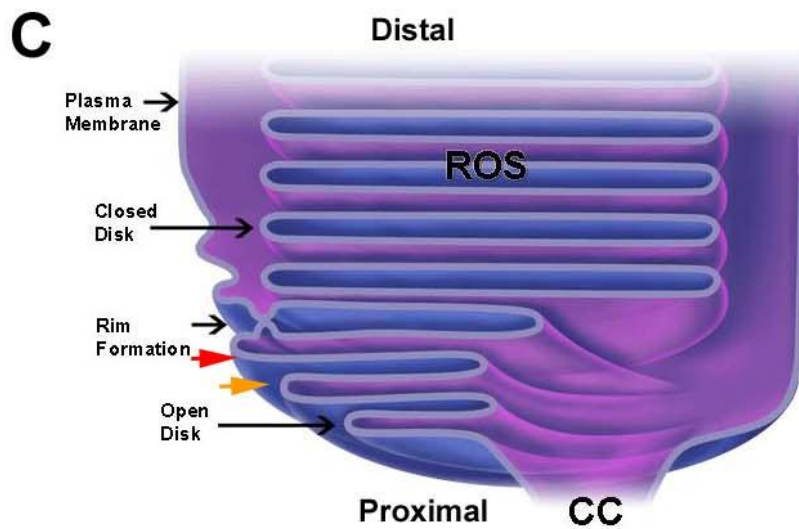
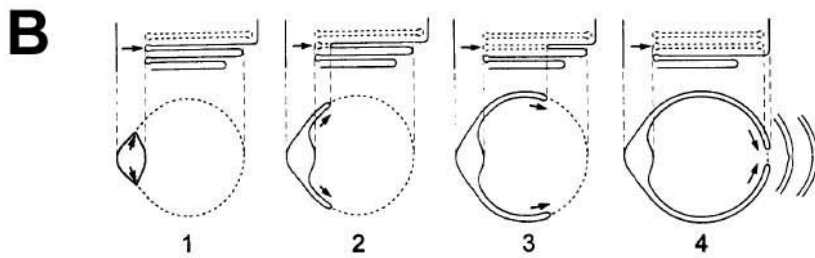
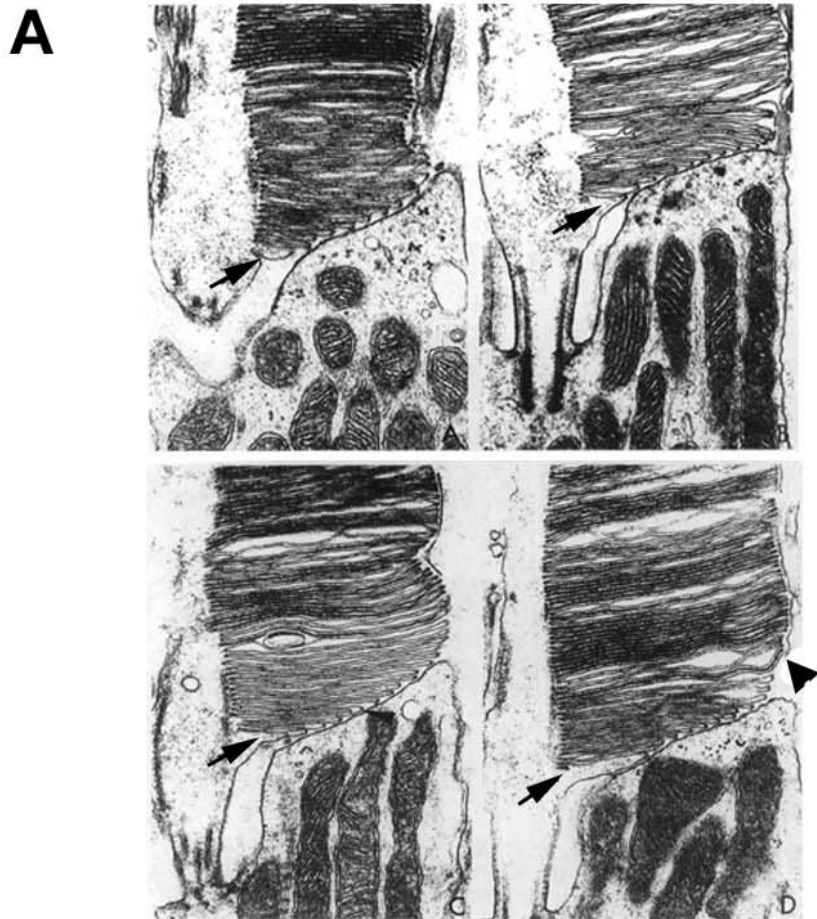


**Figure 1-6. The membrane evagination model is separated into two steps: the formation of disk surface (A) and disk rims (B-C).**

(A) Electron micrographs of monkey ROS illustrating the development of disk surface. At the distal connecting cilium, a small bud, representing a newly formed evagination is observed (1, arrow). As the evagination grows away from the connecting cilium, it becomes thinner and continues to remodel into disk shape (2-4, arrows). An arrowhead marks the first mature disk spanning the width of the OS. Note that mature disks are surrounded by plasma membrane, which are absent in nascent disks (Modified from Steinberg, 1980). **(B)** Longitudinal and cross sections of a disk showing the process of rim formation. Rim formation begins at the distal connecting cilium (1). Two adjacent evaginations grow and extend along the disk edge (2-3). The two ends join at a point opposite to the connecting cilium (4) (Modified from Steinberg, 1980). **(C)** Cartoon illustrates the transition from open to closed disk followed by rim formation. Rim formation occurs when proximal side of one evagination (orange arrow) fuses with the distal side of the adjacent evagination (red arrow). The mature disk detaches from the plasma membrane, forming a closed disk. This fusion results in the engulfment of the extracellular space (blue) into the closed disks. Blue indicates surface exposed to the extracellular region whereas purple indicates surface facing the cytoplasm surface. CC=connecting cilium (Modified from Han, Z., thesis).

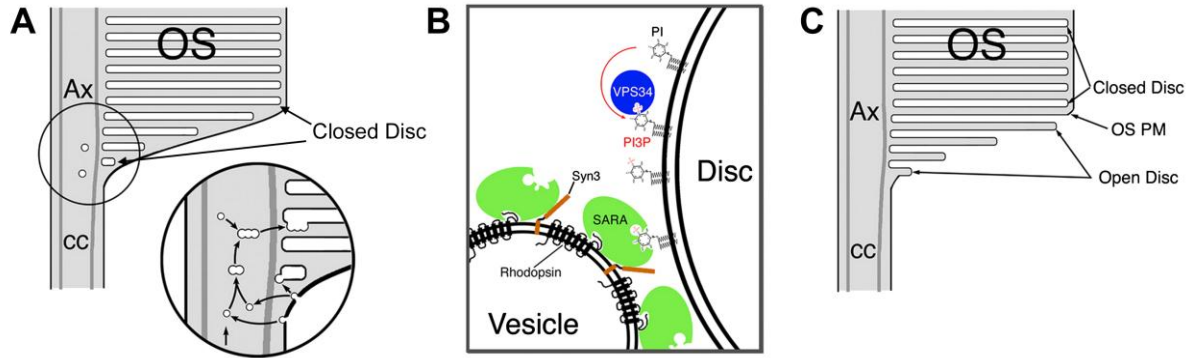


**Figure 1-7. Two contradicting models of rod disk synthesis.**

(A) In the “vesicular targeting model”, all disks, including nascent disks, are enclosed by plasma membrane. The enlarged circle depicts nascent disk formation through vesicle fusion with developing disks. Vesicles are transported directly from the inner segment or derived by endocytosis at the connecting cilium. Ax=axoneme; CC=connecting cilium. (B) Diagram illustrates the molecular machinery involved in the “vesicular targeting model”. Vesicles embedded with rhodopsin and SNARE protein syntaxin3 (Syn3) fuse with nascent disks enriched with phosphatidylinositol 3-phosphate (PI3P). This fusion is regulated by SARA that interacts with rhodopsin, Syn3 and PI3P. (Modified from Sung and Chung, 2010). (C) The “membrane evagination model” describes the presence of open disks at the base of the ROS. Closed disks surrounded by plasma membrane are described in the “vesicular targeting model”(Modified from Sung & Chuang, 2010).

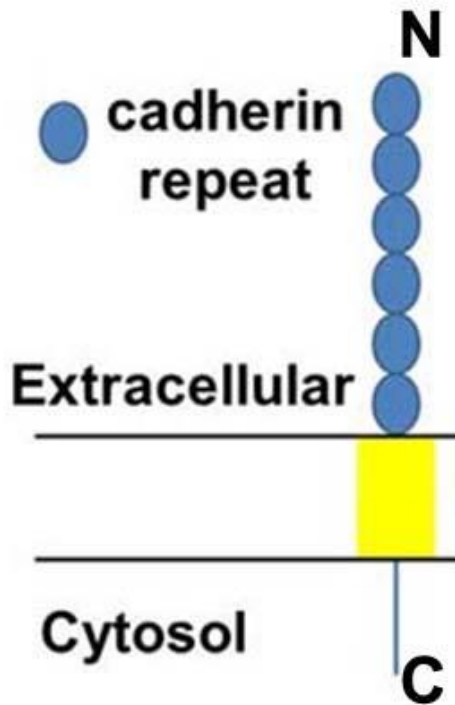


**Figure 1-8. Schematic diagram of pcdh-21 structure.**

Pcdh-21 is a single pass transmembrane protein with a cytosolic C-terminus. The extracellular N-terminus consists of six cadherin repeats.

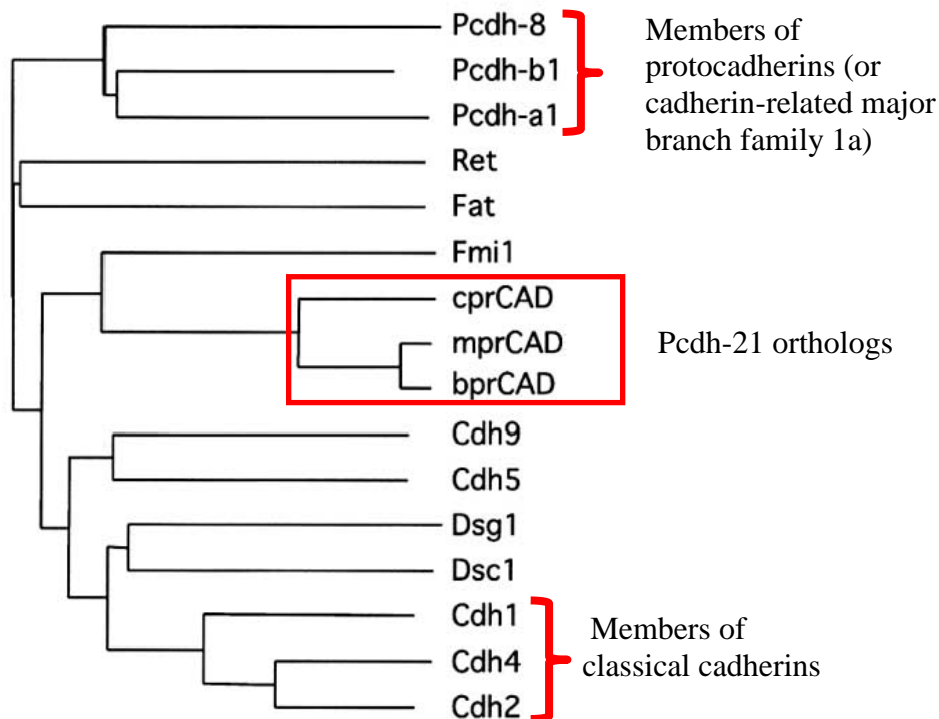


**Figure 1-9. Phylogenetic tree generated by comparing first cadherin domain of pcdh-21 and other cadherin family members.**

The illustrated cadherin members show higher homology to pcdh-21 than other cadherins based on BLAST search of the GenBank database. Chicken (cprCAD), mouse (mprCAD) and bovine (bprCAD) pcdh-21 are closely related to each other. They are not highly related to classical cadherins and protocadherins. (Modified from Rattner, 2001 and Hulpau, 2009). prCAD=photoreceptor cadherin. Cdh1=E-cadherin (GenBank accession number Z13009); Cdh2=N-cadherin(S42303); Cdh4=R-cadherin; Cdh5=VE-cadherin; Cdh9=T1-cadherin; Dsg1=Desmoglien-1; Dsc1=Desmocollin-1; Fat=Fat; Fmi1=Flamingo1; Pcdh-a1=Protocadherin- $\alpha$ 1 (CNR); Pcdh-b1=Protocadherin- $\beta$ 1; Pcdh-8=Protocadherin-8 (Arcadlin). (Modified from Rattner, 2001).

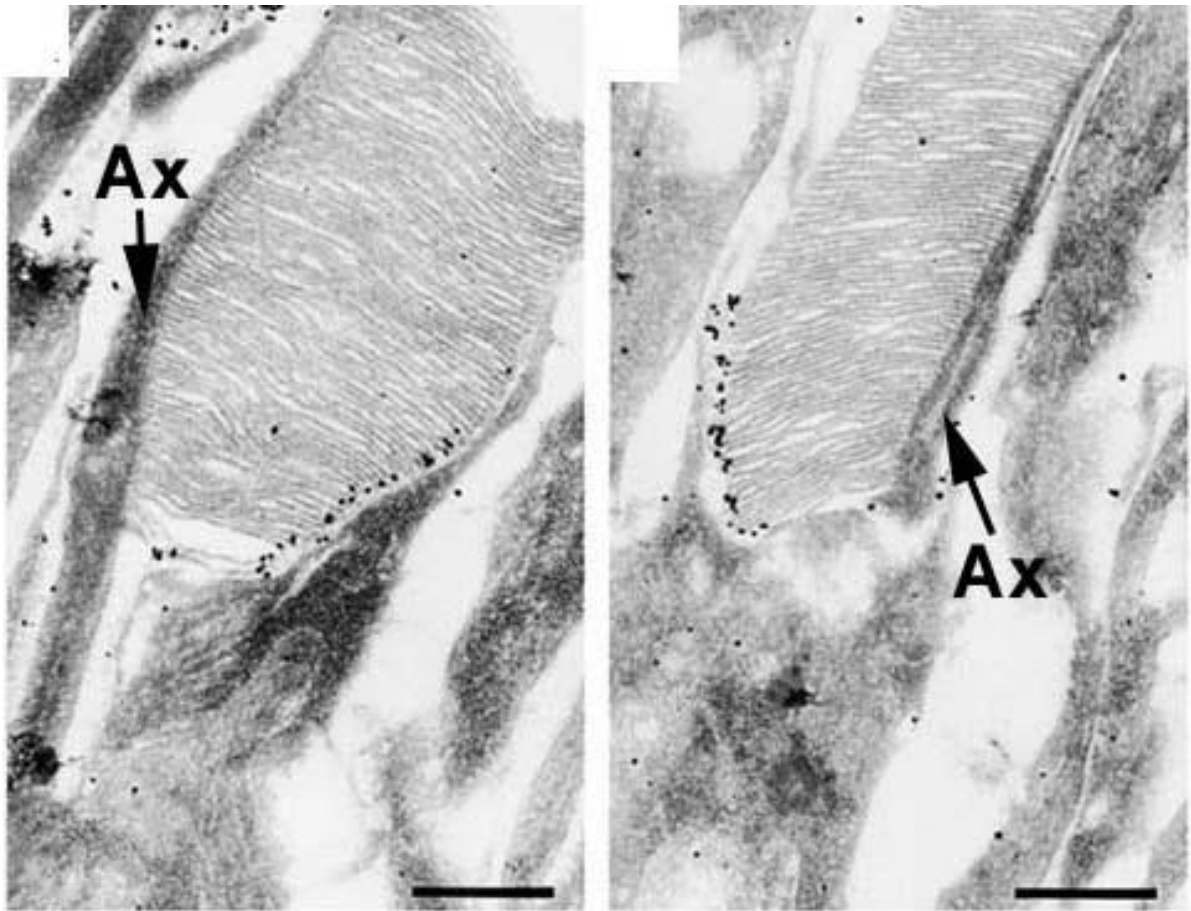


**Figure 1-10. Pcdh-21 localization in mouse rods.**

Pre-embedding labeling of mouse rods using anti-C-pcdh-21 antibody. Labeling is concentrated at the basal ROS rims opposite to the axoneme. Ax=axoneme. (Modified from Rattner, 2001).

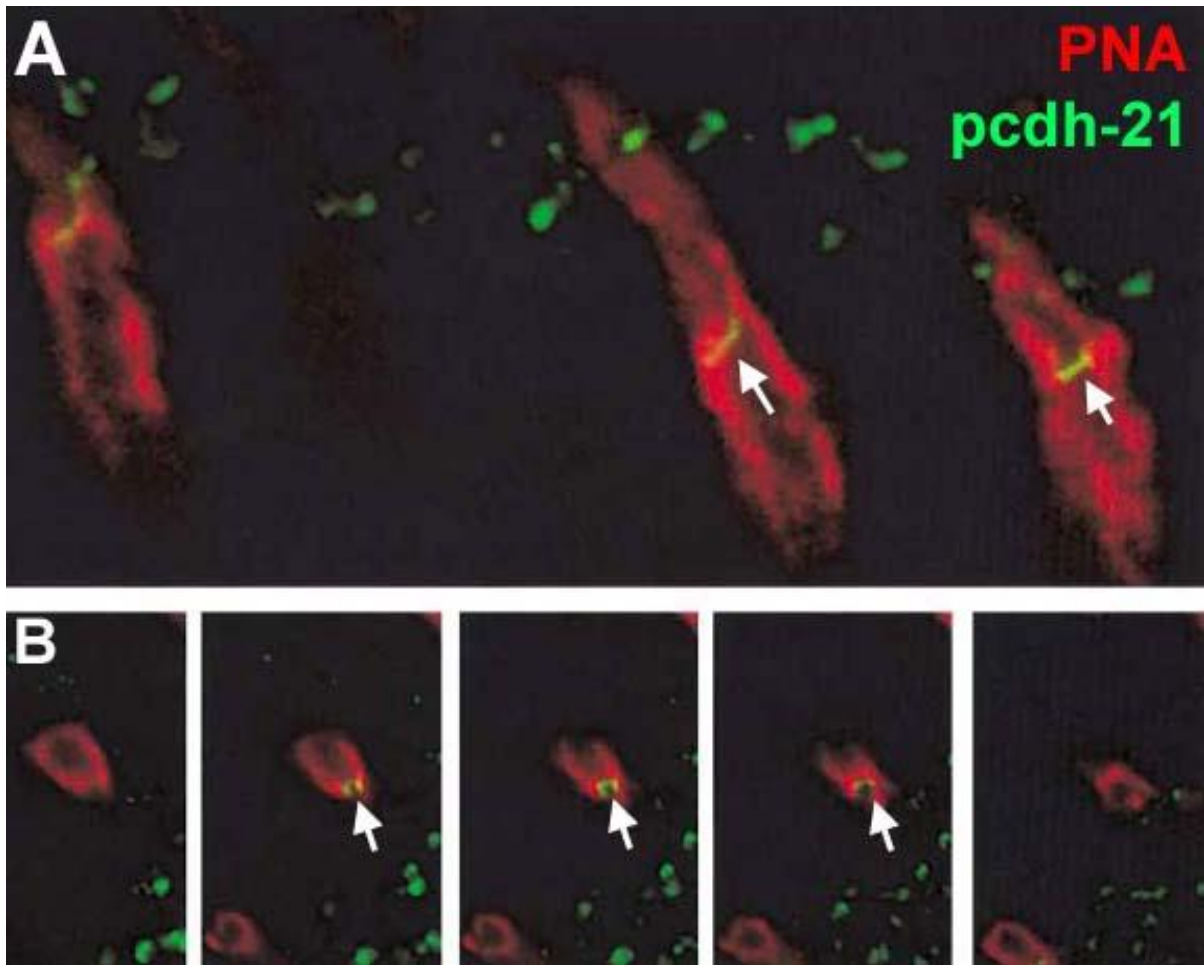


**Figure 1-11. Pcdh-21 localization in mouse cones.**

Mouse retinal sections were double labeled with anti-pcdh-21 and peanut agglutinin (which labels the extracellular matrix ensheathing COS). (A) Pcdh-21 (arrows) is exclusively localized to the base of the COS, labeling the basal disks as a thin line. (B) Serial optical sections imaged at a plane close to the connecting cilium showed that pcdh-21 (arrows) is confined to the COS. (Modified from Rattner, 2001).

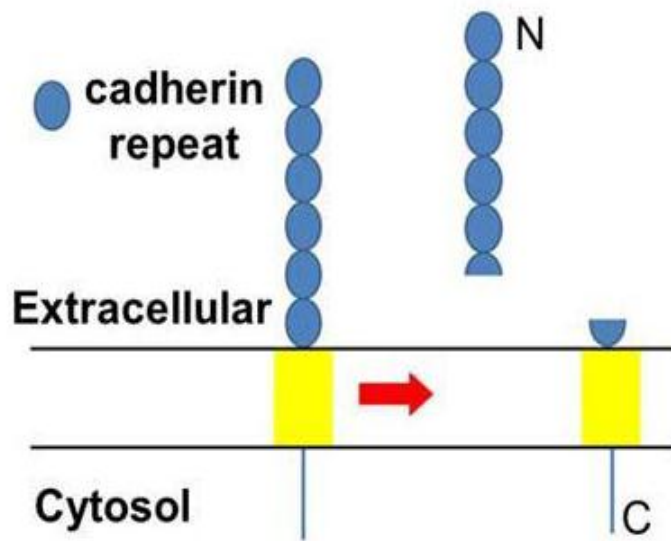


**Figure 1-12. Pcdh-21 cleavage in mouse and bovine retinas.**

Pcdh-21 is cleaved at the last cadherin domain, releasing a soluble N-terminal fragment and a membrane associated C-terminal fragment (Rattner, 2001).

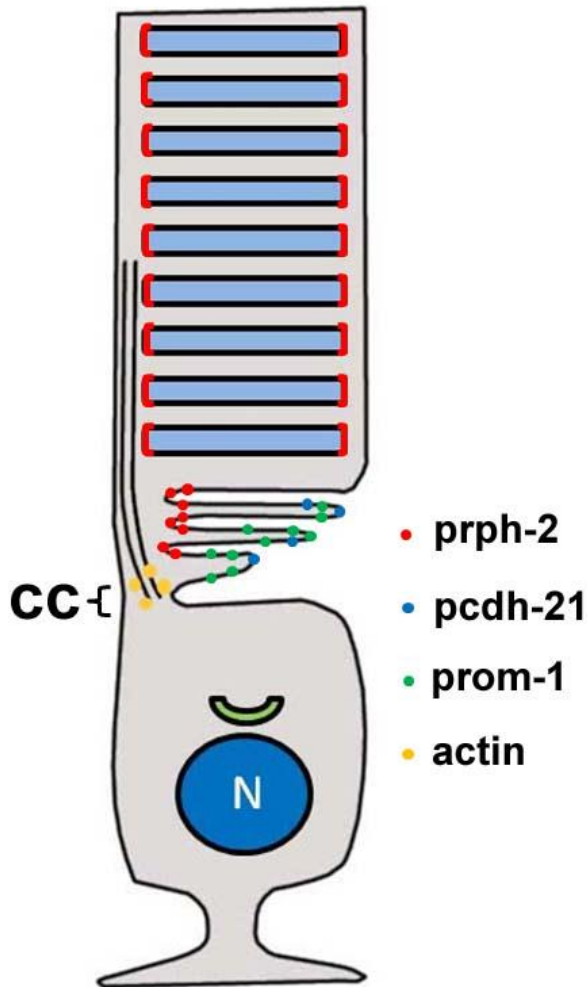


**Figure 1-13. Localization of OS proteins involved in disk synthesis in rodent rods.**

Nascent disks are depicted as membrane evaginations (also named “open disks”), based on the membrane evagination model. Actin is localized to the distal connecting cilium (Chaitin & Bok, 1986). Prom-1 and pcdh-21 colocalize at the base of the ROS, likely at the rims opposite to the connecting cilium (Rattner, 2004; Yang, 2008). Low levels of prom-1 are present in nascent disk surfaces (Maw, 2000). At the base of the OS, prph-2 distribution is complementary to that of pcdh-21 (Arikawa, 1992; Rattner, 2004). Prph-2 is restricted to rims near the connecting cilium. At the distal OS, prph-2 is localized to both rims of mature disks (also named “close disks”) (Arikawa, 1992). N=nucleus. CC=connecting cilium.

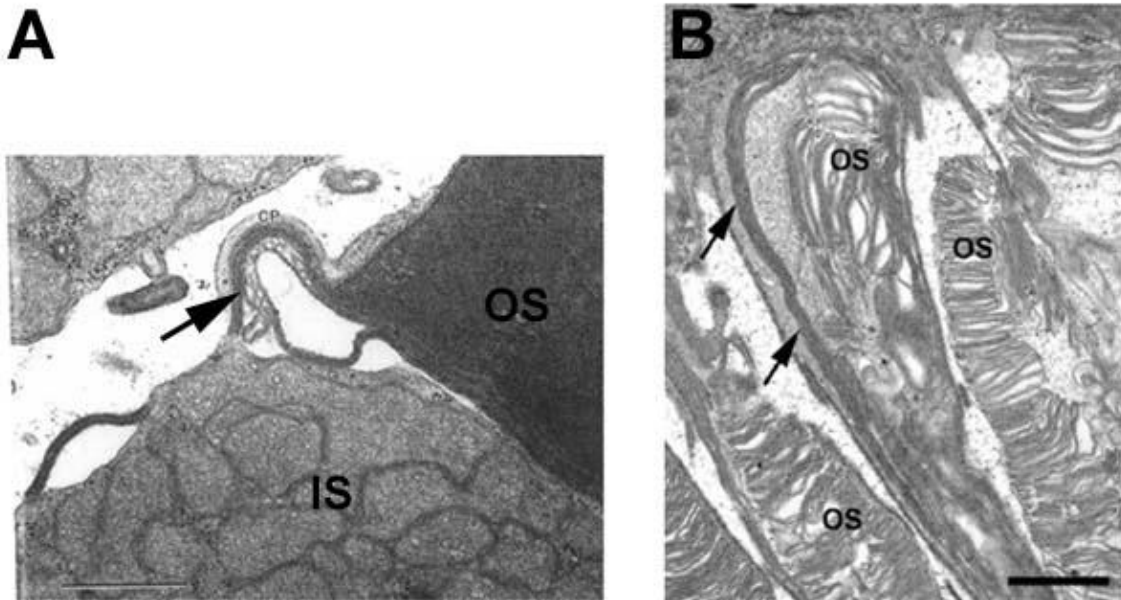


**Figure 1-14. *X.laevis* with defects in actin polymerization (A) and transgenic mice containing a prom-1 R373C mutation (B) have abnormally large disks.**

(A) At the base of the outer segment, the overgrown nascent disks (arrows) extend along the inner segment plasma membrane. The mature disks at the distal outer segment are normal. (B) Enlarged disks (arrows) grow along the outer segment plasma membrane. OS=outer segment; IS=inner segment (Williams ,1988; Yang, 2008)

**Table 1-1. *PCDH-21* and *PROM-1* mutations associated with inherited photoreceptor degeneration.**

<b>Gene</b>	<b>Mutation</b>	<b>Disease</b>
<i>PCDH-21</i>	c.524dupA *	AR CORD (Ostergaard, 2010)
	c. 337delG *	AR disease unknown (Henderson, 2010)
	c.1459delG *	AR disease unknown (Henderson, 2010)
<i>PROM-1</i>	c.1878delG *	AR disease unknown (Maw, 2000)
	c.C1726T	AR RP (Zhang, 2007)
	c.R373C	AD CORD, AD MD (Yang, 2008)
	c.869delG *	AR RP (Permanyer, 2010)
	c.1349insT *	AR CORD (Pras, 2009)

dup=duplication; del=deletion; ins=insertion; AR=autosomal recessive; \*=frameshift mutation; AD=autosomal dominant; CORD=cone-rod dystrophy; MD=macular dystrophy; RP=retinitis pigmentosa

## Chapter 2: Subcellular localization of pcdh-21

### 2.1 Introduction

*Pcdh-21* is evolutionary conserved across species. *Pcdh-21* transcripts are exclusively found in the PR layers of fish, *X.laevis* and mice (Rattner, 2004). However, its localization at the protein level has only been determined in mice. In mouse rods, it is restricted to the nascent disk rims opposite the axoneme (Rattner, 2001). It is also localized to the nascent disks of mouse cones, but its ultrastructural localization within the nascent disks is unknown.

Because of its exclusive localization in nascent disks, pcdh-21 is thought to play a role in disk synthesis. *Pcdh-21* <sup>-/-</sup> mice had shorter and fragmented OS (Rattner, 2004). *PCDH-21* mutations are linked to retinal degenerative diseases (Ostergaard, 2010; Henderson, 2010). In mice, pcdh-21 undergoes proteolytic cleavage, which may be essential for disk synthesis (Rattner, 2004).

Observations from primates and amphibians suggest that nascent disks are first synthesized as membrane protrusions and are subsequently remodeled into disk structures (membrane evagination model) (Steinberg, 1980; Wrigely, 2000). This model has been challenged by studies from mice (Chuang, 2007). The authors proposed that disk synthesis occurs by fusion between vesicles and developing disks (vesicular targeting model). One plausible explanation for such inconsistency is that mammalian and non-mammalian rods may employ different disk synthesis mechanisms (Sung, 2010). This is supported by multiple studies revealing differences in OS ultrastructure across vertebrates (Cohen, 1965; 1960; Frederick, 1973; Papermaster, 1982).

To gain clues about the function of *pcdh-21* in disk synthesis across species, it is necessary to determine its subcellular localization. Our current knowledge of *pcdh-21* localization is limited and is based on mice that have small OS, low number of cones and relatively slow disk renewal rate.

We evaluated and compared *pcdh-21* localization across species and in transfected cells with immunofluorescence microscopy. Using *X.laevis* with OS diameter five times larger than mice and twice as high a disk synthesis rate as mice (Kinney, 1977), we studied *pcdh-21* abundance in nascent rod disks during disk synthesis. We also examined *pcdh-21* cleavage across species using western blot.

## **2.2 Materials and methods**

### **2.2.1 Generation of *pcdh-21* polyclonal antibody**

Peptides containing sequences from the N-terminus (CYGENGPQNRFE~~LT~~MYEH; amino acid 358-374) and C-terminus (CQEMESGPKNENRNN; amino acid 776-789) of *X.laevis pcdh-21* were fused to either KLH or THY. Immunogens were used to immunize rabbits and their antisera were collected. Procedures were carried out by Yenzym Antibodies (South San Francisco, California).

### **2.2.2 Peptide competition assays on Western blots and immunohistochemistry**

Lyophilized peptides were resuspended to 100mg/ml in DMSO and were incubated in 50°C hot water bath for 3mins. The mixture was vortexed and mixed by inversion at RT for 1hr. Prior to immunolabeling for immunohistochemistry, peptides (100X) were incubated with antibodies and mixed by inversion at RT for 1hr. For immunostaining of western blots,

a mixture containing antibodies and peptides were incubated and mixed by inversion overnight at 4°C. prior to application to the western blot membrane.

### **2.2.3 Preparation of frozen retinal sections from multiple species**

***X.laevis* and *X.tropicalis*:** Tadpoles were fixed in 4% paraformaldehyde in 0.1M NaPO<sub>4</sub> pH 7.4 at 4°C for 1-3 days. Eyes were dissected and cryoprotected with 20% sucrose in 0.1M NaPO<sub>4</sub> pH 7.4 for 2-3 hours. Eyes were embedded in OCT (TissueTek, Torrance, CA) and 12µm sections were cut.

**Zebrafish:** Heads of adult zebrafish were fixed in 4% paraformaldehyde in 0.1M NaPO<sub>4</sub> pH 7.4 at 4°C overnight. Eyes were dissected, processed and sectioned using a protocol identical to that used on *X.laevis* eyes.

**Mouse:** Eyes were obtained from C57BL mice (P22) and were fixed in 4% paraformaldehyde in 0.1M NaPO<sub>4</sub> pH 7.4 for 1hr. After the removal of the corneae and lenses, eyes were fixed for another hour and were gradually infiltrated with increasing concentrations of sucrose (5%, 10%, 15%, 20% in 0.1M NaPO<sub>4</sub> pH 7.4; 10mins at each concentration). Eyes were then embedded in OCT and 12-16µm sections were obtained.

**Fig:** Eyes were shipped on ice from a nearby slaughterhouse and were kept at 4°C until dissection. Sections of the eye were sliced off with a razor blade. Tissues were processed and sectioned using a protocol identical to that used on mouse eyecups.

**Human** Donor eyes with their corneae removed were obtained from UBC Eye Bank (Vancouver, BC, Canada). Eyes were fixed in 4% paraformaldehyde in 0.1M NaPO<sub>4</sub> pH 7.4 for 3 days at 4°C. After the removal of the lenses and ciliary bodies, several incisions were made to flatten the eye and pieces of tissue were obtained using an 8mm trephine. Punched

tissues were gradually infiltrated with increasing sucrose concentration (5%, 10%, 15%, 20% in 0.1M NaPO<sub>4</sub> pH 7.4; 5-10mins at each concentration). In another protocol, prior to dissection, eyes were immersed in 10% sucrose in 0.1M NaPO<sub>4</sub> pH 7.4 (overnight at 4°C) and were transferred to 30% sucrose in 0.1M NaPO<sub>4</sub> pH 7.4 (overnight at 4°C). After punches of tissues were collected, they were further cryoprotected in 30% sucrose in 0.1M NaPO<sub>4</sub> pH 7.4 for 1 hr. Tissues were embedded in OCT and 20µm sections were obtained.

#### **2.2.4 Immunofluorescence labeling of frozen retinal sections**

Cryosections were blocked and permeabilized in PBS containing 1% goat serum and 0.1% Triton X-100. Sections were immunolabeled overnight with primary antibodies diluted in PBS containing 0.1% goat serum and 0.1% Triton X-100. Antibodies used were as followed: anti-N pcdh-21 (1:10000), anti-acetylated tubulin (1:250; Sigma-Aldrich, St. Louis, MO), anti-peripherin 5A11 (1:10; a gift from R.S. Molday, UBC), anti-rhodopsin blgn (1:10; gift of W. C. Smith, University of Florida), anti-cone arrestin 7G6 (1:100; gift from Peter Mcleish, Morehouse School of Medicine) and anti-N-prom-1 (1:150; gift from Zhou Han, University of Connecticut). Sections were washed with PBS and labeled with Cy3- (anti-mouse 1:750; anti-rabbit 1:1000; Jackson Immunoresearch, West Grove, PA), Cy5- (anti-mouse 1:500; anti-rabbit 1:500; Jackson Immunoresearch, West Grove, PA) or Alexa488-conjugated secondary antibodies (anti-mouse 1:500; anti-rabbit 1:100; Molecular Probes, Eugene, OR). Some sections were also counterstained with Alexa488 (1:100) or Alexa555-conjugated wheat germ agglutinin (1:1000; Molecular Probes, Eugene, OR), Alex546-conjugated phalloidin (1:40; Molecular Probes, Eugene, OR) and Hoechst 33342 (1:1000; Sigma-Aldrich, St. Louis, MO). Sections were imaged using a Zeiss (Oberkochen, Germany)

510 laser scanning confocal microscope equipped with a 10X numerical aperture (N.A.) 0.3 objective and a 40X N.A. 1.2 water immersion objective. Images in z-series were spaced 1µm apart. Z-series projections were constructed using Zeiss LSM5 software. Figures were assembled using Adobe Photoshop (Adobe Systems, San Jose, CA). Gamma was freely adjusted in images of wheat germ agglutinin (to improve image detail), but was not adjusted in images of antibody labeling (to maintain linearity of signal).

### **2.2.5 Expression and purification of mouse and *X.laevis* pcdh-21 from COS-7 cells**

Plasmids used for transfection were generated by subcloning eGFP, mpcdh-21, xpcdh-21 and human rhodopsin cDNA into the *EcoRI* and *NotI* site of the pMT3 vector (Oprian,1987). COS-7 cells were plated onto 60mm and 10cm culture vessels and maintained in Dulbecco's modified Eagle's medium with 10% (v/v) fetal calf serum. 24µg of pMT3 mpcdh-21 and pMT3 xpcdh-21 plasmids were transfected in 10cm culture dishes; whereas 8µg of pMT3 GFP were transfected in 60mm cultured dishes. All transfections were performed using lipofectamine 2000, according to the manufacturer's instructions (Invitrogen, Carlsbad, CA) and harvested 40-42hrs after transfection. Lysates from cells expressing xpcdh-21 and mpcdh-21 were solubilized in 500µl of buffer (PBS, 1% Triton X-100, 2mM EDTA, 1mM PMSF), whereas lysates from cells expressing GFP were solubilized in ~170µl of buffer. Lysates were vortexed and centrifuged for 5mins to pellet insoluble materials. Supernatants were transferred to separate microcentrifuge tubes and equal volumes of 2X loading buffer containing 8% β-mercaptoethanol were added. For localization studies, cells were plated on 8-well cell culture slides and were transfected with 2µg of DNA. All plasmids were transfected using lipofectamine 2000 and fixed 40-48hrs post-transfection.

### **2.2.6 Immunofluorescence labeling of COS-7 cells**

After the removal of media, cells were washed with PBS and fixed in 4% paraformaldehyde in 0.1M NaPO<sub>4</sub> pH 7.4 for 30mins. To terminate fixation, fix was removed and cells were rinsed with PBS, followed by incubation with primary antibodies for 1hr. Antibodies were prepared in buffer containing PBS, 0.1% goat serum and 0.1% TritonX-100. Identical buffer, excluding Triton X-100, were used to dilute antibodies for labeling of non-permeabilized cells. The following primary antibodies were used: anti-N rhodopsin (B630N) (1:20; cell line was a gift from W. C. Smith, University of Florida), anti-C rhodopsin (1D4) (1:1000; Calbiochem), anti-N pcdh-21 (1:10000), anti-KDEL (1:80; Stressgen Biotechnologies, Victoria, BC, Canada) and anti-calnexin (1:100; Stressgen Biotechnologies, Victoria, BC, Canada). Sections were washed with PBS and labeled with Cy3- (anti-mouse 1:750; anti-rabbit 1:1000; Jackson ImmunoResearch, West Grove, PA) or Alexa488-conjugated secondary antibodies (1: 100; Molecular Probes, Eugene, OR). Some sections were also counterstained with Alexa488-conjugated wheat germ agglutinin (1:100; Molecular Probes, Eugene, OR), and Hoechst 33342 (1mg/ml; Sigma-Aldrich, St. Louis, MO). Sections were imaged as previously described.

### **2.2.7 Retinal extracts from multiple species**

Eight *X. laevis* tadpole retinas were solubilized in 80ul of solubilization buffer (PBS, 2.5% SDS, 5mM Tris pH 6.8, 20% sucrose, bromophenol blue, 2mM EDTA, 1mM PMSF, 4% β-mercaptoethanol) and homogenized using a motorized plastic pestle. Retinas from ten adult zebrafish, pig and human were solubilized and homogenized in 100μl of buffer

(150mM NaCl, 50mM Tris pH 7.5, 1% Triton X-100, 1mM EDTA, protease inhibitor cocktail (Sigma Aldrich). Mouse retina (C57BL, P25) was solubilized and homogenized in 80µl of buffer. After incubation on ice for 5mins, lysates were centrifuged to remove the nuclear fraction and other insoluble material. Supernatants containing cytoplasmic and membrane proteins were transferred to a separate tube and equal volume of 2X loading buffer (2.5% SDS, 5mM Tris pH 6.8, 20% sucrose, 8% β-mercaptoethanol, bromophenol blue) were added.

### **2.2.8 SDS page and western blotting**

14µl of protein samples were separated on 10% SDS-polyacrylamide gels (SDS-PAGE) using the Laemmli discontinuous buffer system. After electrophoresis, proteins were transferred to PVDF membrane using a Biorad wet transfer apparatus. Blots were blocked with 1% blocking buffer (skim milk and PBS) and probed with anti-N pcdh-21 (1:10000). Blots were then incubated with IRDye800-CW-conjugated anti-rabbit secondary antibodies (1: 10000; Rockland, Gilbertsville, PA) and analyzed on a LI-COR Odyssey imager (Li-Cor, Lincoln, NE).

## **2.3 Results**

### **2.3.1 Characterization of anti-pcdh-21 antibodies and proteolytic cleavage of pcdh-21 across species**

Two polyclonal antibodies were raised against the N- and C-termini of *X.laevis* pcdh-21 (xpcdh-21). Peptides corresponding to sequences from the fourth extracellular cadherin

domain or the cytoplasmic domain were chemically linked to KLH or THY and used to immunize rabbits (Fig.2-1).

Previous studies have demonstrated that mouse pcdh-21 (mpcdh-21) (100kDa) is cleaved, producing a soluble N-terminal fragment (75kDa) and a membrane associated C-terminal fragment (25kDa) (Fig.1-12). Immunoblot analysis was used to determine whether this cleavage is present in retinas across species. COS-7 cells extracts expressing GFP, mpcdh-21 or xpcdh-21 served as controls.

The anti-N-pcdh-21 antibody detected a single 90kDa band, likely representing the full length xpcdh-21, in *X.laevis* retinal lysate (Fig.2-2, top left, arrow). The band had a relative mobility slightly lower than that predicted by the xpcdh-21 sequence. In xpcdh-21 transfected cell lysate, four bands were detected (150kDa, 100kDa, 90kDa and 60kDa). The two most intense bands appeared to be 100kDa and 90kDa. The 100kDa band, which was not present in *X.laevis* retinal lysate, is likely to represent alternatively glycosylated xpcdh-21. The faint, high molecular band (150kDa) may represent xpcdh-21 aggregates or xpcdh-21 that is post-translationally modified or alternatively spliced. The 60kDa band may be degradation products or fragments result from cleavage at a site different from that predicted in mouse retinas (Rattner, 2004). Antibody incubated with the corresponding peptide did not detect the 90kDa band in *X.laevis* retinal lysate as well as the four bands in xpcdh-21 transfected cell lysate (Fig.2-2, top right), demonstrating labeling specificity.

Immunoblotting with the anti-C-pcdh-21 antibody detected 100kDa and 90kDa (Fig.2-2, bottom left, arrow) bands in xpcdh-21 transfected cell lysate, identical to those recognized by the anti-N-pcdh-21 antibody. The predicted 25kDa C-terminal fragments that would be produced via proteolytic cleavage were not detected, suggesting that xpcdh-21 was not

cleaved in transfected cells. No band was detected in *X.laevis* retinal lysate, possibly due to low sensitivity of the antibody. The absence of labeling in mpcdh-21 transfected cell lysate implies that the anti-C-pcdh-21 antibody does not cross react with the mouse orthologue. Antibody specificity was demonstrated when antibody preincubated with peptide failed to detect any band in xpcdh-21 transfected cell lysate (Fig.2-2, bottom right).

The antigenic sequence used to generate the anti-N-pcdh-21 antibody had a high degree of homology with other species. We tested the cross reactivity of this antibody with ppcad-21 in zebrafish and mammalian retinas, including mouse, pig and human. The antibody was not able to detect zebrafish pcdh-21, since the only observed band (120kDa) was not inhibited when probed with preincubated antibody (Fig.2-2, top left). In mpcdh-21 transfected cells, the antibody recognized two bands at 100kDa (Fig.2-3, top left, arrow) and 90kDa. The 100kDa band likely represents the full length mpcdh-21. Its relative mobility is slightly lower than what was previously reported (Rattner, 2004). The 90kDa band was also observed in xpcdh-21 transfected cells that were not able to cleave xpcdh-21. Therefore, it is unlikely that the 90kDa band represents the N-terminal cleaved fragment. Similarly, previous studies reported that cleavage was not detected in 293 cells expressing mpcdh-21 (Rattner, 2004).

In mouse retinas, three bands with molecular masses of 100kDa, 90kDa and 80kDa were detected (Fig.2-3,left). However, only the highest molecular weight band (100kDa), was inhibited by preadsorption of antibody with peptide (Fig.2-3, right). This implies that our antibody might not be able to detect the cleaved N-terminal fragment and it might detect an unrelated protein at 80kDa. A 100kDa band was observed in pig and human retinas. However, this band was not inhibited with preadsorbed antibody in human retinas. A 150kDa band was detected in pig retina that was inhibited by preadsorbed peptide. This band was also detected

in control cells transfected with GFP, suggesting that the 150kDa detected in pig retina may not be pcdh-21.

### **2.3.2 Distribution of pcdh-21 in *X.laevis* rods**

To determine pcdh-21 localization in *X.laevis* retinas, frozen sections were labeled with the anti-N- and anti-C-pcdh-21 antibodies. Both antibodies showed similar labeling patterns. The labeling intensity obtained with the anti-N-pcdh-21 antibody was stronger than that obtained with the anti-C-pcdh-21 antibody. This difference might be due to variation in antibody sensitivity (due to e.g. differences in affinity), as demonstrated by the results from western blots (Fig.2-2). Other potential causes might include limited accessibility of the intracellular epitope. Since there was no evidence that xpcdh-21 is cleaved (unlike the mouse homolog, see section 2.3.1), we assumed that the same protein was detected with both antibodies. All subsequent immunolabeling studies were therefore performed using the anti-N-pcdh-21 antibody, unless stated otherwise.

In *X.laevis* rods, pcdh-21 labeling was most intense in the RIS and ROS plasma membrane (Fig.2-4A, arrows). It labeled the base of the ROS as a faint, thin band in some, but all not rods (Fig.2-4A, arrowhead). A Z-series projection indicated that low levels of pcdh-21 were present in the ROS, exhibiting a striated labeling pattern (Fig.2-4B, arrows). To determine whether these structures represent labeling of incisures (invaginations of disk rims, Fig.1-2B), transverse sections were double labeled with antibody against peripherin-2 (5A11) in the incisures. (Fig.2-5A). Peripherin-2 was localized to the interior of the ROS, where pcdh-21 was absent, indicating that the striated pattern noted in Fig. 2-4B is not due to incisure labeling.

In some cross sections of ROS, pcdh-21 antibody did not label the circumference of the ROS continuously with uniform intensity (Fig.2-5A), as one would expect for a plasma membrane protein. Instead, it labeled the circumference of the ROS in a punctate manner. This led to the speculation that pcdh-21 is localized to the calycal process or the spaces in between them (Fig.1-2B). Calycal processes contain actin filaments and can be identified by staining with phalloidin. Phalloidin labeling appeared as dots that were uniformly spaced around the base of the ROS (Fig.2-5B, arrows). Pcdh-21 was not localized exclusively at the calycal processes, nor was it found exclusively in the spaces between them. Pcdh-21 labeled the ROS in a pattern suggestive of plasma membrane labeling (Fig.2-5B, arrows).

The faint, thin band labeling the base of ROS reflects pcdh-21 expression in a few nascent disks (Fig.2-4A, arrowhead). In a minority of rods, stacks of disks were labeled throughout the disk surface, showing a thick band labeling pattern. Most bands extended from the base (Fig.2-4C) or tip of the ROS (Fig.2-4D) and their thickness ranged from 2-18 $\mu$ m. This suggests that in a small number of rods, all disks synthesized for a period of some days expressed high levels of pcdh-21. However, on average, only ~1% of the rods exhibited this type of labeling, although this number varied significantly between animals. In transverse sections, in which epitopes are exposed to the disk surfaces and are equally accessible to antibody labeling, only a minority of rods were labeled in the disk surfaces (Fig.2-5C), similar to what we observed in labeling of longitudinal sections. Furthermore, labeling longitudinal sections with anti-C pcdh-21 antibody specific to the intracellular epitope produced identical labeling pattern. These results eliminated the possibility that the thick band labeling is an artifact caused by increased antibody accessibility in damaged OS (i.e. rods bisected by sectioning).

Our results showed that in *X.laevis*, pcdh-21 is localized to multiple regions of the ROS and is in distinct contrast with those previously reported in mice, where it is concentrated at the base of the ROS (Rattner, 2001).

### **2.3.3 Distribution of pcdh-21 in *X.laevis* cones**

Similar to our findings in rods, we observed that the base of the COS (Fig.2-6A, arrowhead) and CIS plasma membrane (Fig.2-6A, arrows) were labeled. Compared to adjacent rods, pcdh-21 labeling in cones was more intense, suggesting that pcdh-21 may be expressed at higher levels in cones than rods (Fig.2-6A).

A 3D reconstruction of serial optical sections demonstrated that pcdh-21 was localized exclusively at the COS rims (Fig.2-6B). Notably, pcdh-21 did not completely circumscribe the COS and exhibited a C-shaped labeling pattern (Fig.2-6B, arrows). Double-labeling with anti-acetylated-tubulin antibody, specific for the axoneme, showed that pcdh-21 was not localized to the rims adjacent to the axoneme. This suggests that pcdh-21 is only localized to the open rims of COS. The apparent labeling of disk surfaces in some cones (indicated in longitudinal sections (Fig.2-6A)) likely represent tangential imaging of the COS surface.

Occasionally, we observed bright spots of pcdh-21 labeling at the periphery of basal COS (Fig.2-6A, arrows). To confirm whether these spots were at the connecting cilium, a passage for exporting OS proteins synthesized in the IS (Fig.1-2A), transverse sections were double labeled with anti-acetylated tubulin antibody, a connecting cilium marker (Fig.2-6B). These spots of pcdh-21 colocalized with anti-acetylated tubulin labeling (Fig.2-6B, arrows), indicating that pcdh-21 was abundant at the connecting cilium. A timecourse analysis

(discussed more extensively in section 2.3.5), showed that pcdh-21 expression in cones was constant throughout the day (Fig.2-8B). We therefore speculated that these spots represent delivery of newly synthesized pcdh-21 to the COS, providing a continuous supply of pcdh-21.

Immunofluorescence studies of mouse cones showed that pcdh-21 is localized exclusively at the base of the OS (Rattner, 2001). This contrasts dramatically with our findings in *X.laevis*, where in addition to the basal COS, we observed pcdh-21 is also localized to open COS disk rims and CIS plasma membrane.

#### **2.3.4 Peptide competition assays for testing antibody specificities**

To verify labeling specificities, the anti-N- and anti-C-pcdh-21 antibodies were pre-incubated with their respective immunogenic peptides prior to immunolabeling (Fig.2-7). In the blocked sections, pcdh-21 labeling at the rod plasma membrane (Fig.2-7B, arrows; Fig.2-7D) and base of the ROS (Fig.2-7B, arrowheads; Fig.2-7D) were abolished. In sections labeled with the anti-N-pcdh-21 antibody, immunoreactivity was detected in the COS, although the intensity was substantially weaker (Fig.2-7B, asterisks). It is possible that pcdh-21 in tCOS is expressed at such high levels that more concentrated peptide would be required to completely inhibit the signal.

#### **2.3.5 Variation in pcdh-21 labeling intensity in *X.laevis* retinas during disk synthesis**

Pcdh-21 is thought to regulate disk synthesis in mice (Rattner, 2001; Rattner, 2004). We therefore hypothesized that pcdh-21 abundance in nascent disks might increase with disk synthesis rate, or alternatively, that pcdh-21 abundance at the base of the OS might increase with increased abundance of nascent disks. We sought to verify this hypothesis using *X.laevis*,

an amenable model for correlating protein expression and disk synthesis. In *X.laevis* rods, disk synthesis is stimulated upon light exposure and the synthesis rate varies in different phases of a standard light cycle (Besharse, 1977).

*X.laevis* tadpoles raised in diurnal cycles (12hrs light: 12hrs dark) were collected at five different timepoints when disk synthesis rate has been previously described as varying most dramatically (Fig.2-8A, red arrows) (Besharse, 1977). We imaged the entire retina and measured the number of rods with thin basal band labeling (Fig.2-8B). We frequently observed bands that only labeled 10-20% of the ROS width (Fig.2-8, C and D). To determine whether this is an artifact due to imaging of an oblique section or surface of the ROS, the entire depth of the ROS was imaged with serial optical sections. These “partial bands” did not always become bands that spanned the entire width of the ROS. For consistency of our analysis, only bands that spanned at least 90% of the ROS were measured.

Our results suggested that *pcdh-21* abundance at the basal ROS did not correlate with phase of light cycle, and consequently, with disk synthesis rate. First, we observed thin bands spanning the base of the ROS in retinas collected at 1am when almost no disks are synthesized (Fig.2-6B, arrows) (Besharse, 1977). Second, within a single retina, less than half of the rods were labeled at the basal ROS. It has been reported that younger cells at the peripheral retina have higher ROS renewal rate than more mature cells at the central retina (Kinney, 1978). However, rods that were labeled at the basal ROS were not found in greater numbers in the peripheral than central retina. Lastly, although the animals were raised under the same lighting condition, there was substantial variation between retinas collected at the same time, in terms of the width of the band and the number of ROS with thin basal band. In contrast to the variable labeling seen at the basal ROS, the ROS plasma membrane was

always uniformly labeled in all rods. In addition, pcdh-21 labeling in cones was uniform, with no obvious variation between day and night.

In summary, we did not observe any time-dependent variations in any pcdh-21 labeled ROS and COS structures, including the labeling intensity, band width and number of ROS with thin basal band.

### **2.3.6 Distribution of pcdh-21 in non-mammalian retinas**

Pcdh-21 distribution in *X.laevis* retinas differs from that reported in mice, in which pcdh-21 is exclusively at the base of the OS (Rattner, 2001). We thus set out to determine if localization to other regions of the OS is unique to non-mammalian retinas. Immunolabeling of *X.tropicalis* and zebrafish retinal sections with anti-N-pcdh-21 antibody showed that pcdh-21 localization was similar between *X.tropicalis* and *X.laevis* retinas. It was localized to the base of the ROS (Fig.2-9A, arrows) and rod plasma membrane (Fig.2-9A, arrowheads). In cones, pcdh-21 was localized to the disk rims (Fig.2-9B, arrowheads) and base of the COS (Fig. 2-9B, arrows). In adult zebrafish that have cone-dominant retinas, pcdh-21 was only detected in cones, where it was similarly present at the disk rims (Fig.2-9C, arrowheads) and base of the COS (Fig.2-9C, arrows). In conclusion, the distribution of pcdh-21 we observed in *X. laevis* retina is not unique to this species. In non-mammalian PR, pcdh-21 localization is not restricted to the base of the OS, but is also localized to the rod plasma membrane and cone disk rims. Differential localization in the two membrane domains of rods and cones is distinctive and has not been reported for any other OS protein.

### 2.3.7 Distribution of pcdh-21 in mammalian retinas

Our result of pcdh-21 localization in non-mammalian retinas is different from previous reports. Three possibilities may give rise to these differences. First, the epitopes used to generate the antibodies were different, and therefore the antibodies may have different sensitivities. Second, different procedures were employed for sample preparation that may alter antigenicity. Third, mice may have a pcdh-21 distribution that differs from fish and frog species. To rule out these possibilities, mouse retinal sections were labeled with antibodies used in previous studies in mice (Rattner, 2001; 2004). These antibodies recognized epitopes in the cytosolic C-terminus and first N-terminal cadherin domain of mouse pcdh-21. Immunolabeling was performed in parallel with antibody against the fourth cadherin domain of *X.laevis* pcdh-21, which cross reacts with the mouse homolog as demonstrated in immunoblot (Fig.2-3). For direct comparison, images were obtained using identical settings. Labeling with three different antibodies showed that in mice, pcdh-21 was most concentrated at the base of the OS (Fig.2-10). The intensity used to scan the sections labeled with the mouse specific antibody was too high for imaging the sections labeled with xpcdh-21 antibody. Signal at the base of the OS was saturated and background was observed in the IS (Fig.2-10C). When the same section was scanned at a lower intensity (Fig.2-11A), the image showed a similar signal to noise ratio as Fig.2-10A and B, suggesting that the antibody raised against xpcdh-21 is likely more sensitive. Antibody labeling was specific since signal at the base of the OS was abolished when antibody was preincubated with respective peptide (Fig.2-11B).

Thus, three antibodies generated against three different epitopes produced similar labeling patterns in mice, suggesting that exclusive pcdh-21 localization at the base of the OS

is not an artifact, and likely represents a distribution of pcdh-21 unique to mouse or to mammalian retinas. To verify this, we labeled pig retinal sections with the anti-N-pcdh-21 antibody raised against xpcdh-21. As observed in mouse retinas, pcdh-21 was greatly enriched at the base of the OS (Fig.2-12, arrowheads). In addition, weak immunoreactivity was detected in the apical OS (Fig.2-12; A,C, arrows). Due to the relatively small sizes of the PR, it is uncertain whether this labeling represents the plasma membrane or other structures of the apical OS.

In both mouse and pig retinal sections, we found that anti-pcdh-21 antibody also labeled one side of the basal OS (Fig.2-12; B,D, arrows). This labeling pattern was only observed occasionally in cells that were positioned closer to the outer nuclear layer, where cells were less densely packed, allowing us to more clearly visualize the basal OS.

Ultrastructural analysis of mouse rods has reported that pcdh-21 was concentrated at the rims opposite to the axoneme (Rattner, 2001). To determine whether our observation at the light microscopic level agrees with ultrastructural results, we double labeled mouse sections with anti-acetylated tubulin antibody. We found that in some cells, pcdh-21 is localized to the axonemal side of the OS (Fig.2-13B, arrows), which contradicts this previous report.

However, due to the thin diameter of the OS, we could not conclude its precise localization in some cells (Fig.2-13B, arrowhead).

### 2.3.8 Distribution of pcdh-21 in human photoreceptors

To examine pcdh-21 distribution in human rods, human retinal sections were labeled with anti-N-pcdh-21 antibody. Pcdh-21 was localized as a thin line spanning the base of the OS (Fig.2-14A, arrowhead). Occasionally, pcdh-21 was also localized to one side of the basal OS, in a pattern which extended from the base to ~30% of the length of the OS. In a minority of rods, pcdh-21 labeling was observed along almost the entire OS. In these cells, pcdh-21 labeling was more abundant at the basal ROS and was distributed along the distal ROS in discrete puncta (Fig.2-14B, arrows). In Fig.2-14B, the puncta labeled with anti-N-pcdh-21 antibody appeared to align with a subtle banding pattern of wheat germ agglutinin (WGA), which detects glycoproteins in the OS. This labeling pattern may reflect the periodicity of disk synthesis (Kaplan, 1982), suggesting that there may be a correlation between disk synthesis and pcdh-21 expression, although we failed to describe any such association in our timecourse analysis of *X.laevis* rods.

Double-labeling with anti-acetylated-tubulin antibody showed that pcdh-21 was localized adjacent to the axoneme, where disk synthesis begins (Fig.2-14C, arrows). Due to the resolution limit of light microscopy, we could not determine whether pcdh-21 is localized to the disk rims or plasma membrane of human rods. We speculate that pcdh-21 is likely to localize to the plasma membrane as observed in *X.laevis* rods. Labeling specificity was verified with antibody preadsorbed with their respective peptides (Fig.2-15).

In human cones (identified by anti-cone arrestin antibody) pcdh-21 was exclusively found at the base of the OS (Fig.2-14D arrows). In contrast to *X.laevis* cones, we did not observe labeling in the disk rims. Previous ultrastructural studies have reported that human cones consists of mostly closed disk rims that are not accessible to the extracellular matrix

except at the basal third of the OS, whereas *X.laevis* cones have open disks throughout the OS. We therefore speculate that this difference in pcdh-2 distribution may be related to the different distribution of open disks in cones of the two species.

In conclusion, similar to non-mammalian and other mammalian species, pcdh-21 in human rods was localized to the basal ROS. However, its localization at the distal ROS adjacent to the axoneme was not observed in other mammalian species and may be unique to humans or primates.

### **2.3.9 Localization of pcdh-21 in COS-7 cells**

Immunofluorescence of *X.laevis* retinal sections indicated that pcdh-21 is localized to the ROS plasma membrane. However, such localization is unclear in mice due to the thin diameter of their ROS. We therefore investigated pcdh-21 localization in COS-7 cells expressing either mpcdh-21 or xpcdh-21. We also compared their localization with rhodopsin that is distributed to the plasma membrane and disk surfaces of rods, and the plasma membrane of COS-7 cells. Pcdh-21 and rhodopsin were detected with antibodies against their extracellular (anti-N-pcdh-21, anti-rhodopsin B630N) or intracellular region (anti-rhodopsin 1D4), in the presence or absence of permeabilizing agent (TX-100). Cells were double labeled with WGA, which labels glycoproteins in the plasma membrane and therefore serves as a cell surface marker.

In permeabilized cells expressing rhodopsin (Fig.2-16; A,C), xpcdh-21 (Fig.2-16E) or mpcdh-21 (Fig.2-16G), the majority of the labeling was intracellular. Double labeling using ER markers, KDEL or calnexin, demonstrated that most of the rhodopsin (Fig.2-17A) and pcdh-21 (Fig.2-17; B,C) were localized to the ER, likely representing newly synthesized

proteins, or proteins prevented from ER exit due to quality control mechanisms. Due to their high expression in the cell body, it is difficult to conclude whether pcdh-21 and rhodopsin colocalized with WGA label in the plasma membrane. In a minority of cells, labeling in the cell processes (Fig.2-16; A,C,E,G arrows) was clearly evident.

In the absence of permeabilizing agent, ER labeling was reduced dramatically, enabling detection of proteins at the plasma membrane (Fig.2-16; B,D,F,H). Compared to cells expressing rhodopsin (Fig.2-16; B,D), labeling of xpcdh-21 (Fig.2-16F) and mpcdh-21 (Fig.2-16H) at the cell surface was weak. These results suggested that pcdh-21 was not efficiently transported to the plasma membrane. Cells expressing rhodopsin labeled with antibody against the intracellular epitope (1D4) also showed weak labeling at the cell surface (Fig.2-16D), indicating that a small degree of permeabilization occurred in the absence of detergent.

Double labeling using an ER marker and anti-N-pcdh-21 antibody showed different labeling patterns of xpcdh-21 (Fig. 2-18C) and mpcdh-21 (Fig. 2-18D) in the ER. Rhodopsin (Fig. 2-18B) and xpcdh-21 (Fig. 2-18C) were distributed diffusely in the ER. These cells had normal ER morphologies, in a pattern that is also typical of ER labeling of non-transfected cells (Fig. 2-18A). In contrast, mpcdh-21 was retained in the ER in a reticular manner and these cells had unusual ER morphologies (Fig. 2-18D). Similar localization and abnormal ER structures were observed in transgenic *X.laevis* overexpressing mpcdh-21 (Section 3.3.2, Fig. 3-5B, arrows). These results suggest that mpcdh-21 disrupted ER structures, and possibly induced ER stress.

## 2.4 Discussion

### 2.4.1 Differential pcdh-21 localization in rods and cones of the same species

We found that pcdh-21 localization is different in rods and cones of the same species (Fig.2-17). This was most evident in *X.laevis* and human retinas. In *X.laevis* rods, pcdh-21 labeling was most intense in the IS and OS plasma membrane, whereas in *X.laevis* cones, it labeled the open rims of cone disks. In human rods, it labeled the base and possibly the disk rims of OS, whereas in human cones, pcdh-21 was localized exclusively at the base of the OS. It is an unusual observation that this OS protein has different localizations in the two types of PR. The major OS proteins that have been identified so far have similar localizations in both rods and cones. For example, peripherin-2, rom-1 and ATP-binding cassette transporter (ABCA-4) are all found at the rims of mature rod disks as well as at the rims of cone disks (Arikawa, 1992; Moritz, 1996; Papermaster, 1982). To date, the only OS protein that shows similar differential localization is prom-1 (Han, 2012). In *X.laevis* retinas, prom-1 and pcdh-21 shows overlapping localization pattern at the base of the OS and cone disk rims (Han, 2012). Since the two proteins interact in mouse PR (Yang, 2008), it is likely that they also interact in *X.laevis* PR, leading to overlapping localization pattern.

As mentioned above, in contrast to most major OS proteins, which have similar localizations in both rods and cones, we observed that in *X.laevis*, pcdh-21 is differentially localized to the ROS plasma membrane and the open rims of COS opposite to the axoneme. This begs the question as to how pcdh-21 can be targeted to these distinct membrane domains. We propose that the non-axonemal side of COS rims may be analogous to ROS plasma membrane. It is not surprising that COS and ROS may share similar membrane domains since rods and cones shared a common ancestor (Lamb, 2007). After the divergence,

ROS developed a plasma membrane that was absent in COS. To verify this hypothesis of “membrane domain homology”, it may be interesting to determine whether cone homologs of other ROS plasma membrane proteins (eg. CNGC, Na<sup>+</sup>Ca<sup>2+</sup> exchanger) are localized to the non-axonemal side of COS rims.

#### **2.4.2 Pcdh-21 may be involved in maintaining open disk structure in *X.laevis***

Differential localization of pcdh-21 in *X.laevis* rods and cones may be related to ultrastructural differences between these cell types. One notable difference is the distribution of open disks along the OS, which appears to correlate with pcdh-21 expression level. We found that pcdh-21 expression is greatest in cones that are composed entirely of open disks. Pcdh-21 localization also correlates with the distribution of open disks. It is restricted to the open rims of cone disks and open basal rod disks (Fig.2-19).

In *X.laevis* retinas, pcdh-21 localization is in direct contrast to that of prph-2, which is localized to the closed rims of COS and ROS (Arikawa, 1992). Based on *in vitro* studies, prph-2 has been hypothesized to form closed rims by promoting fusion of adjacent disk membranes (Arikawa, 1992; Boesze-battaglia, 1997). Because of the contrasting localizations of pcdh-21 and prph-2 in both rods and cones, the two proteins may play opposing roles in disk synthesis. We therefore speculate that pcdh-21 may maintain the open disk structure by preventing membrane fusion. It has also been suggested that the prph-2 dimerization and oligomerization is responsible for adhering adjacent disk membranes, thereby forming disk rims that are closer together compared to those of open disks (Wrigley, 2000; Fetter & Corless, 1987). If pcdh-21 function is opposite to prph-2, pcdh-21 may be involved in maintaining the spaces between open disk membranes. Microsome studies have

demonstrated that expression of prph-2 is sufficient to induce membrane morphology characteristics of OS (Wrigely, 2000). It may be of interest to express pcdh-21 in vesicles and contrast changes in their membrane structure with those induced by prph-2 insertion.

Prom-1 is another protein that is thought to maintain open disk structure. Similar to pcdh-21, prom-1 and prph-2 reside in mutually exclusive domains in *X.laevis* cones (Han, 2012). If pcdh-21 and prom-1 form a complex in maintaining open disk structure, it provides a molecular explanation as to the origin of structural differences between rods and cones, a question that has been of great interest of PR cell biologists for years.

To address whether pcdh-21 is involved in maintaining open disks in other species, one can compare pcdh-21 localization in the COS of other species. Unlike *X.laevis* that have open disks along the COS, only the basal third disks and some of the distal disks of squirrel and mouse COS are open (Anderson, 1978). If this open disk distribution is similarly observed in humans, it may explain why pcdh-21 is only observed exclusively at the base of COS. These results may have implication in understanding whether open disks are present at the base of human ROS, where pcdh-21 labeled the width of basal ROS as a thin line. Interestingly, in human rods, pcdh-21 was also localized to the axonemal side where open disk rims are absent. Therefore, the axonemal localization of pcdh-21 is unlikely to be related to open disks.

#### **2.4.3 Conserved localization of pcdh-21 in basal OS support its role in disk synthesis**

In all species examined, pcdh-21 is localized to the nascent disks at the base of ROS and COS, suggesting that its role in disk synthesis is conserved. In mice, compared to other proteins that are essential for normal OS morphology, pcdh-21 is expressed earlier during

development when rods begin to differentiate (Rattner, 2001; Cook, 1989; Bascom, 1992; Liu, 2002). Moreover, pcdh-21 expression is restricted to the developing OS (Rattner, 2004). Previous studies hypothesized that disk synthesis occurring at the base of adult OS is equivalent to that which occurs in developing photoreceptors (Nilsson, 1964; Sung & Chuang, 2010). Examining the expression pattern of pcdh-21 in developing retinas of other species may be useful to confirm the role of pcdh-21 in disk synthesis.

If pcdh-21 regulates disk synthesis in all species, the results of this study demonstrating differential pcdh-21 localization in mammalian and non-mammalian species supports the hypothesis that the mechanisms of disk synthesis are not evolutionarily conserved (Sung, 2010). Two contradicting models of disk synthesis have been proposed by Steinberg (1980) and Chuang (2007). The evidence that gave rise to the Steinberg model is based on the presence of open disks at the base of the ROS, which have been interpreted as unfolding of the plasma membrane (Steinberg, 1980). In general, studies that support the presence of open disks were performed in frogs, however, these open disks were not observed in mice (Obata and Usukura, 1992; Chuang, 2007). In biochemical studies that test whether an extracellular dye is incorporated into ROS after the open disks are sealed off, inconsistent results have been reported in amphibians and mammalian retinas (Matsumoto and Besharse, 1985; Laties, 1976). Ultrastructural localization of pcdh-21 at the basal ROS of different species using electron microscopy or sub-resolution light microscopy will allow us to examine subtle differences in pcdh-21 distribution and correlate pcdh-21 localization with the distribution of open disk in these species.

Pcdh-21 labeling pattern in human rods may reflect the process of disk synthesis. At the most basal part of the ROS where the most nascent disks were found, pcdh-21 labeling

was most intense. Pcdh-21 was also localized to the axonemal side of the ROS, where disk synthesis is initiated (Steinberg, 1980). In the distal ROS where mature disks were found, weak and punctate labeling was detected. The puncta may result from disk remodeling during disk maturation. It is possible that in this process, pcdh-21 is degraded once it has completed its role in disk synthesis. Alternatively, pcdh-21 may be displaced by insertion of other OS structural proteins, such as prph-2. It is worth noting that the punctate labeling of pcdh-21 appeared to align with bands of WGA labeling with similar variations in intensity, which have been hypothesized to be related to altering periods of disk synthesis.

#### **2.4.4 Pcdh-21 likely performs species- and cell type-specific structural roles**

Pcdh-21 is differentially localized to other regions of ROS and COS across species, including disk rims, plasma membrane and structures adjacent to the axoneme, suggesting species and cell type specific structural roles. For example, we speculate that pcdh-21 is involved in maintaining open disk structures in *X.laevis* cones, as described in section 2.4.2.

Given that OS ultrastructure varies between species, pcdh-21 may be a component that is important for achieving the structural diversity between photoreceptors. Pcdh-21 is detected in distal regions of *X.laevis* and human ROS, but not mouse and pig ROS. At the ultrastructural level, human and *X.laevis* rods are similar that they both have multiple, deep incisures that surround the ROS, whereas mouse rods have a single, shallow incisure near the axoneme. In addition, mouse rods do not have distinct calycal process surrounding the basal ROS, as observed in *X.laevis* and higher primates (Cohen, 1960; Cohen, 1965).

Our data show that pcdh-21 localization in basal ROS is reversed in human and mouse. We found that in human, pcdh-21 is localized to disk rims near the axoneme, whereas

previous studies in mouse rods showed that pcdh-21 is concentrated to the rims opposite to the axoneme (Rattner, 2001). We speculate that the more intense labeling at the basal ROS in humans may be a result of its distinct disk ultrastructure. In rods of higher primates, at the basal ROS, one side of the disks seems to be displaced by the axoneme. Therefore, it may force pcdh-21 to cluster towards one region of the disks. This unique organization of the basal ROS has only been reported in human and monkey (Cohen, 1965). To confirm that the more intense labeling is due to this special organization at basal ROS, it may be of interest to examine pcdh-21 localization in monkey rods.

#### **2.4.5 Pcdh-21 abundance at the basal ROS does not increase with disk synthesis or open disks**

*X.laevis* is an ideal model organism for correlating pcdh-21 distribution with change in disk synthesis rate (Besharse, 1977). This question is difficult to address in mouse because light only has a minor effect in stimulating disk synthesis, comparing to *X.laevis* (Young, 1967). Furthermore, the presence of open disks is controversial in mouse rods (Chuang, 2007).

Ultrastructural studies have shown that *X.laevis* have open, nascent disks (Besharse, 1977). Based on our hypothesis that pcdh-21 and prom-1 together form a complex in maintaining open disks (section 2.4.2), we expect that pcdh-21 labeling will be greater at the base of ROS, as disk synthesis increases and more open disks are present. However, our immunofluorescence results did not indicate variation in thin basal band labeling. To test whether pcdh-21 abundance increases with the number of open disks, we can perform immunolabeling of ultrathin sections, which will allow us to determine whether pcdh-21 is

specifically associated with open disk rims and whether this labeling varies at different phases of the light cycle.

Previous studies have examined prom-1 abundance at the basal rod disks in *X.laevis* raised in cyclic light (Han, 2012). In the dark (4.30am) when no disk was synthesized, prom-1 was absent at the basal disks; whereas, in the day (4.30pm), prom-1 was more abundant at the basal disks. However, the authors reported great variations between animals which made the difference between timepoints statistically insignificant. Such variations were also observed in our analysis with pcdh-21. To determine circadian regulation of pcdh-21 and prom-1, semi-quantitative approaches, such as RT-PCR and western blots, may be useful. However, immunohistochemical studies suggest that pcdh-21 and prom-1 are expressed at much higher levels in cones. As a result, they may not truly reflect the circadian regulation of pcdh-21 and prom-1 in rods.

In contrast to the weak and heterogeneous expression at the base of the ROS, labeling intensity was much higher in ROS plasma membrane and was observed in all rods. This may imply that in *X.laevis* rods, pcdh-21 may have other roles in addition to disk synthesis.

#### **2.4.6 Xpcdh-21 and mpcdh-21 have different localizations and effects**

Xpcdh-21 and mpcdh-21 are different in various aspects: (1) Cleavage of pcdh-21 is likely unique to mouse retinas. (2) Overexpression of mpcdh-21, but not xpcdh-21, in PR and cultured cells resulted in ER abnormalities. (3) Xpcdh-21 and mpcdh-21 are localized differently in cultured cells and PR.

Given their differences in primary sequences, it is possible that the two homologs adopt different conformations and/or interact with different proteins. Immunoblot analysis of

retinal lysates showed that xpcdh-21 has lower molecular mass compared to mpcdh-21. Treatment of retinal lysates with enzymes that remove glycosylation and phosphorylation will allow us to determine whether the shift is a result of post-translational modifications. However, this difference in molecular mass was not observed in COS-7 cell lysates, suggesting that pcdh-21 expressed in COS-7 cells and retinas are processed differently.

#### **2.4.7 Pcdh-21 cleavage is not conserved across species**

Pcdh-21 has been shown to be cleaved in mouse and bovine retinas (Rattner, 2004). In two strains of transgenic mice with abnormal disks, pcdh-21 cleavage is impaired, leading to accumulation of full length pcdh-21 (Yang, 2008; Rattner, 2004). This phenotype led to the hypothesis that pcdh-21 cleavage is essential for normal OS structure.

To determine the significance of pcdh-21 cleavage in disk synthesis, it is important to identify the enzyme that is responsible for this cleavage. One candidate enzyme is a member of a Disintegrin and Metalloprotease (ADAM) family, which is a zinc dependent metalloprotease that cleaves other cadherin family members at the last cadherin domain, similar to the observed cleavage of pcdh-21 (Reiss, 2005; Scholz, 2005; Satfig, 2008). Matrix metalloprotease is another enzyme that cleaves many transmembrane proteins at the extracellular domain (Rattner, 2004; Arribas & Borroto, 2002).

Identifying the cleavage enzyme is useful in defining the function of pcdh-21 cleavage on disk synthesis. Theoretically, it would be possible to inhibit cleavage by applying a protease inhibitor or by knocking down the enzyme with siRNA. Furthermore, it would help to determine if some species lack the enzyme or co-factors required for this cleavage and as a result, pcdh-21 is not cleaved in these species, or alternatively, whether

differential processing of pcdh-21 may be related to disk ultrastructural differences between species. It may be interesting to determine whether different species have other mechanisms to compensate for functions performed by pcdh-21 cleavage.

Following pcdh-21 cleavage, a soluble N-terminal fragment and membrane associated C-terminal fragment were generated (Rattner, 2004). Understanding the fate of the N-terminal fragment is crucial for understanding whether pcdh-21 is cleaved across species. Immunostaining of mouse retinal sections using the anti-N-pcdh-21 antibody only detected pcdh-21 at the base OS, rather than throughout the retina, as expected for a soluble protein (Rattner, 2001). It is therefore possible that the N-terminal fragment is degraded following cleavage and the degradation rate may vary between species. A pulse-chase experiment involving incubating cultured cells with radioactive amino acids can be performed to study the rate of pcdh-21 cleavage and half-life of the N-terminal fragment. Culture media that likely contain the released N-terminal fragments can then be analyzed with immunoblot analyses. However, studying pcdh-21 cleavage *in vitro* will require expression in cell lines that are capable of cleaving pcdh-21, such as PR derived cell lines or cells cotransfected with the candidate enzyme. Another approach to verify pcdh-21 cleavage across species is to generate a C-terminal antibody that detects the membrane associated C-terminal fragment.

Although the predicted pcdh-21 cleavage site is highly conserved between mouse and *X.laevis*, our results showed that pcdh-21 cleavage is unique to mouse retinas (Rattner, 2004). We speculate that pcdh-21 cleavage may be specific to rods. Therefore, cleavage may not be detected in species with greater number of cones, such as *X.laevis*. However, we also did not observe cleavage in pig retinas, which have a similar rod to cone ratio as mice. Furthermore, one can take advantage of a strain of transgenic mice with cone dominant retinas (Daniele,

2005). We hypothesize that these mice will have lower levels of cleaved fragments than normal mouse retinas.

Previous studies have found that the ratio of C-terminal fragment: full length pcdh-21 produced after cleavage was significantly higher in bovine OS than mouse retina (Rattner, 2004). If the level of cleavage differs between these two closely related mammalian species, it is not entirely surprising that in *X.laevis* retina, pcdh-21 was not cleaved or the level of cleavage occurred at such low levels that the cleaved fragments were undetectable by our assay.

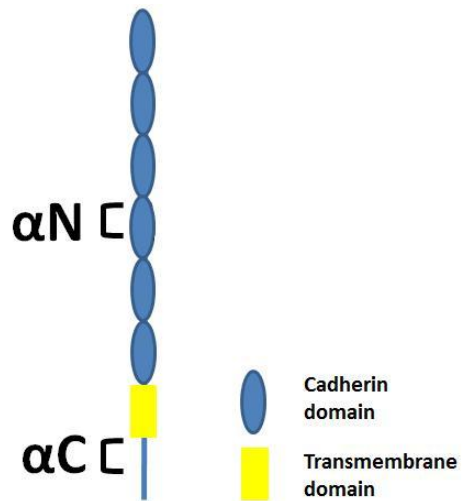


**Figure 2-1. Epitopes recognized by the anti-N and anti-C-pcdh-21 antibodies.**

The locations of the peptides N- (CYGENGPQNR FELTMYEH; amino acid 358-374) and C-terminus (CQEMESGPKNENRNN; amino acid 776-789) used to generate anti-pcdh-21 antibodies are indicated.

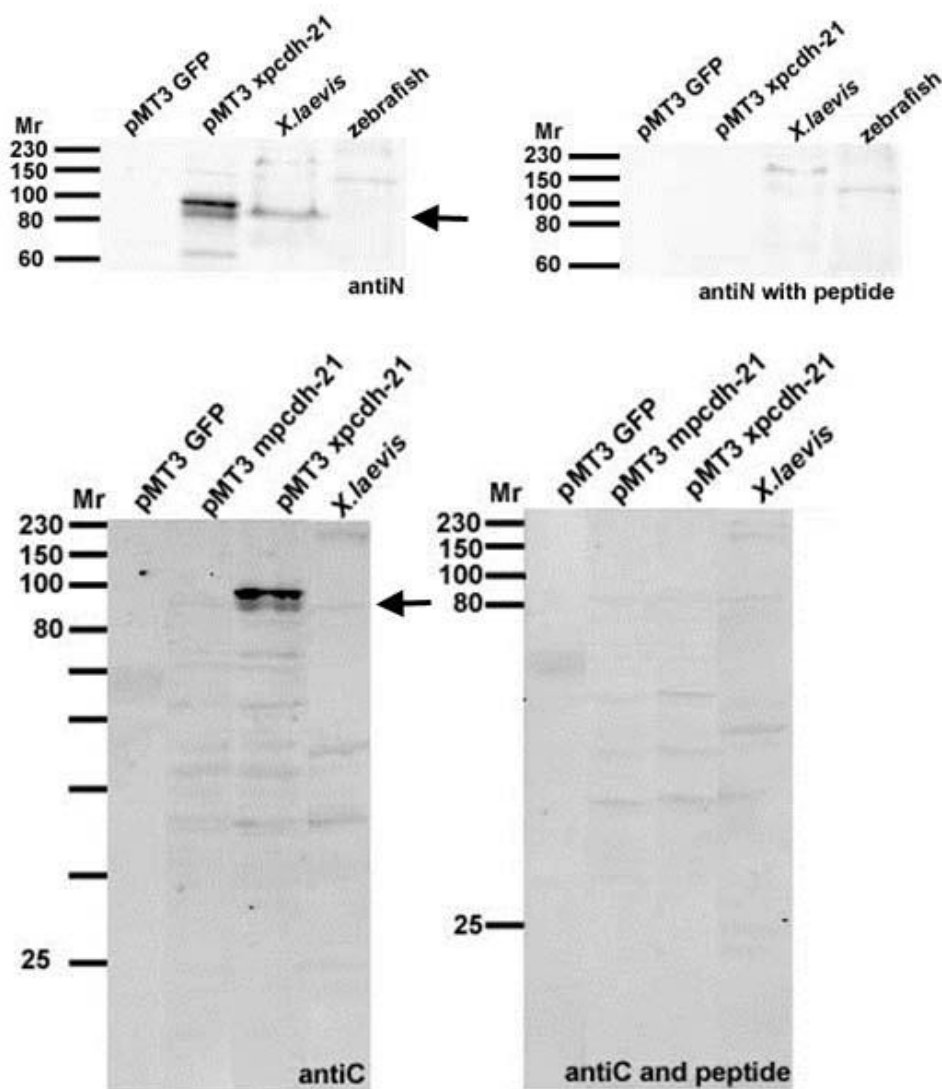


**Figure 2-2. Immunoblot of extracts from transfected cells and non-mammalian retinas probed with anti-N-and anti-C-pcdh-21 antibodies (left). Peptide competition assays for testing antibody specificities (right).**

For blots probing with the same antibody, equal volumes of identical samples were loaded and immunoblotting were performed in parallel. (Left) Both anti-N and anti-C-pcdh-21 antibodies detected two intense bands at ~100kDa and ~90kDa (arrow) in xpcdh-21 transfected cell lysate. Only the ~90kDa band was observed in *X.laevis* retinal lysate using the anti-N-pcdh-21 antibody. Xpcdh-21 was not detected in *X.laevis* retinal lysate using the anti-C-pcdh-21 antibody. The predicted ~25kDa cleaved fragments were not detected in xpcdh-21 transfected cells. (Right) Antibody specificities were verified using antibody preincubated with corresponding peptide. All bands were blocked except for a faint high molecular weight band at ~200kDa in *X.laevis* retinal lysate and ~150kDa in zebrafish retinal lysate.

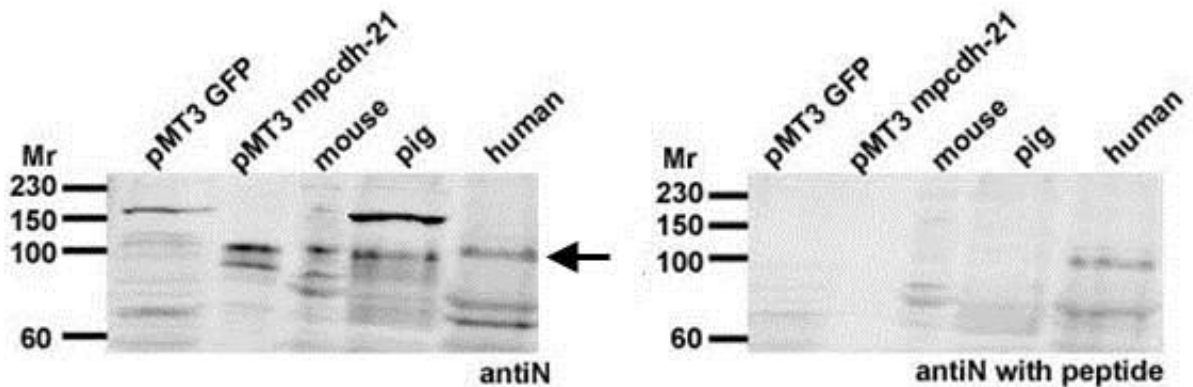


**Figure 2-3. Immunoblot of extracts from transfected cells and mammalian retinas, probed with anti-N-pcdh-21 antibody (left) or antibody incubated with peptide (right).** Equal volumes of identical samples were loaded and immunoblotting were performed in parallel. (Left) In mpcdh-21 transfected cell lysate, two bands at ~100kDa (arrow) and ~90kDa were detected. These bands, in addition to a ~80kDa band, were observed in mouse retinal lysate. Of these bands, only the ~100kDa band was observed in pig and human retinal lysate. (Right) Antibody specificities were verified using antibody preincubated with corresponding peptide. The anti-N-pcdh-21 antibody incubated with peptide did not detect any band in mpcdh-21 transfected cell lysate. The ~100kDa band observed in retinal lysates of all species was inhibited, except in human retina. The ~90kDa and ~80kDa bands were not inhibited in mouse retinal lysate.

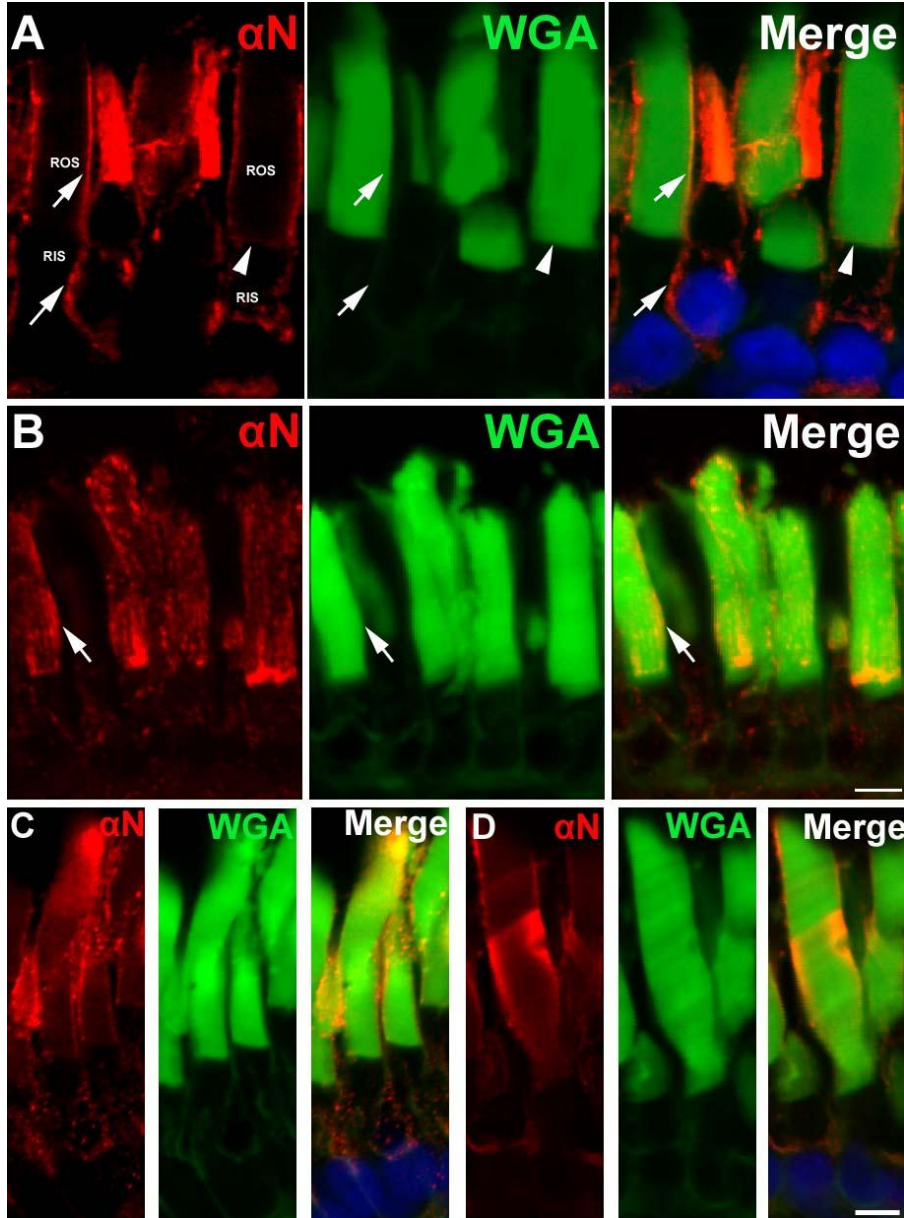


**Figure 2-4. Pcdh-21 localization in longitudinal sections of *X.laevis* photoreceptors labeled with anti-N-pcdh-21 antibody.**

(A) Pcdh-21 was localized to the plasma membrane of ROS and RIS (arrow). The base of the ROS was also labeled as a thin band (arrowhead). Image was contrast-enhanced to show labeling at the basal ROS. (B) A Z-series projection indicated that low levels of pcdh-21 were found in the ROS, exhibiting a striated labeling pattern (arrows). (C-D) In a minority of rods, pcdh-21 was expressed in the disk surfaces at the distal (C) or basal OS (D). Scale bar=5 $\mu$ m.

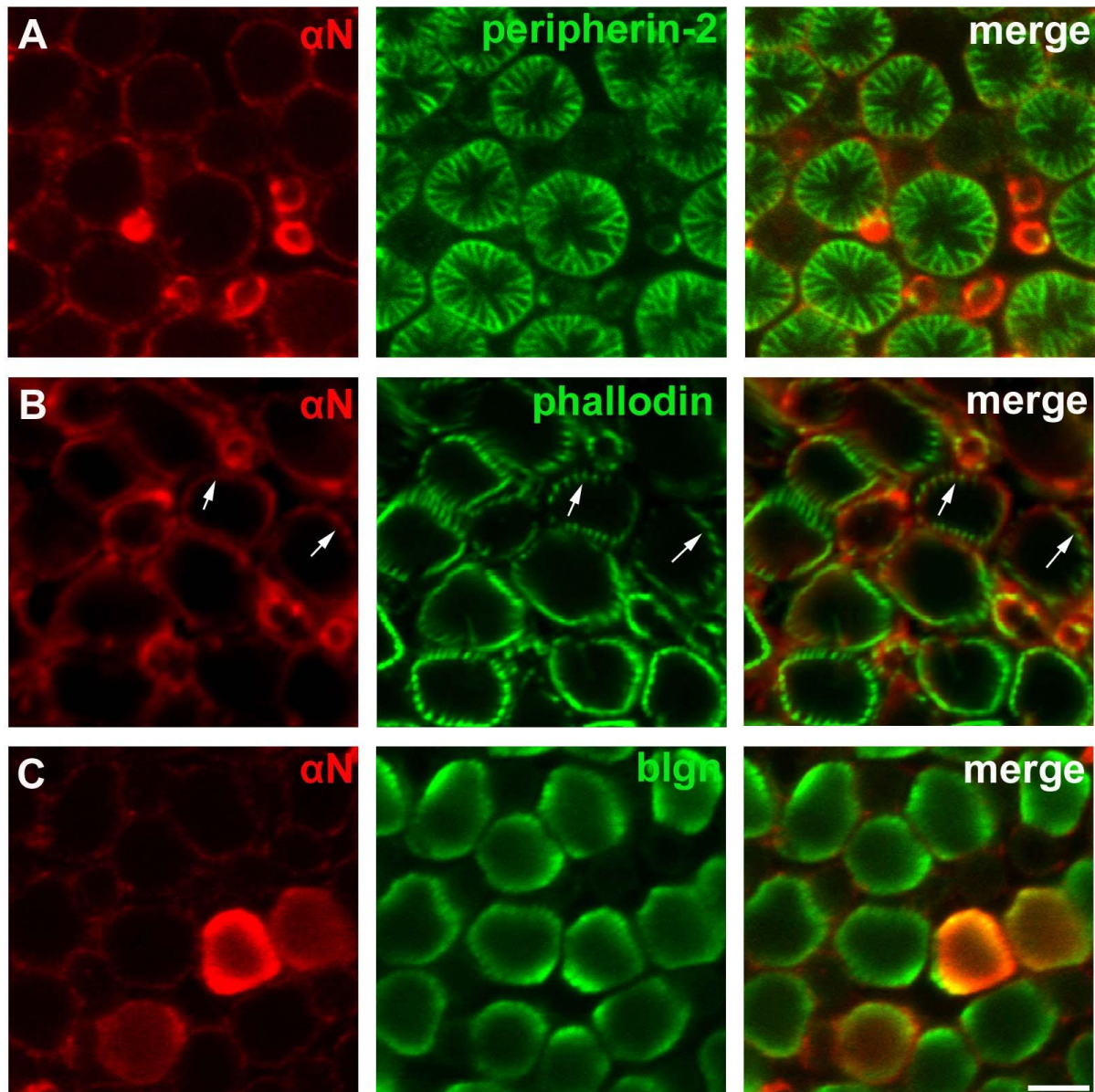


**Figure 2-5. Pcdh-21 localization in cross sections of *X.laevis* photoreceptors.**

Sections were double labeled with anti-N-pcdh-21 antibody and anti-peripherin-2 (5A11) (A), phalloidin (B) or anti-opsin antibody (blgn) (C). (A) Pcdh-21 did not colocalize with peripherin-2 in the incisures. Note the punctate labeling of pcdh-21 at the circumference of the ROS. (B) Phalloidin recognizes actin filaments in the calycal process. It appeared as dots surrounding the ROS at the inner and outer segment junction (arrows). Pcdh-21 antibody labeled the ROS as a continuous line (arrows). It did not colocalize exclusively with phalloidin, nor was it found exclusively in the spaces between them. (C) In a few rods labeled with anti-rod opsin antibody (blgn), pcdh-21 was localized to the disk surfaces. Scale bar=5 $\mu$ m.

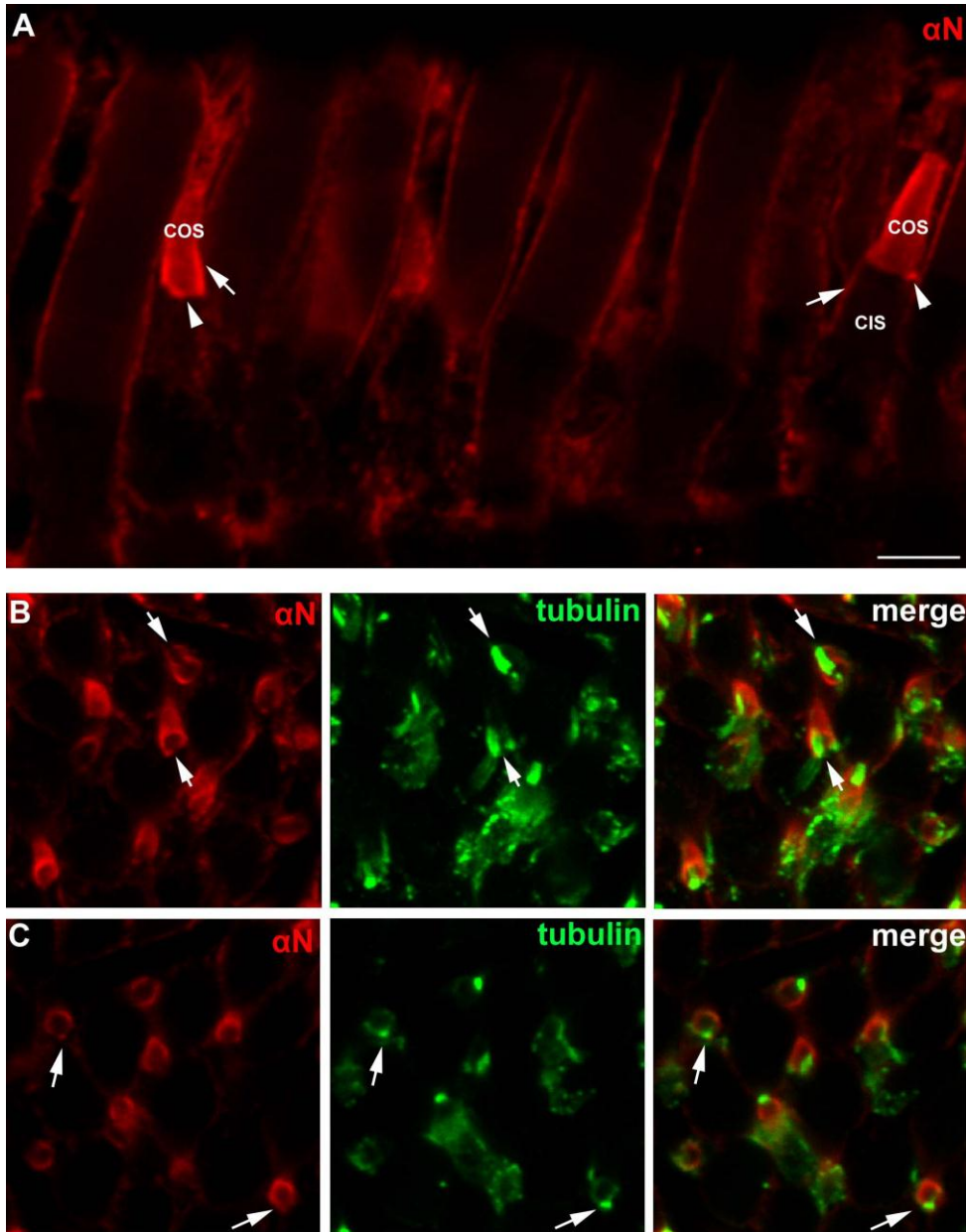


**Figure 2-6. Pcdh-21 localization in longitudinal (A) and cross sections (B-C) of *X.laevis* photoreceptors.**

(A) Pcdh-21 localized to the base (left, arrowhead) and rims of COS (left, arrow). It was also found at the CIS plasma membrane (right, arrow). Bright spots of pcdh-21 were localized to the periphery of basal COS (right, arrowhead). Labeling in COS was more intense than neighboring rods. (B-C) Cross sections double labeled with anti-acetylated-tubulin antibody, a marker for the axoneme and connecting cilium. (B) A Z-series projection showed that pcdh-21 was localized to the COS rims except at the rims adjacent to the axoneme (arrows). (C) In a few cones, bright spots of pcdh-21 attached to COS rims were observed. These bright spots colocalized with anti-acetylated tubulin labeling (arrows). Scale bar=5 $\mu$ m.

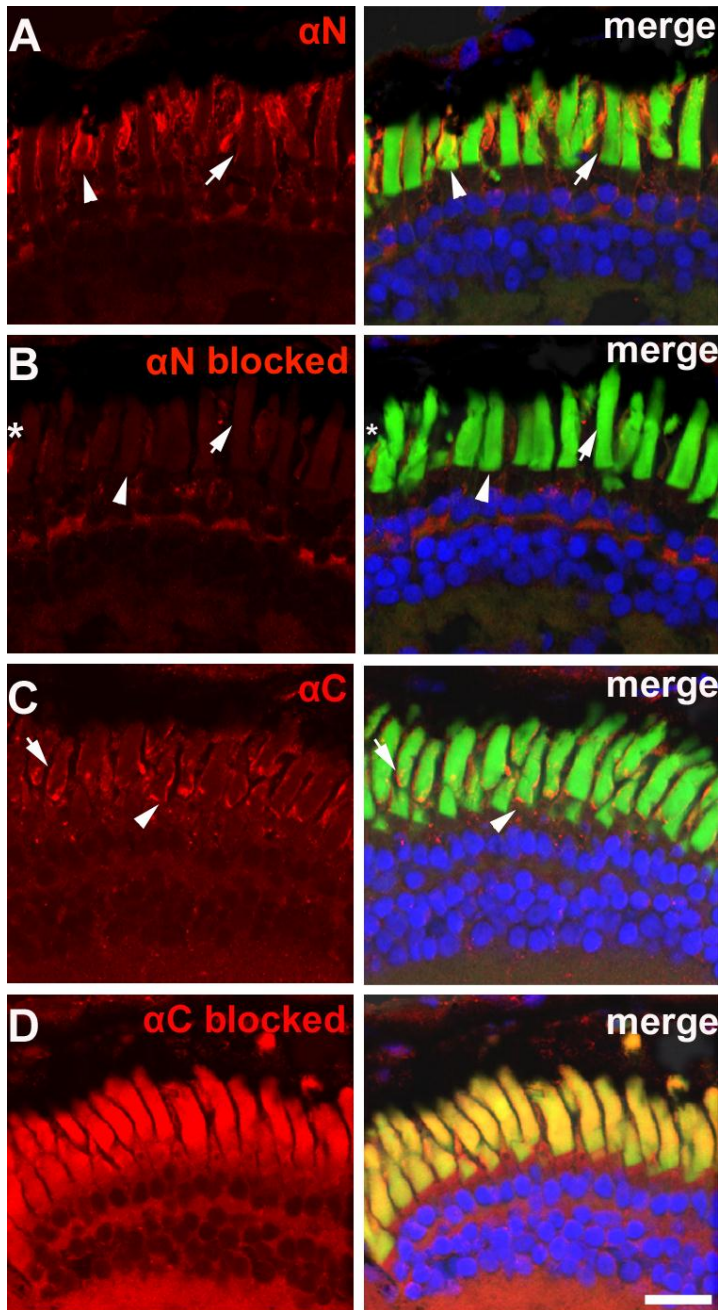


**Figure 2-7. Peptide competition confirmed the specificities of anti-N (A-B) and anti-C-pcdh-21 antibodies (C-D).**

Prior to immunolabeling of *X.laevis* retinal sections, antibodies were preincubated with peptides used to generate the antibodies (B, D). For comparison, images of unblocked sections taken with identical settings were shown (A, C). (B) In the blocked sections, anti-N-pcdh-21 labeling at the ROS plasma membrane (arrows) and basal ROS (arrowhead) were abolished. In addition, labeling of the COS was significantly weaker (asterisk). (D) No rods or cones were labeled when anti-C-pcdh-21 antibodies were preincubated with their respective peptide. Scale bar=20 $\mu$ m. Green=wheat germ agglutinin.

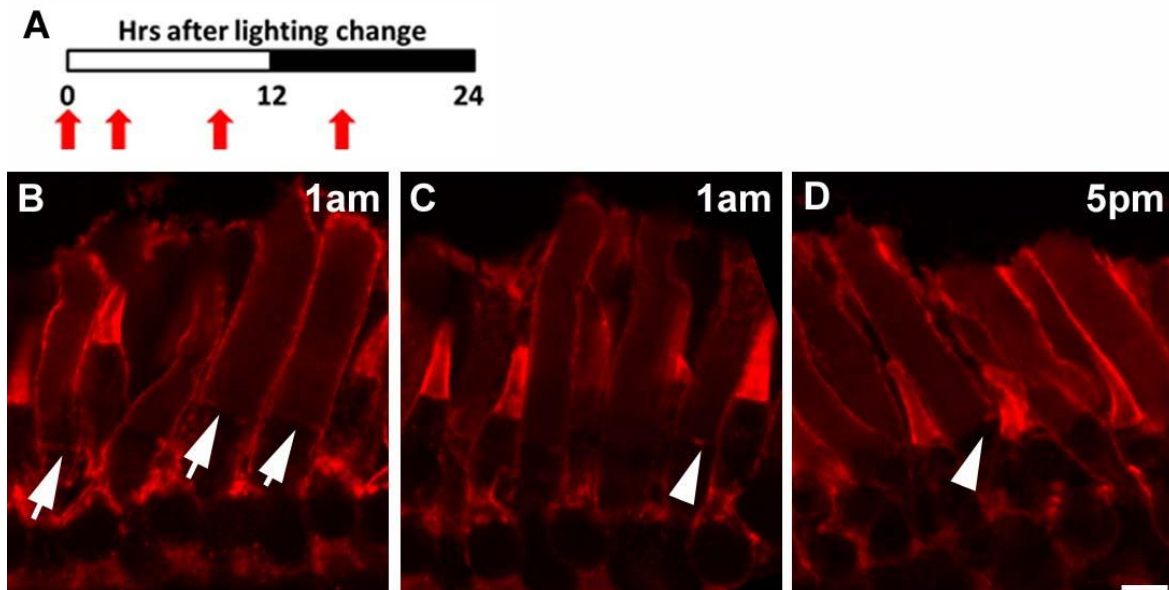


**Figure 2-8. Analysis of pcdh-21 expression at the basal ROS over a diurnal cycle.**

(A) *X.laevis* tadpoles raised in diurnal cycles were collected after 0, 2, 8 hrs of light exposure and 4hrs in the dark (red arrows). Unfilled and shaded region indicate periods in light and dark cycle, respectively. (B-D) Confocal images showing pcdh-21 localization in retinas collected at 1am (B-C) and 5pm (D). In some rods, pcdh-21 labeled the basal ROS as a faint, thin band (B, arrows). In a few rods, only the centre (C, arrowheads) or periphery (D, arrowheads) of basal ROS was labeled. No obvious difference was observed between retinas collected during the day or at night. Note that pcdh-21 was detected in plasma membrane of all rods and labeling intensity is greater in cones than rods. Scale bar=5 $\mu$ m.

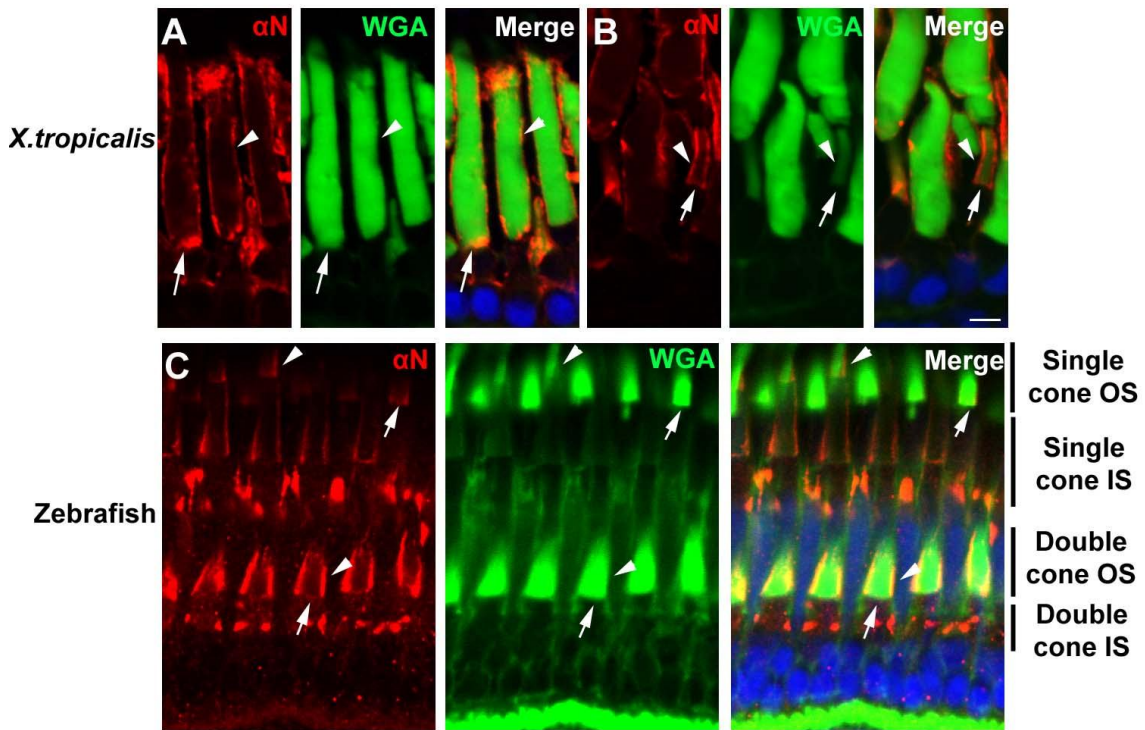


**Figure 2-9. Pcdh-21 localization in *X. tropicalis* and zebrafish retinas.**

In *X. tropicalis* rods (A), pcdh-21 was detected at the base (arrows) and plasma membrane (arrowheads). In *X. tropicalis* cones (B) and adult zebrafish cones (C), pcdh-21 was found in the disk rims (arrowheads) and base of the COS (arrows). Pcdh-21 was localized to the inner segment plasma membrane of zebrafish single cones, but not in the double cones. Pcdh-21 did not appear to express in zebrafish rods. OS=outer segment. IS= inner segment. ONL=outer nuclear layer. Scale bar=5µm.

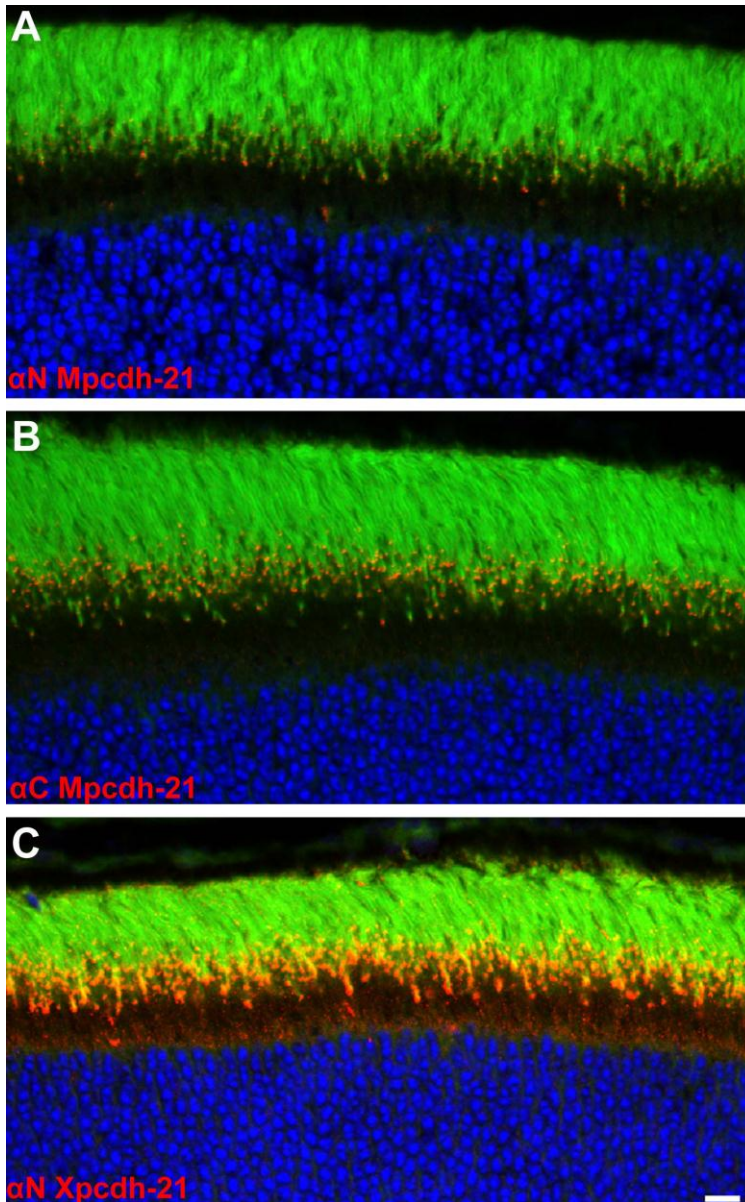


**Figure 2-10. Mouse retinal sections immunolabeled with antibodies against mouse pcdh-21 (A-B) and *X.laevis* pcdh-21(C).**

(A-B) Labeling with anti-N- (A) and anti-C terminus (B) of mpcdh-21 showed that pdh-21 was concentrated at the base of the OS, (C) Labeling with antibody against the N-terminus of *X.laevis* pcdh-21. Section was scanned at the same intensity as Fig.2-10A and B. Signal at the base of the OS was saturated with weak labeling in the IS. Green=WGA; Blue=DAPI. Scale bar=10 $\mu$ m.

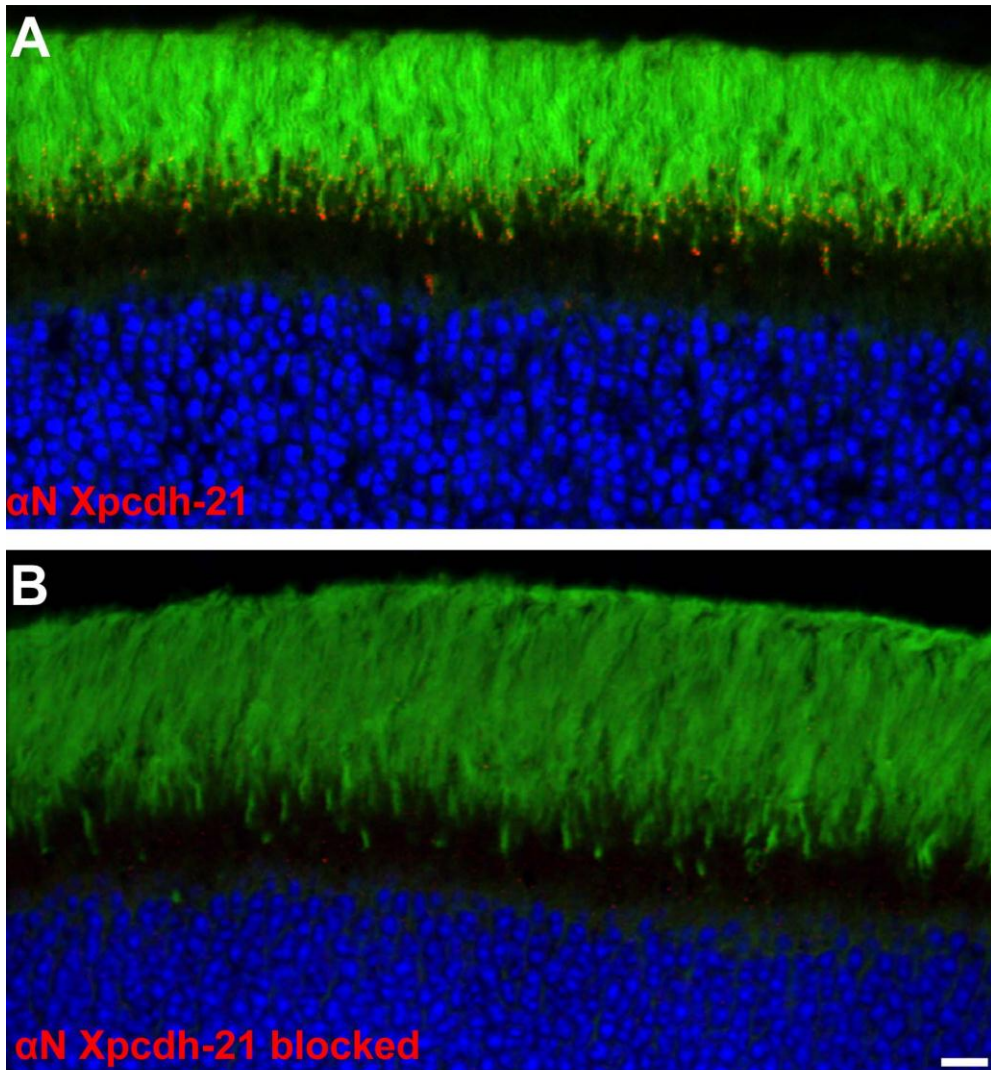


**Figure 2-11. Verification of anti-N xpcdh-21 antibody labeling specificity in mouse retinal sections.**

(A) Sections scanned at a lower intensity compared to Fig.2-10C. Labeling at the base of the OS was weaker and no signal was detected in the IS. (B) Blocked section imaged with the same settings as (A). No signal was detected at the base of the OS. Green=WGA; Blue=DAPI. Scale bar=10 $\mu$ m.

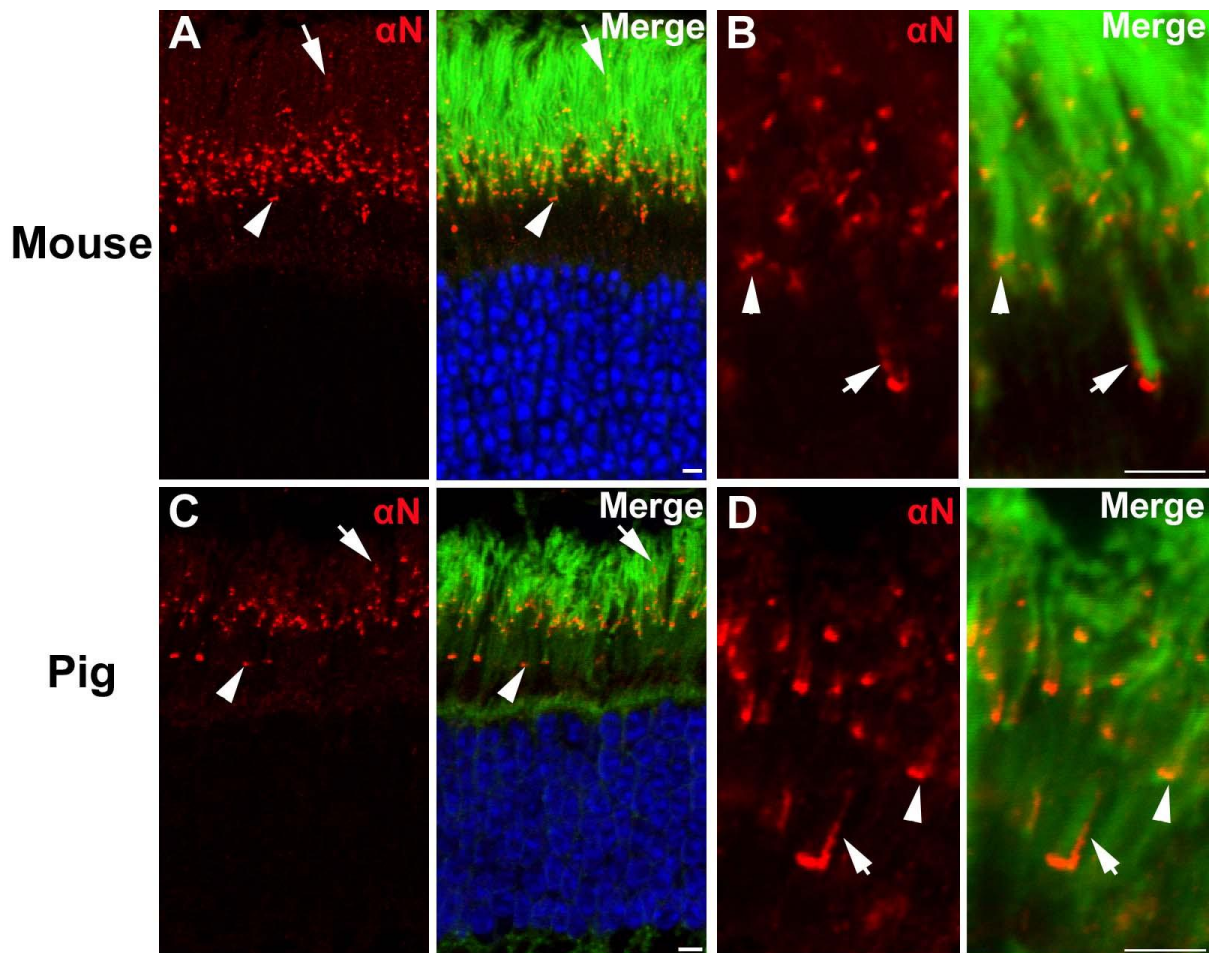


**Figure 2-12. Mouse and pig retinal sections double labeled with WGA and anti-N-xpcdh-21.**

In mouse (A-B) and pig (C-D) retinas, pcdh-21 labeling was most intense at the base of the OS (arrowheads) and weak labeling was detected in the distal part of the OS (arrows). **(B-D) Higher magnification of mouse and pig retinas.** At the base of the OS, pcdh-21 labeled the basal ROS as a thin line (arrowhead) In a minority of rods, the basal half of the ROS at one side, exhibiting a L-shaped labeling pattern. High magnification of the rods are shown to illustrate the. Scale bar=5 $\mu$ m.

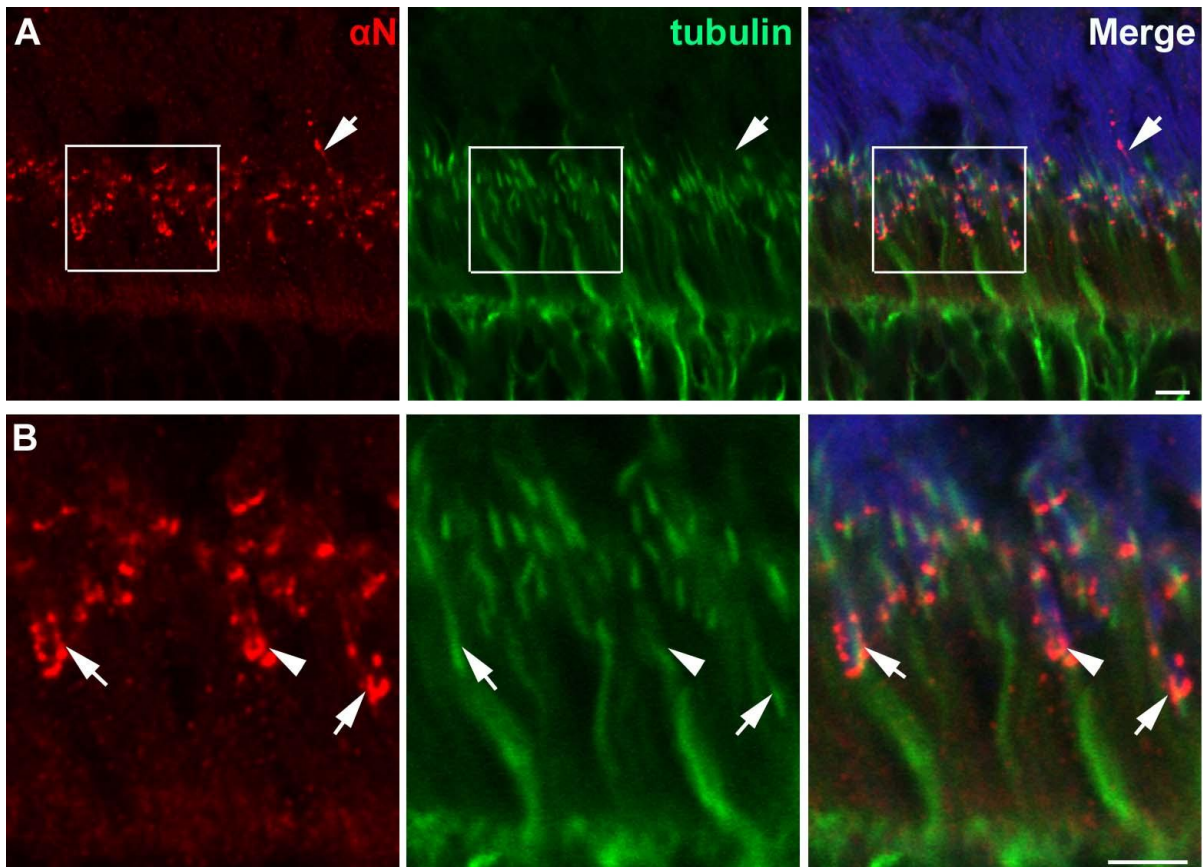


**Figure 2-13. Mouse retinal sections labeled with anti-N-pcdh-21, anti-acetylated tubulin antibody and wheat germ agglutinin.**

(A) Tubulin labeling is most intense at the inner and outer segment junction. Axoneme in the OS was not detectable. Note that pcdh-21 was detected in the distal part of the OS (arrows). (B) **Higher magnification of the boxed region in (A).** In some cells, pcdh-21 appeared to localize to the axonemal side of the OS (arrows). Due to the thin diameter of the OS, the precise localization of pcdh-21 was not clear in other cells (arrowhead). Blue=WGA. Scale bar=5 $\mu$ m.

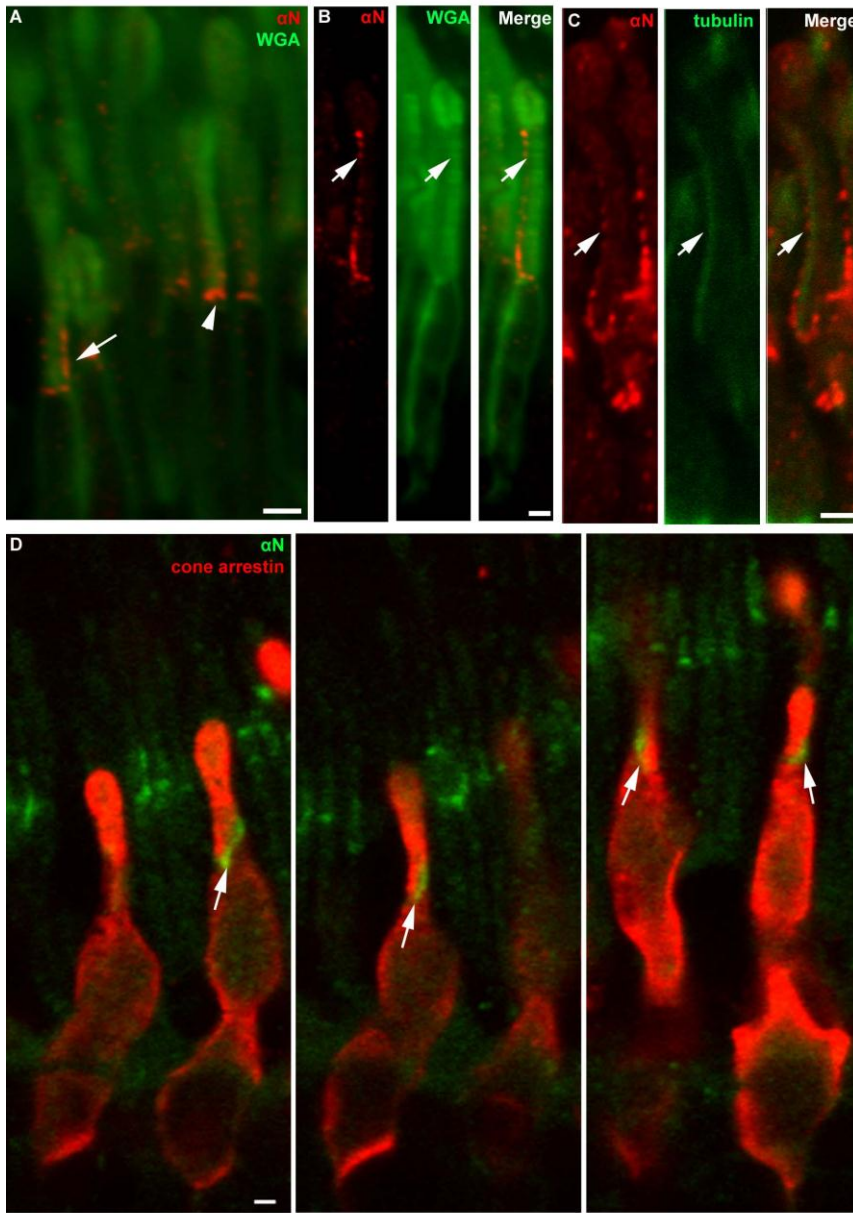


**Figure 2-14. Longitudinal sections of human retinas were double labeled with anti-N-pcdh-21 and WGA (A-B) or anti-acetylated- $\alpha$ -tubulin (C) or anti-cone arrestin 7G6 (D).** (A-B) Double-labeling of anti-N-pcdh-21 antibody and WGA showed that most rods were labeled as a thin line spanning the base of the ROS (A, arrowhead). Pcdh-21 was localized along one side of the ROS, spanning 30% (A, arrows) to 90% (B, arrows) of the ROS length. The labeling was most intense at the base of the ROS and was localized in a particulate manner in the distal ROS (B, arrows). (C) Double-labeling of anti-N-pcdh-21 and anti-acetylated-tubulin antibodies revealed that pcdh-21 was adjacent to the axoneme (arrows). (D) Double labeling of anti-cone-arrestin 7G6 and anti-N-pcdh-21 antibodies demonstrated that pcdh-21 was localized exclusively at the base of the COS (arrows). Scale bar=2 $\mu$ m.

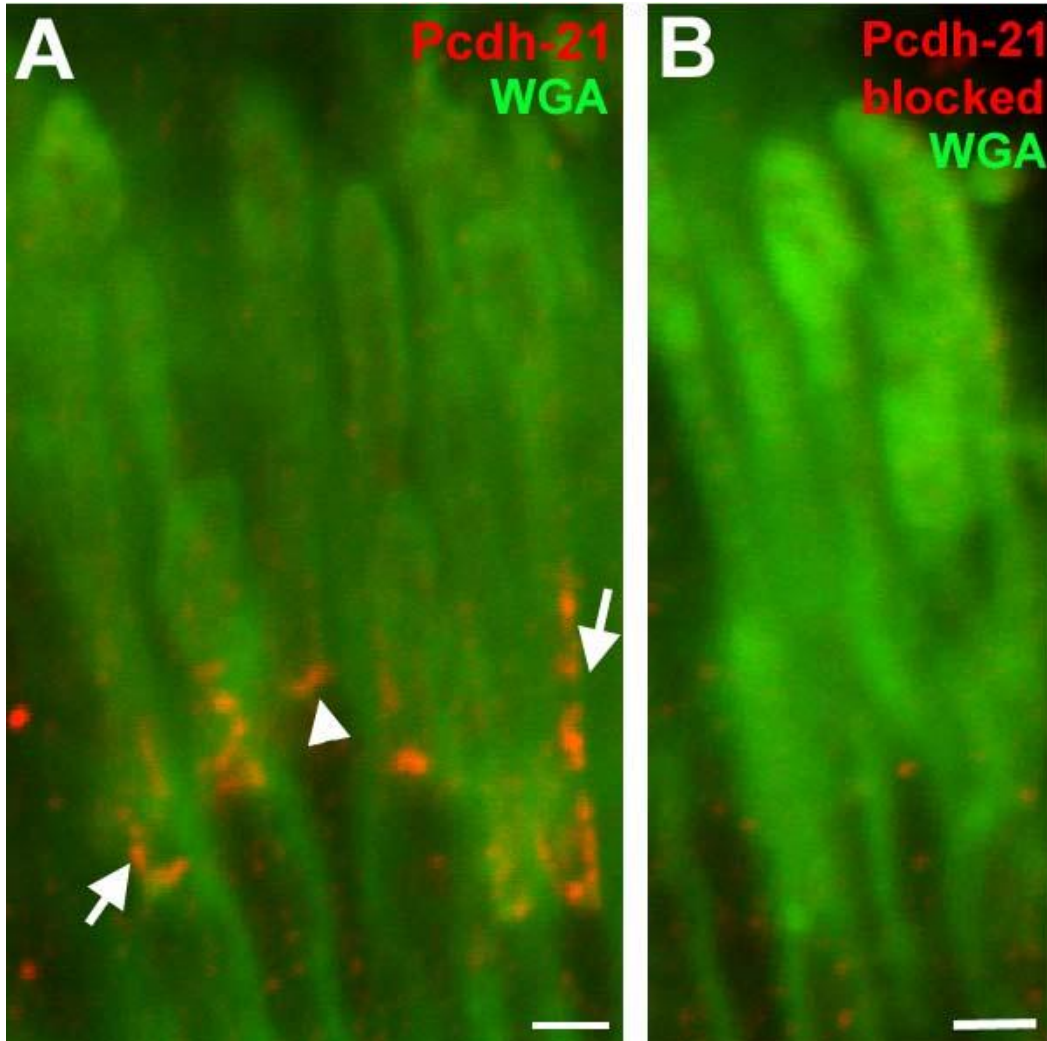


**Figure 2-15. Verification of pcdh-21 antibody labeling specificity in human retinal sections.**

(A) Pcdh-21 labeled the base (arrowhead) and along one side of the ROS (arrows). (B) Labeling at these sites was abolished when antibody was preadsorbed with peptide. Weak background labeling was observed in the inner segment. Scale bar=2 $\mu$ m.

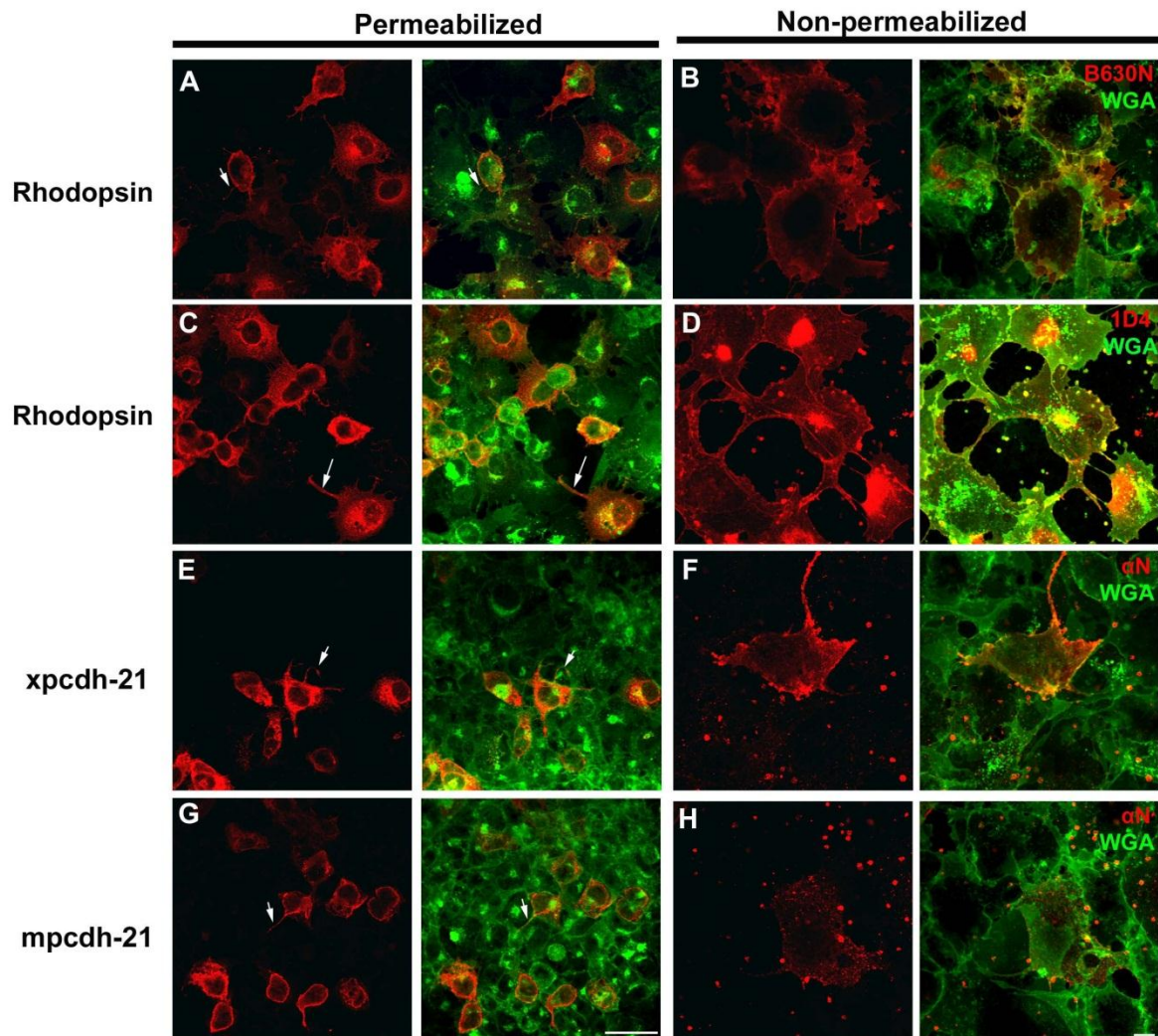


**Figure 2-16. Localization of rhodopsin, xpcdh-21 and mpcdh-21 in permeabilized (left) and non-permeabilized (right) COS-7 cells.**

Transiently transfected cells expressing rhodopsin (A-D), xpcdh-21 (E-F) and mpcdh-21 (G-H) were labeled with anti-rhodopsin (B630N or 1D4) or anti-N-pcdh-21 antibodies in the presence or absence of detergent. Cells were also double-labeled with WGA, a cell surface marker. (Left) In permeabilized cells, the majority of rhodopsin, xpcdh-21 and mpcdh-21 were found in the cytoplasm and they rarely colocalized with WGA. Occasionally, rhodopsin, xpcdh-21 and mpcdh-21 were present in the cell processes (arrows). (Right) In non-permeabilized cells, labeling in the cytoplasm decreased dramatically. Expression in the cell surface was observed in cells expressing rhodopsin and xpcdh-21, but was markedly lower in cells expressing mpcdh-21. Scale bar A,C,E,G=50 $\mu$ m. Scale bar B,D,F,H=10 $\mu$ m.

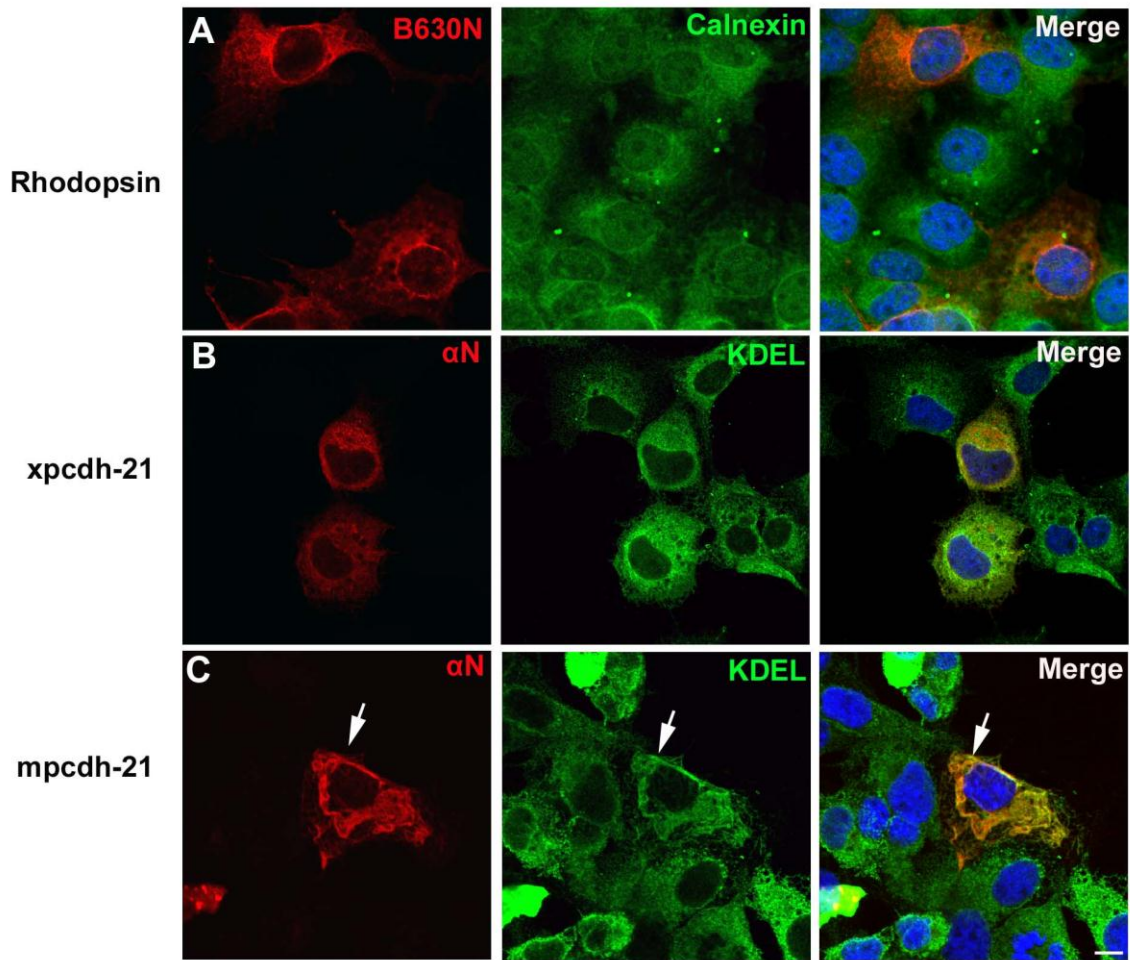


**Figure 2-17. Localization of rhodopsin, xpcdh-21 and mpcdh-21 in the ER of COS-7 cells.**

Transiently transfected cells expressing rhodopsin (A), xpcdh-21 (B) and mpcdh-21 (C) were double-labeled with ER-markers, anti-calnexin (A) or anti-KDEL (B-C), and anti-rhodopsin (B630N) or anti-N-pcdh-21 antibodies. Rhodopsin, xpcdh-21 and mpcdh-21 (arrows) in the cytoplasm colocalized with ER markers. Scale bar=10μm.

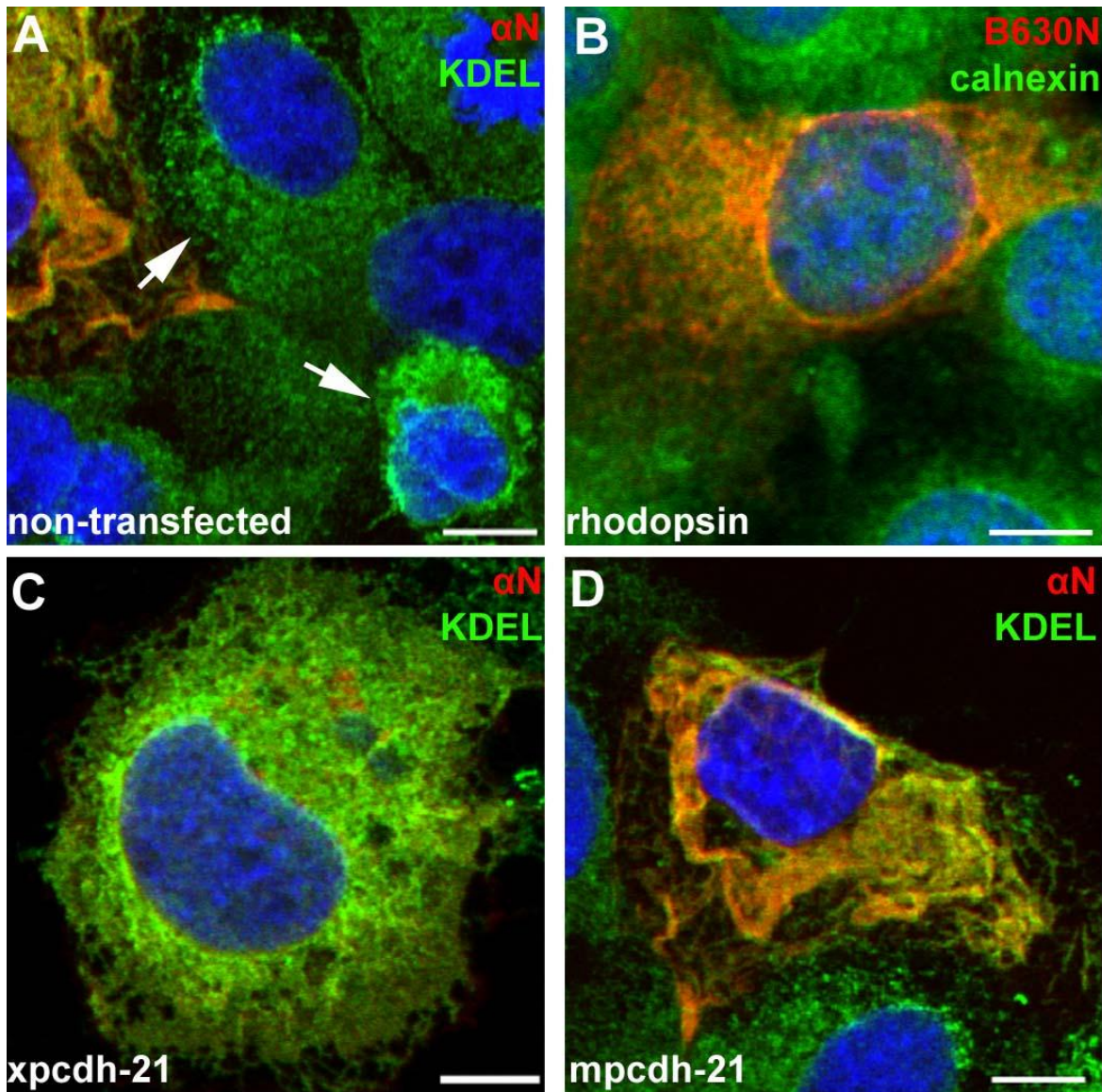


**Figure 2-18. ER morphologies of non-transfected cells (A) and cells expressing rhodopsin (B), xpcdh-21 (C) or mpcdh-21 (D).**

Non-transfected cells (A, arrows), transiently transfected cells expressing rhodopsin (B), xpcdh-21 (C), or mpcdh-21 (D) were double-labeled with ER-markers, anti-calnexin (B) or anti-KDEL (A,C,D), and anti-rhodopsin (B630N) or anti-N-pcdh-21 antibodies. The ER labeling was diffused in non-transfected cells and cells expressing rhodopsin or xpcdh-21. The rhodopsin and xpcdh-21 labeling was also diffused. In contrast, mpcdh-21 was localized to the ER in a reticular manner (D). The abnormal, reticular structures were also observed using the ER marker. Scale bar=10 $\mu$ m

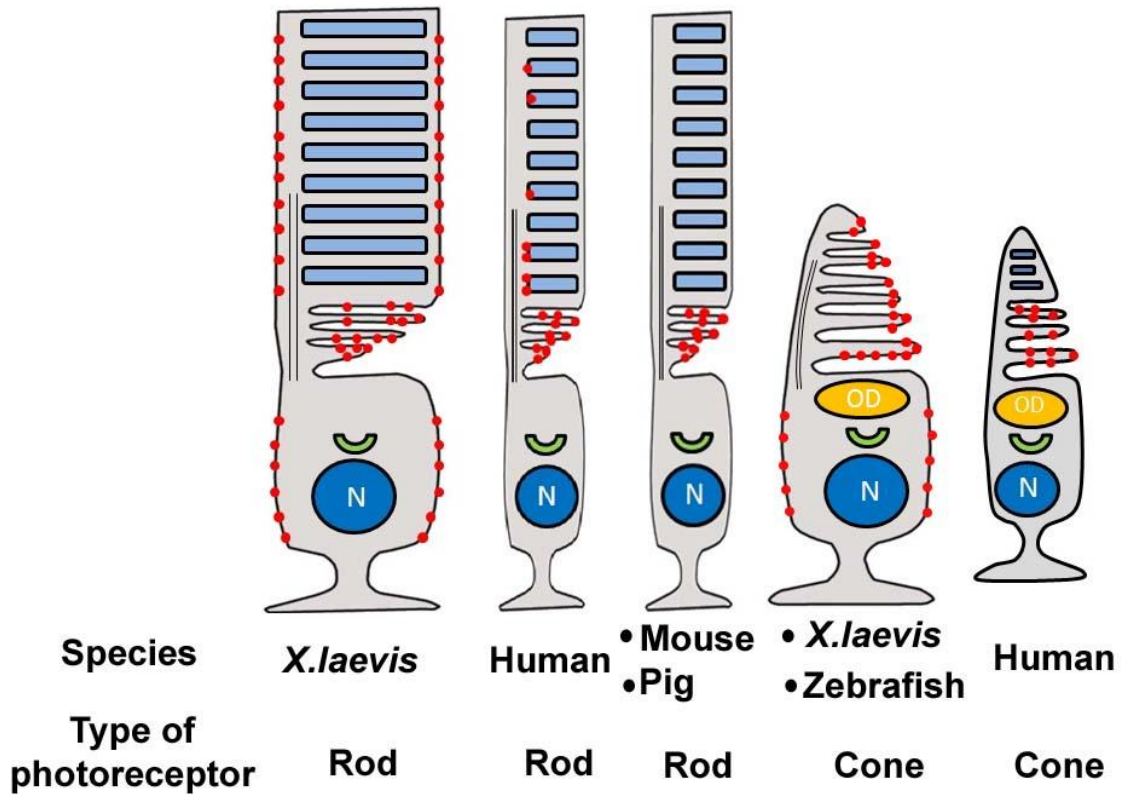


**Figure 2-19. Pcdh-21 distribution in rods and cones of different species.**

Pcdh-21 localization in nascent disks is conserved in rods and cones of different species. In contrast, its distribution in mature disks varies between photoreceptor types across species. In *X.laevis* rods, pcdh-21 is localized to the plasma membrane. In human rods, it may be localized to the disk rims or plasma membrane near the axoneme. In mouse and pig rods, pcdh-21 is not detected in any significant level in distal ROS. In *X.laevis* and zebrafish cones, it is localized to the open disk rims along COS. It is also present in the inner segment plasma membrane of *X.laevis* cones and some types of zebrafish cones. In human cones, pcdh-21 is found exclusively at the base of the COS.

## **Chapter 3: Generation of pcdh-21 mutants to study pcdh-21 function in disk synthesis.**

### **3.1 Introduction**

In mice, prom-1 interacts with pcdh-21 and actin at the base of the OS (Yang, 2008). The absence or disruption of either member of this complex causes abnormal disk synthesis (William, 1988; Rattner, 2001; Yang, 2008). Because prom-1 and actin are often associated with membrane protrusions, which are structurally analogous to the nascent disk precursors described in the membrane evagination model, a complex consisting of prom-1, actin and pcdh-21 is hypothesized to be a molecular participant in disk synthesis (Steinberg, 1978; Yang, 2008).

Transgenic mice expressing a missense mutation in human *PROM-1* (R373C) showed abnormal disks. The mutant protein is thought to cause a dominant negative phenotype. It binds to pcdh-21 and causes pcdh-21 mislocalization. Furthermore, it disrupts interaction between prom-1 and actin filaments (Yang, 2008).

Dominant negative approaches have been used to study cadherin function (Zhu, 1996; Utton, 2001). Cadherin members often interact with intra- or extracellular proteins to perform specific functions (reviewed by Takeichi, 1995). We therefore attempted to generate dominant negative mutations by overexpressing pcdh-21 lacking the extra- or intracellular domain in PR. The underlying hypothesis was that these truncated forms of pcdh-21 would compete with endogenous pcdh-21 for binding partners. However, they would be able to participate in interactions only on one side of the membrane, and unable to interact with binding partners on the other side. Disrupting pcdh-21 function would then lead to defects in disk synthesis and serve as model to study retinal degeneration caused by pcdh-21 mutations.

In mouse retina, pcdh-21 is cleaved into a soluble N-terminal fragment and a C-terminal fragment that is retained in the membrane (Fig.3-1a). Our N-terminal deletion construct was designed to mimic this pcdh-21 cleaved fragment. To ensure entry into the secretory pathway, a signal peptide sequence was added to the N-terminal deletion construct (Fig.3-1b). The C-terminal deletion construct lacked the intracellular domain. The constructs retained the pcdh-21 transmembrane domain in order to ensure the truncated proteins were targeted to membranes.

We overexpressed *X.laevis* and murine (mpcdh-21) forms of these variants in transgenic *X.laevis* rods. Retinal degeneration was determined by measuring rhodopsin levels using dot blot analysis and examining OS structure in frozen retinal sections. Subcellular localizations of transgenes were visualized by confocal microscopy. Disk ultrastructure was studied with transmission electron microscopy.

Transgenic *X.laevis* are relatively easy to generate due to their rapid developmental time, and large number of transgenic animals can be generated in single transgenesis experiment. In addition, *X.laevis* have high disk turnover rates and large PR, making them particularly amenable to studies of disk membrane synthesis. For these reasons, extensive knowledge regarding OS protein targeting has been revealed using transgenic *X.laevis* (Tam, 2000; Tam, 2004; Baker, 2008).

## **3.2 Materials and methods**

### **3.2.1 Generation of constructs**

Full length mpcdh-21 and xpcdh-21 cDNAs were received as gifts from Jeremy Nathans (John Hopkins University). Full length mpcdh-21 cDNA was amplified by PCR

using forward primers containing an *EcoRI* restriction site and reverse primers including a *NotI* site. For synthesis of xpcdh-21 FL, xpcdh-21 $\Delta$ C and mpcdh-21 $\Delta$ C constructs, in addition to the *EcoRI* and *NotI* sites, 15 bases of homologous sequences flanking the *EcoRI* and *NotI* sites were added, allowing the cDNA to be cloned into the vector through homologous recombination (In-fusion cloning kit; Clontech, Mountain View, CA). Xpcdh-21 $\Delta$ N and mpcdh-21 $\Delta$ N were synthesized as described in Fig.3-2. All PCR products were cloned into the *EcoRI/NotI* sites of the XOP0.8-eGFP-N1 vector and all final constructs were sequenced. For the synthesis of TacP-eGFP-N1, *X.laevis* opsin promoter from XOP0.8-eGFP-N1 was excised using *EcoRV* and was replaced with the zebrafish cone transducin promoter (T- $\alpha$ cP). A fragment containing T- $\alpha$ cP was excised from TacP-eGFP-1 (gift of Dr. Brendan Kennedy, University College, Dublin) using *EcoRI* and *BamHI*. To create blunt ends, the TacP fragments were incubated with large fragment of DNA polymerase I (Invitrogen) and 10mM dNTPs, allowing the extension of single stranded DNA in the presence of template and dNTPs. TacP fragments with blunt ends were cloned into vector XOP0.8-eGFP-N1. For expression in transgenic animals, expression constructs were linearized with *FseI* (New England Biolabs, Beverly, MA) and purified (QIAquick Gel Extraction Kit; Qiagen, Valencia, CA).

### **3.2.2 Generation and rearing of transgenic *X.laevis***

Transgenic *X. laevis* were generated using the restriction enzyme mediated integration method, modified as previously described (Kroll and Amaya, 1996; Moritz, 1999). Embryos were treated with 18 $\mu$ g/ml G418 to eliminate non-transgenic embryos (Invitrogen, Carlsbad, CA) and kept in an 18°C incubator on a 12-hour dark/ 12-hour light cycle. All

procedures were carried out in adherence with The ARVO Statement for the Use of Animals in Ophthalmic and Vision Research, and met UBC animal care committee approval. At 14 days postfertilization, normally developed animals were sacrificed. One eye was processed for confocal microscopy and the contralateral eye was either solubilized, or processed for transmission electron microscopy.

### **3.2.3 Dot blot**

Eyes were solubilized using procedures similar to those described previously (section 2.2.8). 2 $\mu$ l of solubilized eyes were diluted 150X in 20mM NaHPO<sub>4</sub> buffer, pH 7.4. 30 $\mu$ l of diluted samples were loaded into a bio-dot apparatus (Bio-Rad, Hercules, CA) and drawn through a PVDF membrane (Millipore, Bedford, MA). Blots were blocked with blocking buffer (1% skim milk and PBS) and probed with anti-rhodopsin (B630N) (1:20; cell line was a gift from W. C. Smith, University of Florida). Blots were then incubated with IRDye800-CW-conjugated anti-mouse secondary antibodies (1:10000; Rockland, Gilbertsville, PA) and analyzed on a LI-COR Odyssey imager (Li-Cor, Lincoln, NE). The fluorescent signal was used to estimate rhodopsin levels in each transgenic animal. Values were normalized to the averaged levels from control (TacP-eGFP). Statistical analysis was performed using SPSS (SPSS, Chicago, IL). Plots were generated using SigmaPlot (Systat, Chicago, IL).

### **3.2.4 SDS page and Western blot**

Solubilized eyes (15 $\mu$ l) were analyzed with SDS-page and Western blot as described previously (section 2.2.9). Blots were probed with anti-N-mpcdh-21 antibodies that only detect the mouse protein (1: 200; a gift of Jeremy Nathans, John Hopkins University) and

labeled with IRDye800-CW-conjugated anti-rabbit secondary antibodies (1:10000; Rockland, Gilbertsville, PA).

### **3.2.5 Immunohistochemistry and confocal microscopy**

Frozen sections of transgenic *X.laevis* were obtained and immunolabeled as previously described (Section 2.2.3-4). The following primary antibodies were used: anti-N-mpcdh-21 (1: 200; a gift of Jeremy Nathans, John Hopkins University), anti-KDEL (1: 10; Stressgen Biotechnologies, Victoria, BC, Canada) and anti-N-xpcdh-21(1: 10000). Sections were counterstained and labeled with secondary antibodies, as previously described in section 2.2.4.

### **3.2.6 Transmission electron microscopy**

*X.laevis* tadpoles were fixed in double aldehyde fixative containing 1% glutaraldehyde and 4% formaldehyde in 0.1M cacodylate buffer pH 7.4 at 4°C. After 30mins of fixation, corneas were slit and tadpoles were fixed again for up to 48hrs. Fixative was then removed by incubating tissue in buffer for at least 1hr at 4°C. To preserve lipids, dissected eyes were fixed for one hour with 1% osmium tetroxide in 0.1M cacodylate buffer pH 7.4. Eyes were washed with buffer for a minimum of an hour and then washed in 0.1M cacodylate buffer. Tissues were dehydrated in a graded series of ethanol (30%, 50%, 70%, 95%, and 100%). They were infiltrated gradually in a mixture of 100% ethanol and Pelco Eponate 12 resin (Ted Pella Inc., Redding, CA) and then in pure resin. Eyes were subsequently embedded in flat molds with the lens facing down to obtain longitudinal retinal sections. Resin was polymerized in a 60°C incubator for up to 72 hrs. Ultrathin sections

(70nm) were cut using a Sorvall MT 5000 ultramicrotome (Dupont, Wilmington, DE) equipped with a diamond knife and collected on Formvar-coated copper grids. Sections were stained with 2% uranyl acetate and 2% lead citrate for 2mins each. They were imaged with the aid of an H-7600 transmission electron microscope (Hitachi, Berkshire, UK) at 80kv.

### **3.3 Results**

#### **3.3.1 Retinal degeneration in transgenic *X.laevis* expressing mpcdh-21 variants**

To examine retinal degeneration in transgenic *X.laevis* expressing mpcdh-21 variants, frozen retinal sections immunolabeled with anti-C-pcdh-21 specific to mouse ( $\alpha$ -mpcdh-21) were examined with confocal microscopy. Transgenic *X.laevis* expressing eGFP under the control of a cone promoter (T $\alpha$ cP-eGFP) served as a control for a lack of retinal degeneration. Histology showed that mpcdh-21  $\Delta$ N (Fig.3-3B) and  $\Delta$ C (Fig.3-3C) were expressed in most rods, whereas mpcdh-21 FL was mostly found in rods located in the peripheral retina (Fig.3-3A). Although mpcdh-21 FL was expressed at lower levels, shorter OS, indicating retinal degeneration, were only observed in this group. The apparent low expression level of mpcdh-21 FL was likely a result of the large number of degenerating cells. This is supported by the observation that cells expressing mpcdh-21 FL were found at the periphery, where new PR are located. It is expected that they would also eventually degenerate due to the toxicity of the transgene. The distribution of degenerating cells also suggests that the overexpression of mpcdh-21 FL caused progressive cell death.

Loss of rods results in lower rhodopsin levels. To rigorously determine PR survival, total rhodopsin levels in transgenic *X.laevis* whole eye lysates were measured by dot blot. ANOVA indicated that there was significant difference between groups (Fig.3-3E). Multiple

comparison analysis using Dunnett's test showed that only retinas expressing mpcdh-21 FL had significantly lower rhodopsin levels, compared to control ( $p=0.009$ ), confirming our results obtained with histology.

### **3.3.2 Subcellular localization of mpcdh-21 variants**

We examined the distribution of mpcdh-21 variants with confocal microscopy. Of the three mpcdh-21 variants, only mpcdh-21 FL (Fig.3-4A, arrow) was convincingly expressed at the base of the OS and this was observed only in a minority of cells (<1%). The majority of mpcdh-21 FL was mislocalized to the IS in a reticular (Fig.3-4; B,C) and punctate distribution (Fig.3-4D). Unlike the endogenous xpcdh-21 (see section 2.3.2), mpcdh-21 FL was not localized to the plasma membrane, suggesting plasma membrane localization of pcdh-21 is dependent on intrinsic factors (such as a targeting signal).

Mpcdh-21  $\Delta N$  (Fig.3-4E) and  $\Delta C$  (Fig.3-4; F-G) were localized to the IS in a diffuse pattern with a characteristic labeling of the ER. Their localizations at the base of the OS was unclear due to their high expression in the IS, making it hard to identify the IS-OS junction. Mpcdh-21 variants were rarely convincingly observed at the base of the OS (Fig. 3-4G, arrow).

To determine the identity of the reticular structures observed in retinas expressing mpcdh-21 FL, sections were double labeled with Golgi and post-Golgi marker (WGA) as well as ER marker ( $\alpha$ -KDEL). The majority of mpcdh-21 FL colocalized with  $\alpha$ -KDEL, suggesting that they were retained in the ER (Fig.3-5B). Non-transgenic retinas showed diffuse ER labeling (Fig.3-5C), whereas mpcdh-21 FL expressing retinas had abnormal, reticular ER labeling (Fig.3-5B). Transmission electron microscopy provided further

evidence that transgenic retinas had abnormal ER. They had vesiculated and wavy ER membrane (Fig.3-6B), in contrast to non-transgenic retinas with flat and regularly spaced ER membrane (Fig.3-6A). Taken together, immunofluorescence and ultrastructural analysis suggest that accumulation of mpcdh-21 FL may cause ER abnormalities and ER stress.

### **3.3.3 Mpcdh-21 cleavage in transgenic *X.laevis***

Previous studies suggested that pcdh-21 cleavage is required for disk synthesis (Rattner, 2004). To investigate whether *X.laevis* is able to cleave mpcdh-21, whole eye extracts from transgenic *X.laevis* were analyzed using western blot probed with antibody against the C-terminus of mpcdh-21. A single band at ~100kDa (Fig.3-7, arrowhead), corresponding to the molecular weight of mpcdh-21 FL, was detected. The predicted cleaved fragment (~25kDa) was not observed, indicating that mpcdh-21 was not cleaved in *X.laevis* rods. No band was observed in control animals and animals expressing low levels of pcdh-21.

### **3.3.4 Disk ultrastructure in rods overexpressing mpcdh-21 FL**

We examined the effect of mpcdh-21 overexpression on disk ultrastructure using transmission electron microscopy. In transgenic retinas expressing mpcdh-21 FL, OS defects with variable degrees of severity were observed between retinas, which may be related to the differences in transgene expression levels. Minor defects were detected in the distal ROS, including misaligned disks (Fig.3-8B), vesicles (Fig.3-8C, arrow) and large intra- or interdiskal spaces (Fig.3-8B). More dramatic defects were observed at the basal OS, the site of disk synthesis. The basal disks of a few rods were overgrown, although they were orientated correctly perpendicular to the OS (Fig.3-8; E-F).

### **3.3.5 Retinal morphology in transgenic *X.laevis* overexpressing xpcdh-21 variants**

Sections of transgenic retinas expressing *X.laevis* pcdh-21 variants were immunolabeled with anti-xpcdh-21 antibodies that are not able to distinguish between transgenic and endogenous xpcdh-21. All variants had normal OS length (Fig.3-9; B-D) and rhodopsin levels (Fig.3-9E), similar to those observed in control retinas (Fig.3-9A). These results confirmed that expression of the deletion constructs did not result in dominant negative mutations. In contrast to mpcdh-21 variants, xpcdh-21 variants did not accumulate in the IS and their localizations were identical to nontransgenic retinas..

## **3.4 Discussion**

### **3.4.1 Pcdh-21 deletion constructs did not generate dominant negative mutations**

Several reasons may explain why we failed to generate dominant negative effects. First, the deletion constructs may not have been expressed at sufficiently high levels to inhibit endogenous xpcdh-21 function, possibly due to protein instability. However, this seems unlikely since histology shows that the deletion constructs were expressed in cells throughout the retina. The expression was greater and more homogenous than mpcdh-21 FL that caused RD. Second, the deletion constructs were not targeted to the base of the OS, which may be necessary for dominant negative effects. Third, the deletion constructs may not be able to bind to pcdh-21 interacting partners and compete with endogenous pcdh-21 due to misfolding, mistargeting, or species-specific sequence differences in interacting domains.

Dominant negative approaches have been particularly successful to study proteins that assemble into multimers or proteins consisting of domains with separate and independent functions. For example, a number of cadherins form homo- or heterotypic interactions using their extracellular cadherin repeats. The extracellular interaction propagates the signal to the cytoplasmic domain linked to a variety of proteins that is essential for cadherin function (reviewed by Angst, 2001). This is demonstrated by the expression of deletion construct lacking the cytoplasmic domain. These mutants were able to bind and compete for interacting partners of endogenous cadherins, thereby inhibiting cadherin functions (Utton, 2001). Whether pcdh-21 possesses separate interaction and function domains, like other cadherins, is unclear. The possibility of generating dominant negative mutants can be further explored when more is known about pcdh-21, including its binding partners, interacting and functional domains.

In a minority of cells with healthy OS, mpcdh-21 FL was targeted to the base of the OS and did not accumulate in the IS. These cells may be expressing mpcdh-21 FL at low levels that can be processed by the protein machinery. Alternatively, the protein machinery may occasionally have increased folding efficacy or decreased quality control. Understanding the cellular conditions that facilitate the successful targeting to the base of the OS may be helpful in generating dominant negative mutations.

Interetingly, in a few rods with normal OS, mpcdh-21 FL was exclusively at the base of ROS and was not found in the plasma membrane, as observed for endogenous xpcdh-21. In other words, mpcdh-21 expressed in *X.laevis* rods retains a localization equivalent to that observed in mouse PR. This implies that the differences in localization between xpcdh-21

and mpcdh-21 are due to intrinsic properties of these homologs (such as targeting signals), and not due to species differences in PR structures or disk synthesis mechanisms.

### **3.4.2 Mpcdh-21 FL, but not xpcdh-21, caused retinal degeneration and abnormal disk synthesis**

The overexpression of mpcdh-21 FL caused rod cell death and abnormal disks; whereas xpcdh-21 FL overexpressing retinas were normal. Several reasons may contribute to such differences. First, the amino acid sequences of mpcdh-21 and xpcdh-21 are not identical (~50% similarity). Therefore, they may have different conformations, properties and turnover rates. Second, mpcdh-21 may express at higher levels than xpcdh-21. Comparison of mpcdh-21 and xpcdh-21 levels is challenging because antibodies specific to the mouse and *X.laevis* pcdh-21 do not have identical sensitivities. Furthermore, our antibody cannot distinguish endogenous and overexpressed *X.laevis* pcdh-21 in *X.laevis* retinas. Third, abnormal phenotype may be caused by mislocalization in the IS, which was only observed in mpcdh-21 overexpressing retinas.

Previously, we attempted to overexpress epitope tagged xpcdh-21 in *X.laevis* rods. The transgene expression level was extremely low and was barely detectable at the base of the ROS, suggesting that overexpression of xpcdh-21 transgene at high levels may be challenging. However, it is also possible that this low expression was caused by the presence of the epitope tag.

### 3.4.3 Mechanisms by which mpcdh-21 FL causes retinal degeneration

Previous studies have suggested that pcdh-21 and prom-1 interaction at the base of the OS is required for disk synthesis. The expression of human R373C prom-1 in mice exerts a dominant negative effect by causing mislocalization of endogenous pcdh-21 and prom-1 (Yang, 2008). We therefore speculate that the overexpression of mpcdh-21 FL in *X.laevis* may cause retinal degeneration by (1) disrupting endogenous pcdh-21 or prom-1 trafficking or (2) interfering with the ability of endogenous pcdh-21 to interact with its partners, possibly prom-1. However, labeling transgenic retinal sections with antibody specific to endogenous prom-1 or pcdh-21 suggest that prom-1 targeting is unlikely to be affected (Fig.A.1). First, prom-1 did not accumulate in the IS. Occasionally, we observed prom-1 at the base of the OS. However, the transgenesis method can lead to mosaic transgene expression levels that can vary between cells within a single retina. These cells may therefore express transgene at such low levels as to be indistinguishable from non-transgenic cells. This question could be addressed by double labeling with anti-mpcdh-21 and anti-prom-1 antibodies but because both available reagents were generated from rabbits, we were unable to perform a double labeling experiment to determine whether a cell showing reticular mpcdh-21 labeling in the IS showed correct localization of prom-1 in the OS. It may be interesting to compare whether prom-1 is localized correctly when mpcdh-21 is also targeted correctly.

Mpcdh-21 cleavage is thought to be essential for disk synthesis. However, the failure to cleave mpcdh-21 FL in *X.laevis* is unlikely to induce retinal degeneration, because unlike in mice, pcdh-21 is not cleaved in *X.laevis* retinas (see section 2.3.1).

The abnormal ER structures observed in mpcdh-21 FL overexpressing retinas strongly suggests ER stress. This may be caused by overexpression of protein that saturates

the protein synthesis and trafficking machinery and/ or mpcdh-21 FL cannot adopt its proper conformation in *X.laevis*. However, it is notable that the accumulation of deletion constructs in IS did not cause retinal degeneration. This suggests that it is not general overexpression but inherent properties of mpcdh-21 FL that causes the observed phenotype. These properties are unique to mpcdh-21 FL and are not present in the deletion constructs or xpcdh-21 FL.

ER stress activates the unfolded protein response (UPR) that aims to eliminate or slow the accumulation of misfolded protein. Failure to restore the cell to its healthy state triggers cell death and may possibly cause retinal degeneration in mpcdh-21 FL overexpressing retinas. To provide direct evidence of ER stress, it may be of interest to examine expression of genes upregulated in UPR, including BiP, a chaperone that facilitates proper protein folding, CHOP, a pro-apoptotic transcription factor, and xbp-1, an RNA that is alternatively spliced in response to ER stress.

#### **3.4.4 Mpcdh-21 FL results in overgrown disks**

In mpcdh-21 FL overexpressing retinas, we observed abnormally large basal disks, strikingly similar to those reported in cultured *X.laevis* retinas treated with actin depolymerization drug (Williams, 1988). We therefore speculate that the overgrown disks observed in our samples may arise due to a direct or indirect disruption of actin. As mentioned above, ER stress may activate the UPR that aims to slow accumulation of misfolded proteins. To achieve this, the cell reduces overall protein synthesis, possibly including actin. Alternatively, mpcdh-21 FL may disrupt prom-1 function (when mutated, prom-1 affects actin polymerization (Yang, 2008)). The last possibility strongly supports the "membrane evagination model" mechanism of disk synthesis. A complex consisting of actin,

prom-1 and pcdh-1 is proposed to be a molecular player in this process. When one of these components is defective, overgrown nascent disks would be anticipated (Williams, 1998; Yang, 2008).

A small number of abnormal disks are observed in a background of normal disks, suggesting that defects in disk synthesis occurred transiently. Furthermore, the abnormal nascent disks synthesized at the base of the OS are likely incorporated into the distal OS. The occasional periods of abnormal disk synthesis were possibly triggered by a specific condition, such as an increase in transgene expression level. The promoter used to drive the transgene expression has been shown to result in expression levels that may vary on a daily or hourly basis (Moritz, 2001). Compared to the complete loss of OS observed with confocal microscopy, abnormal disk synthesis is a mild defect. Most likely, high transgene expression levels induce ER stress and the more severe phenotype of retinal degeneration and complete loss of OS; whereas a moderate expression level is not toxic enough to cause severe retinal degeneration but causes defects in disk synthesis.

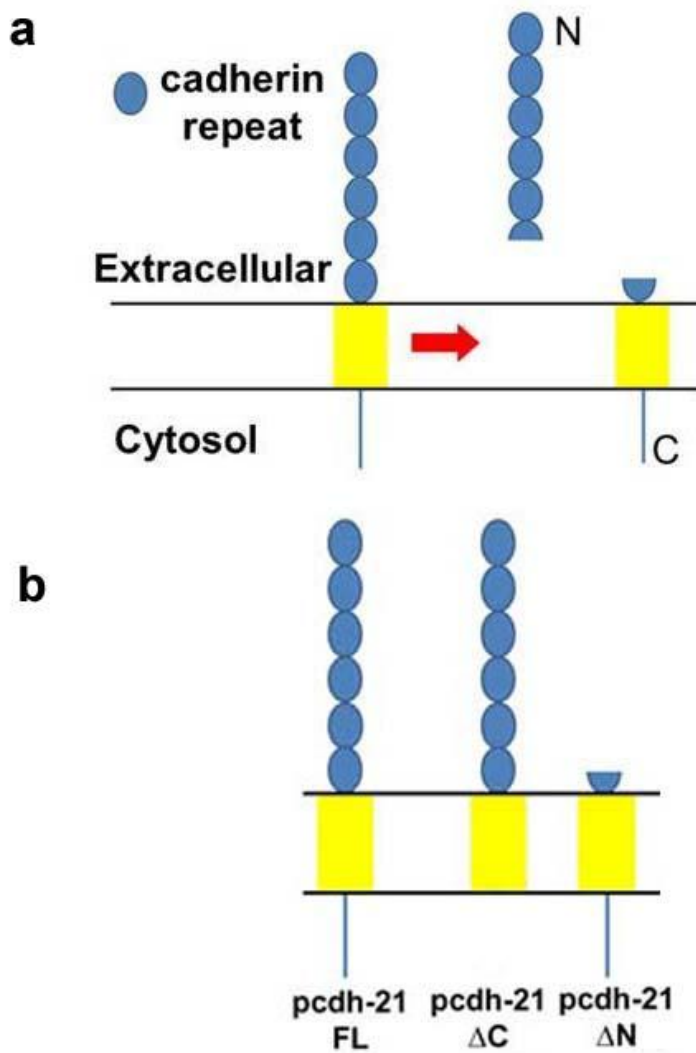


**Figure 2-20. (a) Pcdh-21 cleavage in mice.**

Pcdh-21 is cleaved into a soluble N-terminal fragment and a C-terminal fragment that is retained in the membrane. **(b) Domain structure of the pcdh-21 FL, pcdh-21  $\Delta$ C and pcdh-21  $\Delta$ N constructs.** The N-terminal deletion construct is designed to mimic the endogenous pcdh-21 cleaved fragment. To ensure efficient membrane targeting, a signal peptide sequence was added to this construct.

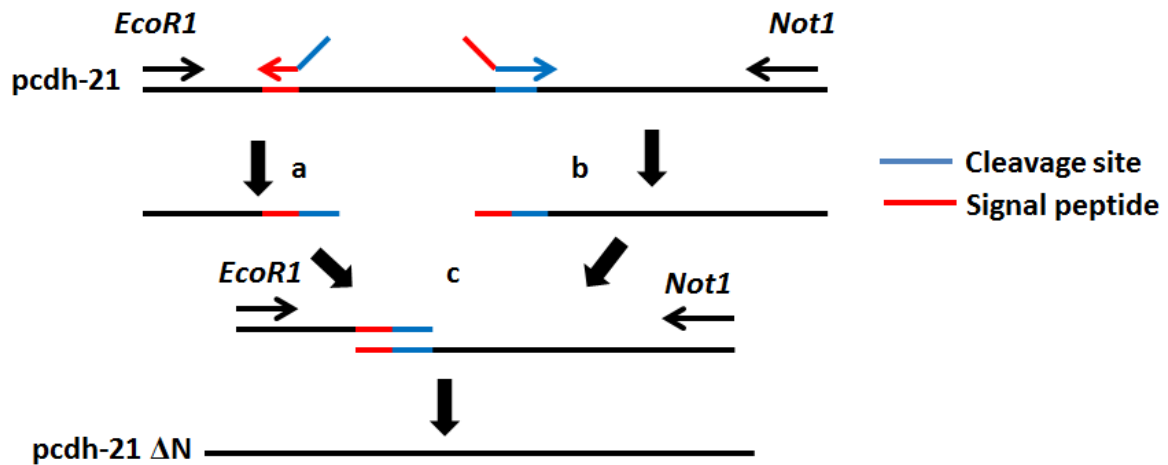


**Figure 2-21. Strategies used to generate the *pcdh-21*  $\Delta$ N constructs.**

(a) Forward primers with the *EcoRI* sites bound to the start of *pcdh-21*. Reverse primers, containing sequences encoding the signal peptide and cleavage site, annealed to the signal peptide. PCR products encoding sequences from the start codon to the signal peptide were synthesized. (b) To remove part of the N-terminus, forward primers, encoding the signal peptide and cleavage site, anneal to the cleavage site. Reverse primers with the *NotI* site bound to the end of *pcdh-21*. The resulting PCR products contain sequences of the cytoplasmic domain. (c) The two PCR products were combined. Overlapping sequences that were introduced in the primers allowed the two PCR products to complementary base pair with each other. The remaining DNA was synthesized by the addition of *EcoRI* and *NotI* primers.

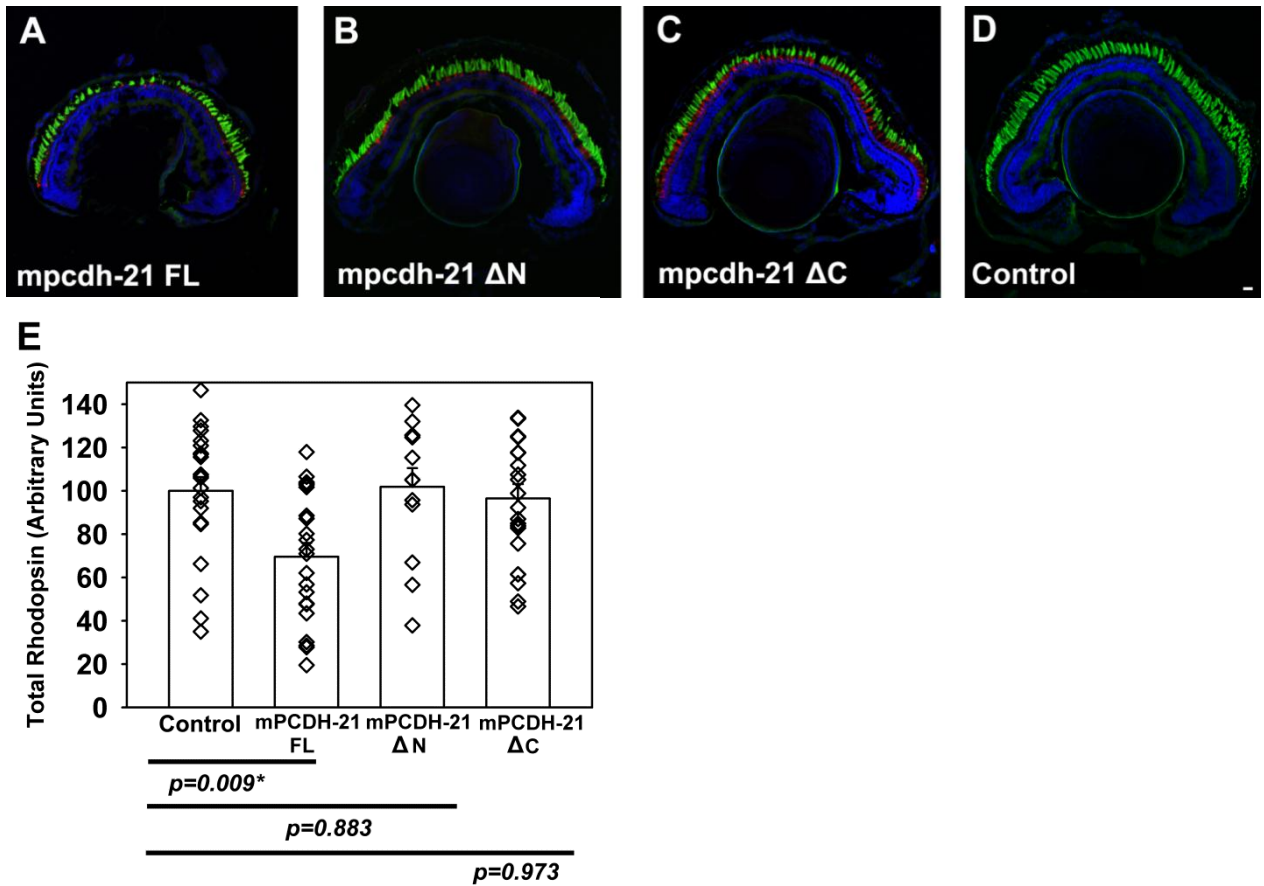


**Figure 2-22. Analysis of transgenic *X.laevis* expressing mpcdh-21 variants by confocal microscopy (A-D) and dot blot (E).**

(A-D) Confocal micrographs showing transgenic retinas expressing mpcdh-21 variants. (A) Mpcdh-21 FL was expressed in a few cells at the periphery of the retina. Cells in the centre of the retina had shorter OS or had completely lost their OS. (B-C) Mpcdh-21  $\Delta$ N (B) and  $\Delta$ C (C) were found in cells throughout the retina and they had healthy OS. (D) Retinas expressing eGFP under the control of a cone-transducin- $\alpha$  promoter (T- $\alpha$ P-eGFP) were used as a control for lack of retinal degeneration. Green=WGA (OS), red=mpcdh-21, blue=Hoescht.. Scale bar=20 $\mu$ m. (E) Averaged rhodopsin levels (bar) from each group are shown. For each sample (data points), rhodopsin levels were measured by dot blot and values were normalized to the averaged levels from control (T- $\alpha$ P-eGFP). ANOVA indicated significant differences between groups ( $p=0.013$ ). Multiple comparison analysis using Dunnett's test showed that only mpcdh-21 FL had significantly lower rhodopsin levels, compared to control ( $p=0.009$ ) ( $n=14-22$  per group).

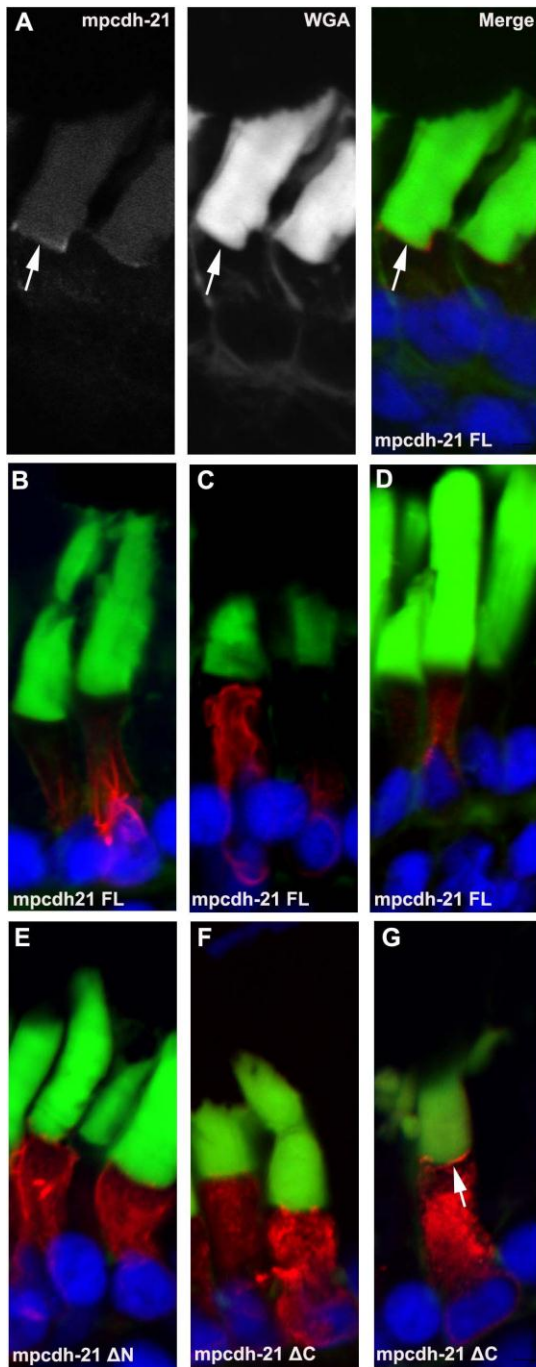


**Figure 2-23. Localization of mpcdh-21 variants in transgenic *X.laevis* rods.**

(A) Mpcdh-21 FL was localized correctly to the base of the OS (arrows). It is important that to note that unlike the endogenous xpcdh-21, mpcdh-21 was not localized to the plasma membrane. (B-D) Mpcdh-21 FL was also expressed in the inner segments in a reticular (B, C) and punctate distribution (D). (E-G) Mpcdh-21  $\Delta$ N (E) and mpcdh-21  $\Delta$ C (F) were primarily localized in the inner segments in a diffuse manner and were rarely convincingly observed at the base of the OS (G, arrow). Green=WGA (OS), red=mpcdh-21; blue=Hoescht. Scale bar=2 $\mu$ m.

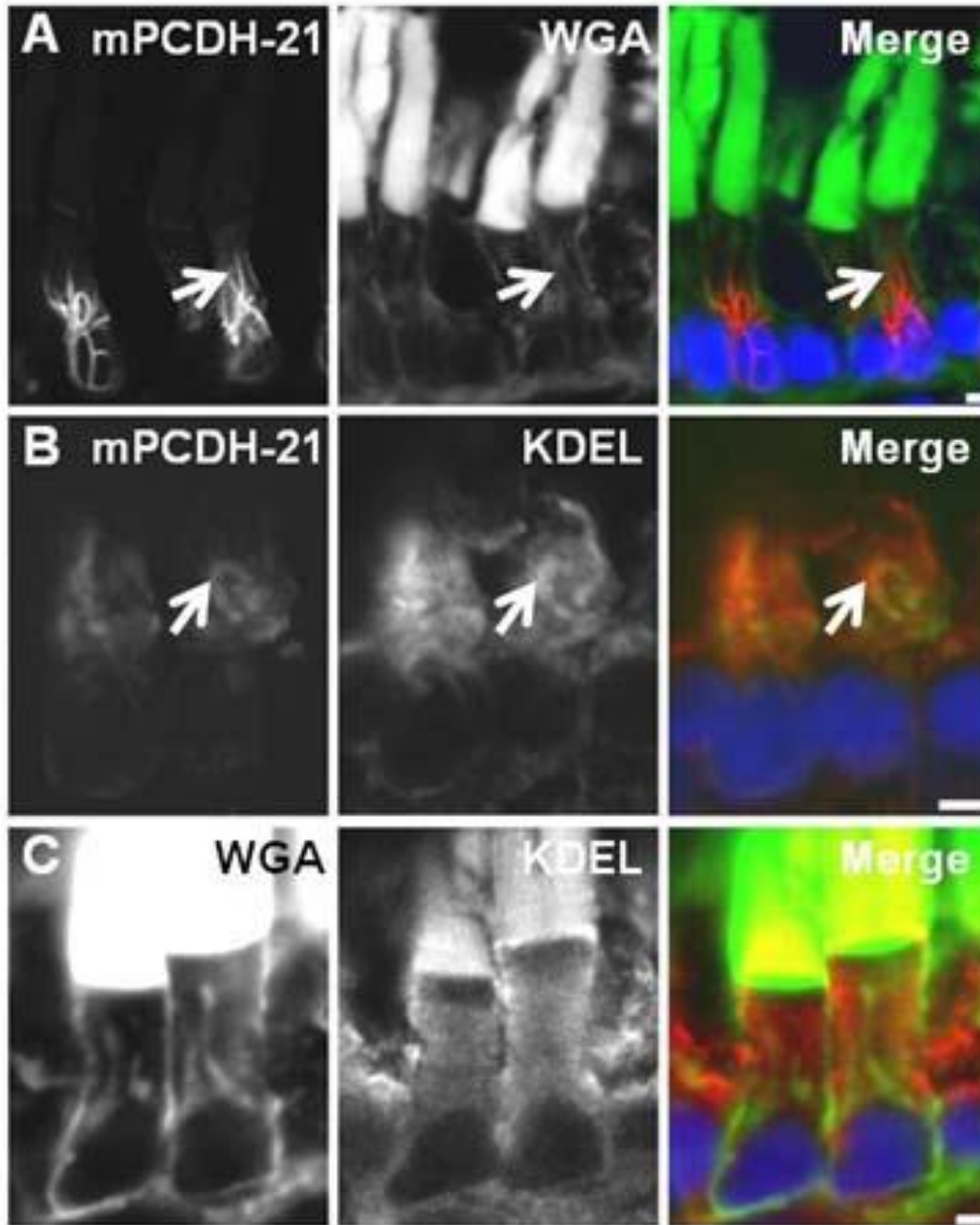


**Figure 2-24. Pcdh-21 localization in the inner segments of transgenic (A-B) and non-transgenic (C) *X.laavis* retinas.**

Double labeling with Golgi and post-Golgi membranes marker, WGA (A) and ER marker,  $\alpha$ -KDEL (B-C). (A) Mpcdh-21 did not colocalize with WGA (arrow). (B) Mpcdh-21 labeling overlapped with  $\alpha$ -KDEL (arrow). Transgenic retinas showed reticular  $\alpha$ -KDEL labeling, indicating abnormal ER morphology. (C) Non-transgenic *X.laavis* ER was diffusely labeled with  $\alpha$ -KDEL. Scale bar=2 $\mu$ m.

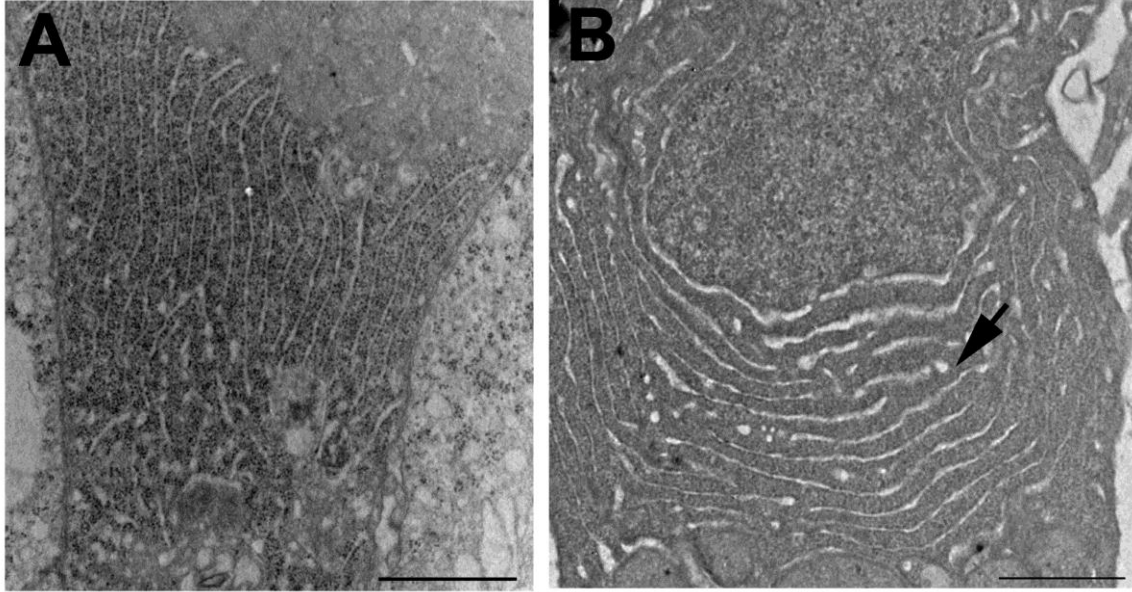


**Figure 2-25. ER ultrastructure of non-transgenic (A) and *mpcdh-21* FL expressing *X.laevis* rods (B).**

(A) The ER membranes of rod photoreceptors of non-transgenic animals were flat and regularly stacked. (B) Rods in transgenic retinas had fragmented ER with vesicles (arrow) located among the membranes. Scale bar=2 $\mu$ m.

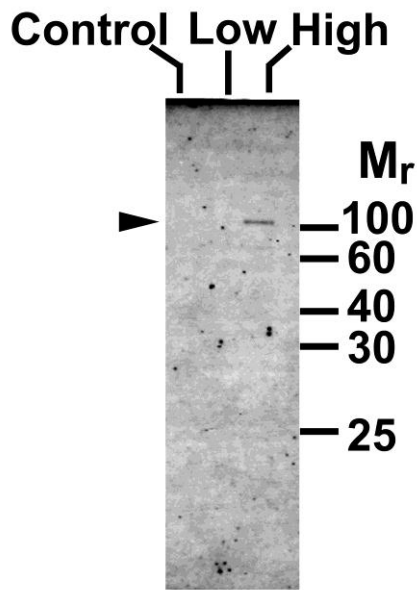


**Figure 2-26. Western blot analysis of mpcdh-21 FL cleavage in transgenic *X.laevis* eyes.** Solubilized eyes from transgenic *X.laevis* expressing mpcdh-21 in rods or eGFP in cones were analyzed by western blot probed with anti-mpcdh-21 C-terminus. Retinas with high and low expression levels were selected. Full length mpcdh-21 (~100kDa) (arrowhead) was detected. The predicted cleaved fragment (~25kDa) was not observed.

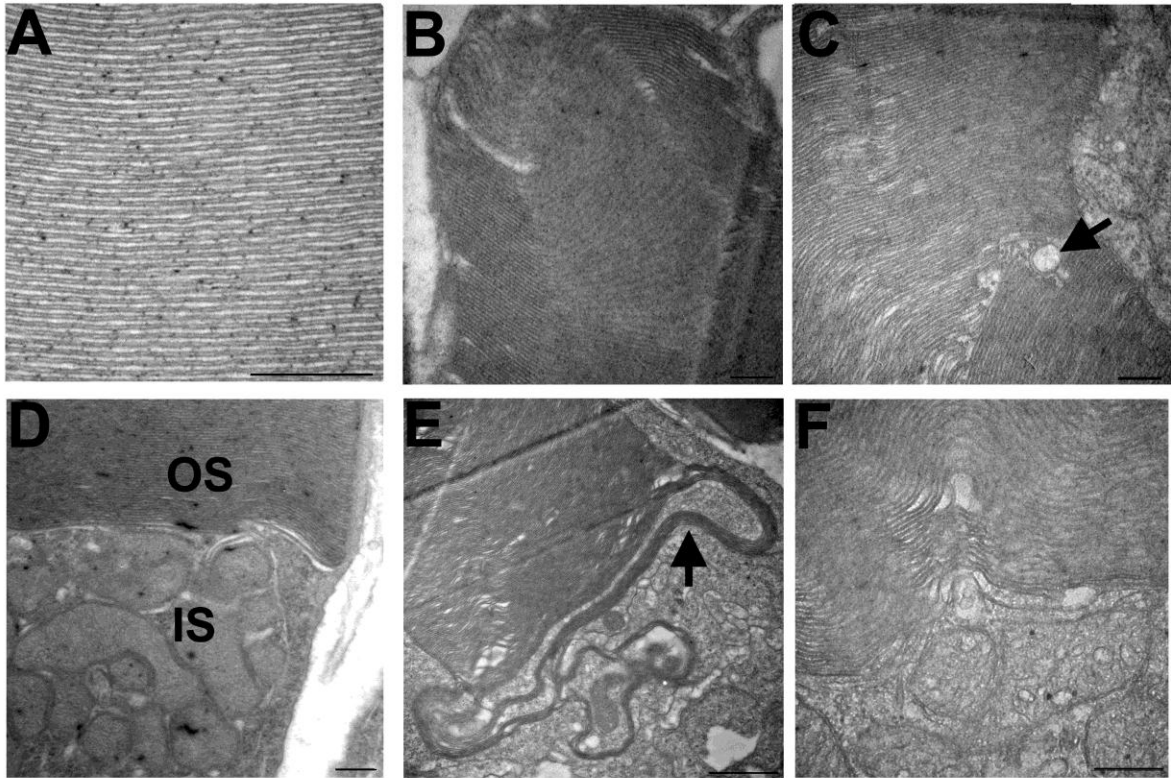


**Figure 2-27. Disk ultrastructure of non-transgenic (A, D) and transgenic *X.laevis* expressing *mpcdh-21* FL (B,C,E,F).**

(A) Non-transgenic retinas had densely packed disks orientated perpendicularly along the long axis of the OS. (B,C,E,F) Transgenic retinas had wavy disks that are orientated at different angles in the distal OS (B). Large intra- or interdiskal spaces (B) and vesicles (C, arrows) were also observed. (D) Non-transgenic retinas had disks with uniform sizes throughout the OS, including the base of the OS. (E) Transgenic retinas had overgrown disks at the base of the OS (arrow) whereas the distal disks were relatively normal. (F) The overgrown disks were bent towards the distal OS. OS=outer segment; IS=inner segment. Scale bar= 500nm (A-D,F); 2 $\mu$ m (E).

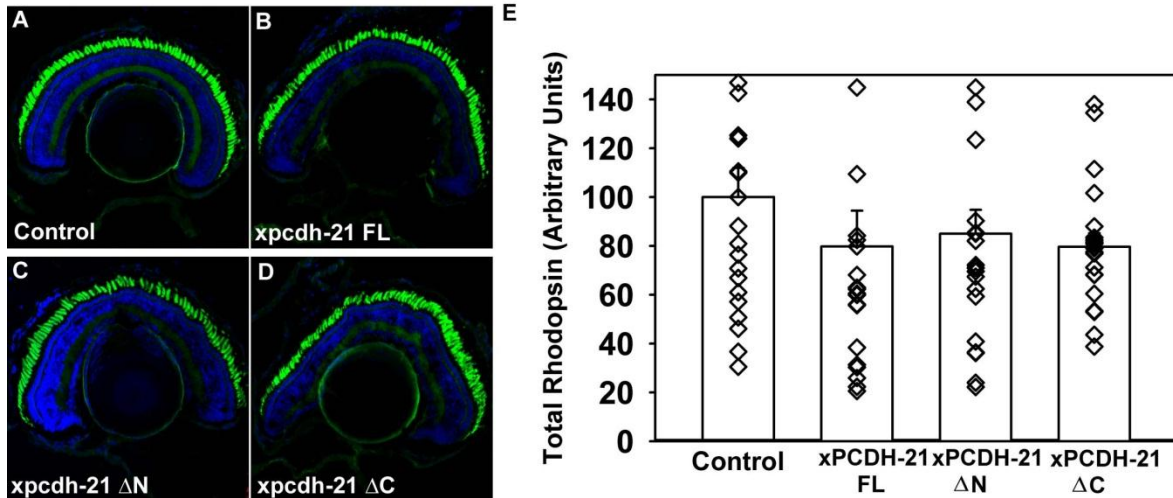


**Figure 2-28. Analysis of transgenic *X.laevis* expressing xpcdh-21 variants by confocal microscopy (A-D) and dot blot (E).**

(A-D) All xpcdh-21 variants all possessed normal OS length and showed no sign of retinal degeneration. Green=WGA, blue=Hoescht. Scale bar=20 $\mu$ m. (E) Experimental procedures were the same as Fig.3-3. ANOVA indicated that no significant differences in rhodopsin levels were observed between groups ( $p=0.561$ ) ( $n=20$  per group).

## Bibliography

- Abd El-Aziz, M. M., Barragan, I., O'Driscoll, C. A., Goodstadt, L., Prigmore, E., Borrego, S., . . . Antinolo, G. (2008). EYS, encoding an ortholog of *drosophila* spacemaker, is mutated in autosomal recessive retinitis pigmentosa. *Nature Genetics*, *40*(11), 1285-1287. doi:10.1038/ng.241
- Anderson, D. H. & Williams, D. S. (2010). In *The encyclopedia of the eye* (Vol. 3, pp. 139-142). San Diego, CA: Elsevier.
- Anderson, D. H., Fisher, S. K., & Steinberg, R. H. (1978). Mammalian cones - disk shedding, phagocytosis, and renewal. *Investigative Ophthalmology & Visual Science*, *17*(2), 117-133.
- Angst, B. D., Marcozzi, C., & Magee, A. I. (2001). The cadherin superfamily: Diversity in form and function. *Journal of Cell Science*, *114*(4), 629-641.
- Arikawa, K., Molday, L., Molday, R., & Williams, D. (1992). Localization of Peripherin/rds in the disk membranes of cone and rod photoreceptors - relationship to disk membrane morphogenesis and retinal degeneration. *Journal of Cell Biology*, *116*(3), 659-667. doi:10.1083/jcb.116.3.659
- Arribas, J., & Borroto, A. (2002). Protein ectodomain shedding. *Chemical Reviews*, *102*(12), 4627-4637. doi:10.1021/cr010202t
- Baker, S. A., Haeri, M., Yoo, P., Gospe, S. M., III, Skiba, N. P., Knox, B. E., & Arshavsky, V. Y. (2008). The outer segment serves as a default destination for the trafficking of membrane proteins in photoreceptors. *Journal of Cell Biology*, *183*(3), 485-498. doi:10.1083/jcb.200806009
- Bascom, R. A., Manara, S., Collins, L., Molday, R. S., Kalnins, V. I., & McInnes, R. R. (1992). Cloning of the cDNA for a novel photoreceptor membrane-protein (rom-1) identifies a disk rim protein family implicated in human retinopathies. *Neuron*, *8*(6), 1171-1184. doi:10.1016/0896-6273(92)90137-3
- Besharse, J. C., Hollyfield, J. G., & Rayborn, M. E. (1977). Turnover of rod photoreceptor outer segments .2. membrane addition and loss in relationship to light. *Journal of Cell Biology*, *75*(2), 507-527. doi:10.1083/jcb.75.2.507
- Besharse, J. C., & Pfenninger, K. H. (1980). Membrane assembly in retinal photoreceptors .1. freeze-fracture analysis of cytoplasmic vesicles in relationship to disk assembly. *Journal of Cell Biology*, *87*(2), 451-463. doi:10.1083/jcb.87.2.451
- Boesze-Battaglia, K., Dispoto, J., & Kahoe, M. A. (2002). Association of a photoreceptor-specific tetraspanin protein, ROM-1, with triton X-100-resistant membrane rafts from

rod outer segment disk membranes. *Journal of Biological Chemistry*, 277(44), 41843-41849. doi:10.1074/jbc.M207111200

- Burns, M. E., & Arshavsky, V. Y. (2005). Beyond counting photons: Trials and trends in vertebrate visual transduction. *Neuron*, 48(3), 387-401. doi:10.1016/j.neuron.2005.10.014
- Chandler, M., Smith, P., Samuelson, D. A., & MacKay, E. O. (1999). Photoreceptor density of the domestic pig retina. *Veterinary Ophthalmology*, 2(3), 179-184.
- Chuang, J., Zhao, Y., & Sung, C. (2007). SARA-regulated vesicular targeting underlies formation of the light-sensing organelle in mammalian rods. *Cell*, 130(3), 535-547. doi:10.1016/j.cell.2007.06.030
- Cohen, A. (1960). The ultrastructure of the rods of the mouse retina. *American Journal of Anatomy*, 107(1), 23-48. doi:10.1002/aja.1001070103
- Cohen, A. (1961). The fine structure of the extrafoveal receptors of the rhesus monkey. *Experimental Eye Research*, 1(2), 128-136.
- Cohen, A. (1965). New details of ultrastructure of outer segments and ciliary connectives of rods of human and macaque retinas. *Anatomical Record*, 152(1), 63-&. doi:10.1002/ar.1091520108
- Cohen, A. (1968). New evidence supporting linkage to extracellular space of outer segment saccules of frog cones but not rods. *Journal of Cell Biology*, 37(2), 424-&. doi:10.1083/jcb.37.2.424
- Cook, N., Molday, L., Reid, D., Kaupp, U., & Molday, R. (1989). The cGMP-gated channel of bovine rod photoreceptors is localized exclusively in the plasma-membrane. *Journal of Biological Chemistry*, 264(12), 6996-6999.
- Corbeil, D., Roper, K., Fargeas, C., Joester, A., & Huttner, W. (2001). Prominin: A story of cholesterol, plasma membrane protrusions and human pathology. *Traffic*, 2(2), 82-91. doi:10.1034/j.1600-0854.2001.020202.x
- Corbeil, D., Roper, K., Hellwig, A., Taviani, M., Miraglia, S., Watt, S., . . . Huttner, W. (2000). The human AC133 hematopoietic stem cell antigen is also expressed in epithelial cells and targeted to plasma membrane protrusions. *Journal of Biological Chemistry*, 275(8), 5512-5520. doi:10.1074/jbc.275.8.5512
- Daniele, L., Lillo, C., Lyubarsky, A., Nikonov, S., Philp, N., Mears, A., . . . Pugh, E. (2005). Cone-like morphological, molecular, and electrophysiological features of the photoreceptors of the nrl knockout mouse. *Investigative Ophthalmology & Visual Science*, 46(6), 2156-2167. doi:10.1167/iops.04-1427

- Davie, E., Fujikawa, K., & Kisiel, W. (1991). The coagulation cascade - initiation, maintenance, and regulation. *Biochemistry*, *30*(43), 10363-10370. doi: 10.1021/bi00107a001
- Fargeas, C., Corbeil, D., & Huttner, W. (2003). AC133 antigen, CD133, prominin-1, prominin-2, etc.: Prominin family gene products in need of a rational nomenclature. *Stem Cells*, *21*(4), 506-508. doi:10.1634/stemcells.21-4-506
- Fetter, R., & Corless, J. (1987). Morphological components associated with frog cone outer segment disk margins. *Investigative Ophthalmology & Visual Science*, *28*(4), 646-657.
- Fu, Y. (2010). In *The encyclopedia of the eye* (Vol. 3, pp. 397-402). San Diego, CA: Elsevier.
- Hale, I. L., Fisher, S. K., & Matsumoto, B. (1996). The actin network in the ciliary stalk of photoreceptors functions in the generation of new outer segment discs. *Journal of Comparative Neurology*, *376*(1), 128-142.
- Han, Z., Anderson, D. W., & Papermaster, D. S. (2012). Prominin-1 localizes to the open rims of outer segment lamellae in *xenopus laevis* rod and cone photoreceptors. *Investigative Ophthalmology & Visual Science*, *53*(1), 361-373. doi:10.1167/iovs.11-8635
- Henderson, R. H., Li, Z., Abd El Aziz, M. M., Mackay, D. S., Eljinini, M. A., Zeidan, M., . . . Webster, A. R. (2010). Biallelic mutation of protocadherin-21 (PCDH21) causes retinal degeneration in humans. *Molecular Vision*, *16*(6-7), 46-52.
- Hengartner, M. (2000). The biochemistry of apoptosis. *Nature*, *407*(6805), 770-776. doi: 10.1038/35037710
- Hulpiau, P., & van Roy, F. (2009). Molecular evolution of the cadherin superfamily. *International Journal of Biochemistry & Cell Biology*, *41*(2), 349-369. doi:10.1016/j.biocel.2008.09.027
- Jansen, H., & Sanyal, S. (1984). Development and degeneration of retina in rds mutant mice - electron-microscopy. *Journal of Comparative Neurology*, *224*(1), 71-84. doi:10.1002/cne.902240107
- Jaszai, J., Fargeas, C. A., Graupner, S., Tanaka, E. M., Brand, M., Huttner, W. B., & Corbeil, D. (2011). Distinct and conserved prominin-1/CD133-positive retinal cell populations identified across species. *Plos One*, *6*(3), e17590. doi:10.1371/journal.pone.0017590
- Kaplan, M., Robinson, D., & Larsen, L. (1982). Rod outer segment birefringence bands record daily disk membrane synthesis. *Vision Research*, *22*(9), 1119-1121. doi:10.1016/0042-6989(82)90076-1

- Kefalov, V.J. (2010). In *The encyclopedia of the eye* (Vol. 3, pp. 389-396). San Diego, CA: Elsevier
- Kinney, M., & Fisher, S. (1978). Photoreceptors and pigment epithelium of adult xenopus retina - morphology and outer segment renewal. *Proceedings of the Royal Society of London Series B-Biological Sciences*, 201(1143), 131-&. doi:10.1098/rspb.1978.0036
- Kinney, M., & Fisher, S. (1978). Photoreceptors and pigment epithelium of larval xenopus retina - morphogenesis and outer segment renewal. *Proceedings of the Royal Society of London Series B-Biological Sciences*, 201(1143), 149-&. doi:10.1098/rspb.1978.0037
- Laties, A., Bok, D., & Liebman, P. (1976). Procion yellow - marker dye for outer segment disk patency and for rod renewal. *Experimental Eye Research*, 23(2), 139-148. doi:10.1016/0014-4835(76)90197-4
- Maw, M., Corbeil, D., Koch, J., Hellwig, A., Wilson-Wheeler, J., Bridges, R., . . . Denton, M. (2000). A frameshift mutation in prominin (mouse)-like 1 causes human retinal degeneration. *Human Molecular Genetics*, 9(1), 27-34. doi:10.1093/hmg/9.1.27
- Mears, A., Kondo, M., Swain, P., Takada, Y., Bush, R., Saunders, T., . . . Swaroop, A. (2001). Nrl is required for rod photoreceptor development. *Nature Genetics*, 29(4), 447-452. doi:10.1038/ng774
- Miraglia, S., Godfrey, W., Yin, A., Atkins, K., Warnke, R., Holden, J., . . . Buck, D. (1997). A novel five-transmembrane hematopoietic stem cell antigen: Isolation, characterization, and molecular cloning. *Blood*, 90(12), 5013-5021.
- Moritz, O., & Molday, R. (1996). Molecular cloning, membrane topology, and localization of bovine rom-1 in rod and cone photoreceptor cells. *Investigative Ophthalmology & Visual Science*, 37(2), 352-362.
- Nilsson, S. (1964). Receptor cell outer segment development and ultrastructure of disk membranes in retina of tadpole ( *rana pipiens* ). *Journal of Ultrastructure Research*, 11(5-6), 581-&. doi:10.1016/S0022-5320(64)80084-8
- Oprian, D., Molday, R., Kaufman, R., & Khorana, H. (1987). Expression of a synthetic bovine rhodopsin gene in monkey kidney-cells. *Proceedings of the National Academy of Sciences of the United States of America*, 84(24), 8874-8878. doi:10.1073/pnas.84.24.8874
- Ostergaard, E., Batbayli, M., Duno, M., Vilhelmsen, K., & Rosenberg, T. (2010). Mutations in PCDH21 cause autosomal recessive cone-rod dystrophy. *Journal of Medical Genetics*, 47(10), 665-669. doi:10.1136/jmg.2009.069120
- Papermaster, D. S., Reilly, P., & Schneider, B. G. (1982). Cone lamellae and red and green rod outer segment disks contain a large intrinsic membrane-protein on their margins - an

ultrastructural immunocytochemical study of frog retinas. *Vision Research*, 22(12), 1417-1428. doi:10.1016/0042-6989(82)90204-8

Petters, R., Alexander, C., Wells, K., Collins, E., Sommer, J., Blanton, M., . . . Wong, F. (1997). Genetically engineered large animal model for studying cone photoreceptor survival and degeneration in retinitis pigmentosa. *Nature Biotechnology*, 15(10), 965-970. doi:10.1038/nbt1097-965

Petters, R., & Sommer, J. (2000). Transgenic animals as models for human disease. *Transgenic Research*, 9(4-5), 347-351. doi:10.1023/A:1008926303533

Pras, E., Abu, A., Rotenstreich, Y., Avni, I., Reish, O., Morad, Y., . . . Pras, E. (2009). Cone-rod dystrophy and a frameshift mutation in the PROM1 gene. *Molecular Vision*, 15(183-84), 1709-1716.

Rattner, A., Chen, J.C. and Nathans, J. (2004). Proteolytic shedding of the extracellular domain of photoreceptor cadherin - implications for outer segment assembly. *Journal of Biological Chemistry*, 279(40), 42202-42210. doi:10.1074/jbc.M407928200

Rattner, A., Smallwood, P., Williams, J., Cooke, C., Savchenko, A., Lyubarsky, A., . . . Nathans, J. (2001). A photoreceptor-specific cadherin is essential for the structural integrity of the outer segment and for photoreceptor survival. *Neuron*, 32(5), 775-786. doi:10.1016/S0896-6273(01)00531-1

Reiss, K., Maretzky, T., Ludwig, A., Tousseyn, T., de Strooper, B., Hartmann, D., & Saftig, P. (2005). ADAM10 cleavage of N-cadherin and regulation of cell-cell adhesion and beta-catenin nuclear signalling. *Embo Journal*, 24(9) doi:10.1038/sj.emboj.7600671

Reiss, K., Maretzky, T., Ludwig, A., Tousseyn, T., de Strooper, B., Hartmann, D., & Saftig, P. (2005). ADAM10 cleavage of N-cadherin and regulation of cell-cell adhesion and beta-catenin nuclear signalling. *Embo Journal*, 24(4), 742-752. doi:10.1038/sj.emboj.7600548

Rodieck, R. (1973). *The vertebrate retina: Principles of structure and function*. San Francisco, CA: W.H. Freeman and Company.

Steinberg, R. H., Fisher, S. K., & Anderson, D. H. (1980). Disk morphogenesis in vertebrate photoreceptors. *Journal of Comparative Neurology*, 190(3), 501-518.

Sung, C. and Chuang, J. (2010). The cell biology of vision. *Journal of Cell Biology*, 190(6), 953-963. doi:10.1083/jcb.201006020

Takeichi, M. (1995). Morphogenetic roles of classic cadherins. *Current Opinion in Cell Biology*, 7(5), 619-627. doi:10.1016/0955-0674(95)80102-2

- Tam, B. M., Moritz, O. L., Hurd, L. B., & Papermaster, D. S. (2000). Identification of an outer segment targeting signal in the COOH terminus of rhodopsin using transgenic *xenopus laevis*. *Journal of Cell Biology*, *151*(7), 1369-1380. doi:10.1083/jcb.151.7.1369
- Tam, B., Moritz, O., & Papermaster, D. (2004). The C terminus of peripherin/rds participates in rod outer segment targeting and alignment of disk incisures. *Molecular Biology of the Cell*, *15*(4), 2027-2037. doi:10.1091/mbc.E03-09-0650
- Utton, M., Eickholt, B., Howell, F., Wallis, J., & Doherty, P. (2001). Soluble N-cadherin stimulates fibroblast growth factor receptor dependent neurite outgrowth and N-cadherin and the fibroblast growth factor receptor co-cluster in cells. *Journal of Neurochemistry*, *76*(5), 1421-1430. doi:10.1046/j.1471-4159.2001.00140.x
- Vaughan, D. K., & Fisher, S. K. (1989). Cytochalasin-D disrupts outer segment disk morphogenesis insitu in rabbit retina. *Investigative Ophthalmology & Visual Science*, *30*(2), 339-342.
- Weigmann, A., Corbeil, D., Hellwig, A., & Huttner, W. (1997). Prominin, a novel microvilli-specific polytopic membrane protein of the apical surface of epithelial cells, is targeted to plasmalemmal protrusions of non-epithelial cells. *Proceedings of the National Academy of Sciences of the United States of America*, *94*(23), 12425-12430. doi:10.1073/pnas.94.23.12425
- Wikler, K., Williams, R., & Rakic, P. (1990). Photoreceptor mosaic - number and distribution of rods and cones in the rhesus-monkey retina. *Journal of Comparative Neurology*, *297*(4), 499-508. doi:10.1002/cne.902970404
- Williams, D. S., Linberg, K. A., Vaughan, D. K., Fariss, R. N., & Fisher, S. K. (1988). Disruption of microfilament organization and deregulation of disk membrane morphogenesis by cytochalasin-D in rod and cone photoreceptors. *Journal of Comparative Neurology*, *272*(2), 161-176.
- Wright, A. F., Chakarova, C. F., El-Aziz, M. M. A., & Bhattacharya, S. S. (2010). Photoreceptor degeneration: Genetic and mechanistic dissection of a complex trait. *Nature Reviews Genetics*, *11*(4), 273-284. doi:10.1038/nrg2717
- Wrigley, J., Ahmed, T., Nevett, C., & Findlay, J. (2000). Peripherin/rds influences membrane vesicle morphology - implications for retinopathies. *Journal of Biological Chemistry*, *275*(18), 13191-13194. doi:10.1074/jbc.C900853199
- Yang, Z., Chen, Y., Lillo, C., Chien, J., Yu, Z., Michaelides, M., . . . Zhang, K. (2008). Mutant prominin 1 found in patients with macular degeneration disrupts photoreceptor disk morphogenesis in mice. *Journal of Clinical Investigation*, *118*(8), 2908-2916. doi:10.1172/JCI35891

- Young, R. (1967). Renewal of photoreceptor cell outer segments. *Journal of Cell Biology*, 33(1P1), 61-&. doi:10.1083/jcb.33.1.61
- Zacchigna, S., Oh, H., Wilsch-Braeuninger, M., Missol-Kolka, E., Jaszai, J., Jansen, S., . . . Carmeliet, P. (2009). Loss of the cholesterol-binding protein prominin-1/CD133 causes disk dysmorphogenesis and photoreceptor degeneration. *Journal of Neuroscience*, 29(7), 2297-2308. doi:10.1523/JNEUROSCI.2034-08.2009
- Zelhof, A. C., Hardy, R. W., Becker, A., & Zuker, C. S. (2006). Transforming the architecture of compound eyes. *Nature*, 443(7112), 696-699. doi:10.1038/nature05128
- Zhang, Q., Zulfiqar, F., Xiao, X., Riazuddin, S. A., Ahmad, Z., Caruso, R., . . . Hejtmancik, J. F. (2007). Severe retinitis pigmentosa mapped to 4p15 and associated with a novel mutation in the PROM1 gene. *Human Genetics*, 122(3-4), 293-299. doi:10.1007/s00439-007-0395-2
- Zhu, A. J., & Watt, F. M. (1996). Expression of a dominant negative cadherin mutant inhibits proliferation and stimulates terminal differentiation of human epidermal keratinocytes. *Journal of Cell Science*, 109, 3013-3023.

## Appendix A

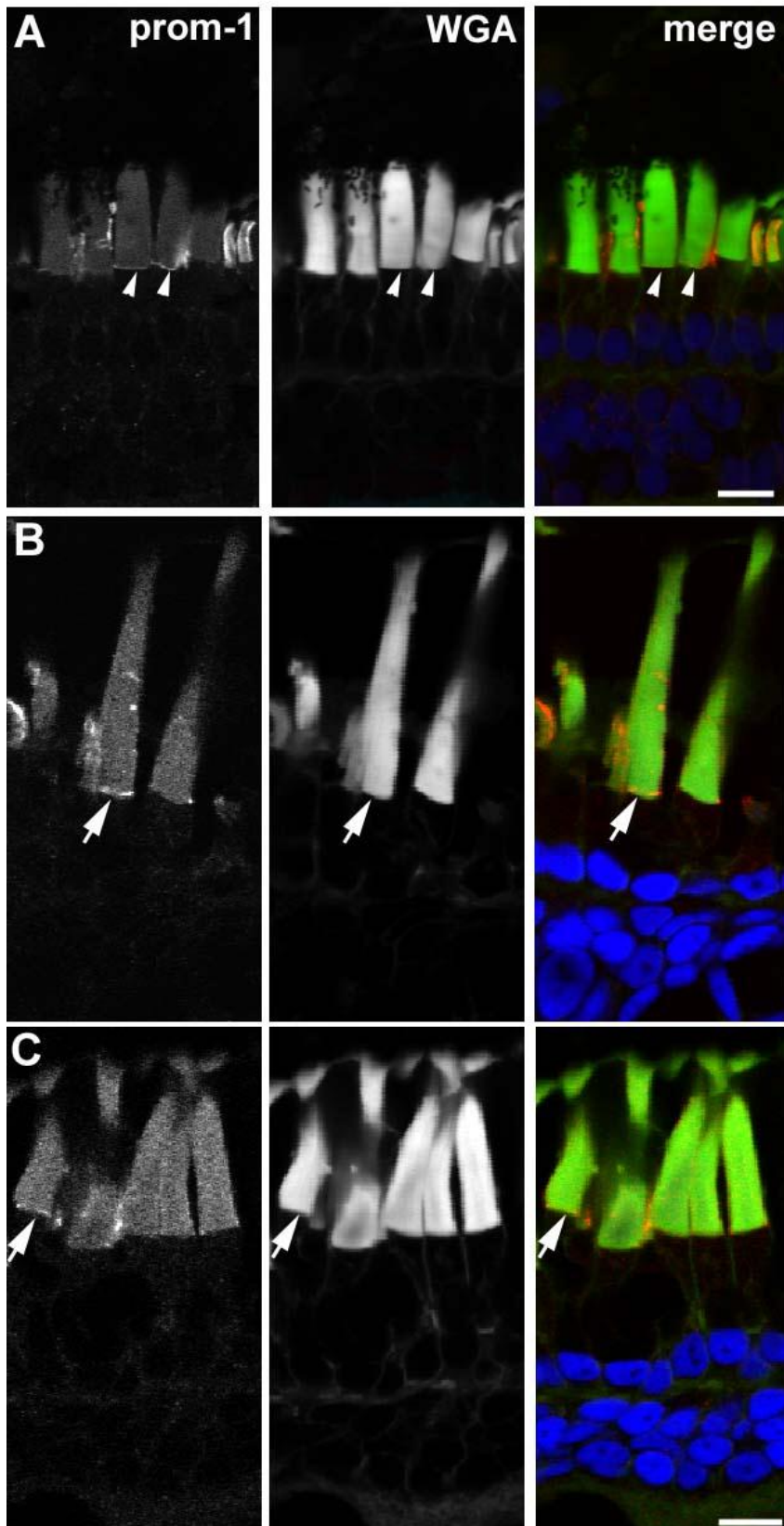


**Fig.A-1. Prom-1 localization in non-transgenic (A) and transgenic *X.laevis* retinas expressing mpcdh-21 FL (B-C).**

Sections were labeled with antibody against the N-terminus of prom-1. (A) In some rods, prom-1 is localized to the base of the ROS as a thin line (arrowheads). (B-C) In transgenic *X.laevis* retinas, prom-1 was correctly targeted to the base of the ROS in a few cells with healthy OS (arrows). Prom-1 did not accumulate in the IS. Scale bar=10 $\mu$ m.

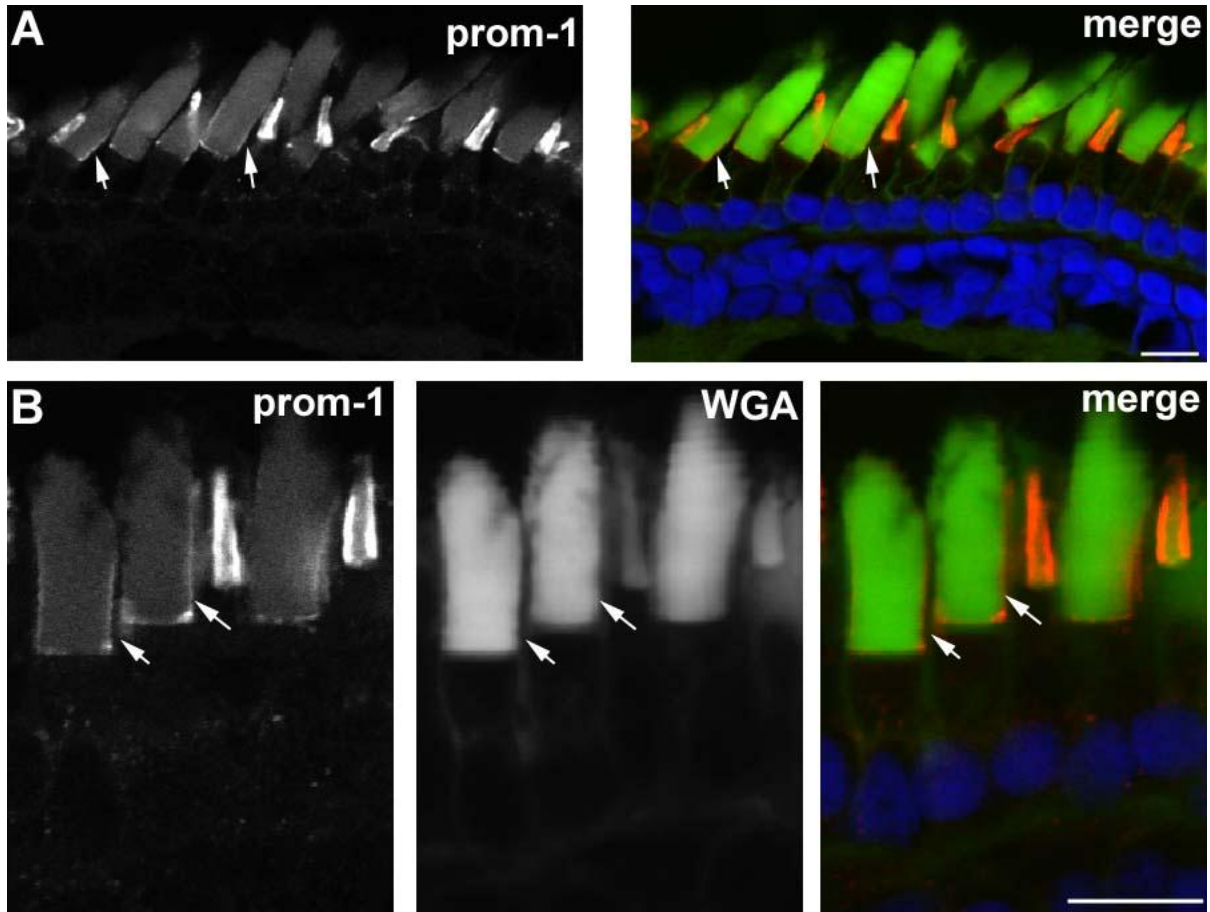


**Fig.A-2. Prom-1 localization in non-transgenic *X.laevis* retina.**

Sections were labeled with antibody against the N-terminus of prom-1. (A) Prom-1 was usually detected at the base of the ROS as a thin line and rarely localized to the ROS plasma membrane (arrows). Prom-1 labeling was more intense in adjacent cones. (B) Higher magnification of rods from a different retina. Rods with prom-1 localization in the plasma membrane were rare, but sometimes occurred in clusters (arrows). Note that prom-1 was not present in the IS plasma membrane. Scale bar=10 $\mu$ m.

```

10      20      30      40      50      60
1  MRGCRWAALALGLLRIGL..AQANFAPHFFDNGVNSTGNMALFSLPEDTPVGSEVYT hpcdh-21
1  MGGPRAIALALGLLFRLL..AQANFAPHFFDNGVNSTGNMALFSLPEDTPVGSEVYT ppcdh-21
1  MRGGRVALVLAGLIRIYL..AQANFAPHFFDNGVNSTGNMALFSLPEDTPVGSEVYT mpcdh-21
1  MKHEWNLGPSIFFSIFHIGLS.VQINIGPYFFDNGVNSTGNMALFSLSEDTPVGAIVYA xpcdh-21
1  MKNARIEIQSSFLLAHFGFVGAQSDIAPYFDNGVNSTGNMALFSLSEDTPEGIQIIVY zpcdh-21
--■-r-----l-1gll-icl--aQanfaPhFfDNGvGStNGNMALfsLpEDTPvGshvYt consensus

70      80      90      100     110     120
57  LNGTDPEGDPISYHISFDPSRSVFSVDPTFGNITLVEELDREREDEIEAIIISIDGLNL hpcdh-21
57  LNGTDPEGDPVSYHISFDPSRSVFSVDPTFGNITLVEELDREREDEIEATISISDGLNL ppcdh-21
57  LNGTDPEGDPISYHISFDPSRSVFSVDPTFGNITLVEELDREREDEIEAIIISIDGLNL mpcdh-21
60  LNCSDPQGDPIYGLTFEPGSEYFAVDPDNGVTLVEELDREREDEIEVIVSISDGLNK xpcdh-21
61  LNGTDPEGQPVKIGLTFEPGSEYFAVDPDNGVTLVEELDREREDEIEVIVSISDGLNK zpcdh-21
LNGTDPEgDpvyhisfdPsersvFsVdP-fGniTLvEeLDREREDEIEaiiSISDgLNl consensus

130     140     150     160     170     180
117  VAEKVVILVTDANDEAPRFIQEPTVALVPEDIPAGSIFKVVHAYDRDTGSGGGSVITFLQN hpcdh-21
117  VAEKVTILVTDANDEAPRFIQEPTVQVPEDILAGSSIAKVVHAYDRDTGSGGGSVITFLQN ppcdh-21
117  VAEKVVILVTDANDEAPRFIQEPTIIRVPEIIPAGSSIFKVVHAYDRDTGSGGGSVITFLQN mpcdh-21
120  VSEKVRVILVTDANDESPGFLNTPYIVIVPEPTPAGSSIFKVEAYDRDTGSGGGSVITFLQE xpcdh-21
121  VVEKYSVIFIMDANDEERQEQMPSIVDYPEPTTEGSSIFKVVHAYDRDTGSGGGSVITFLQS zpcdh-21
VaeKV-ilvtDANDEaPrFIqEpyiv-VPEdipaGsIfKv-AvDrDTGSGGGSvITfLQn consensus

190     200     210     220     230     240
177  .LHSP.FAVDRHSGVLELQAGATLDYERSRTHYITVVAKDGGGRLRGADVVFSAITTVTV hpcdh-21
177  .PESKFAVDRHSGVLELQAGATLDYERSRTHYITVVAKDGGGRLRGADVVFSAITTVTV ppcdh-21
177  .LHSPKFSVDRHSGVLELQAGATLDYERSRTHYITVVAKDGGGRLRGADVVFSAITTVTI mpcdh-21
180  .MGSKFTIDHSGVLEIKAGVSLDFEKSRTHYISVLAKDGGGRLRGKQVFTSITTVTI xpcdh-21
181  SEQSPKFAVDRHSGVLEIKPGESLDYERSRTHYITVVAKDGGGRLRGKQVFTSITTVTI zpcdh-21
-lheskFaiDrHSGVLElqaGatLDyEksRtHfitVvAKDGGGrlrGadvVfsattTvTi consensus

250     260     270     280     290     300
235  NVEDVQDMAPVFGIPYIGVYTEDLPGSEVLKVVADGDGRKPEHILYSLVNGDGAFAFE hpcdh-21
236  NVEDVQDMAPVFGIPYIGVYTEDLPGSEVLTVVADGDGRKPEHILYSLVNGSDGAFAFE ppcdh-21
236  NVEDVQDTAPVFGIPYIGVYTEDLPGSEVLTVVADGDGRKPEHILYSLVNGSDGIFE mpcdh-21
239  NVEDVQDSPPVFGIPYIGVYTEDLPGSEVLTVVADGDGRKPEHILYSLVNGSDGAFIT xpcdh-21
241  NVITQDSPPVFGIPYIGVYTESSPGSEIFIVSADGDGRKPEHILYSLVNGSDGAFIT zpcdh-21
NVEdvQDsaPvFvGTPYyGVYtEdtlpGSEvltVvAdGDGRkPEHilYslvngsDGAfE consensus

```

```

| non conserved
| similar
| conserved
| all match

```

295 INETSGAISITQSPAQMQREVTELEHVQVTEVSPAGSPAAQATVPVTIRIVDLNNEHPPTFY hpcdh-21  
 296 INETSGAIVVQSPAQLRRQVTELEHVQVTEVSSAGSPAAQAMVPVTIRIVDLNNEHPPTFY ppcdh-21  
 298 INETSGAISVLSQSPALLRREVTELEHVQVTEVNSPQSPAAQATVPVTIRIVDLNNEHPPTFY mpcdh-21  
 299 INHATGGITVYIKTPDELKKEVTELEKIQVSEITPECDKVAHAFTVAVRVVDLNNHPPTFY xpcdh-21  
 301 INKTSGVITLRLTPADLRREVTELEKVALEISPECKRLDFATTTVTRIVVDLNNHPPTFY zpcdh-21  
 INetsGaItviqsPa-LrreVyelhvqvtEisp-GspaaqAtvpvTiRiVDLNNHPPTFY consensus

355 GESGPQQRFFELSMTEHPQGEILRGLKITVNDSDQGANAKFNLRVGPGRGIFRVVPQTIVL hpcdh-21  
 356 GESGPQQRFFELSMTEHPQGEILRGLKITVNDSDQGANAKFNLRVGPGRGIFRVVPQTIVL ppcdh-21  
 358 GESGPQQRFFELSMTEHPQGEILRGLKITVNDSDQGANAKFNLRVGPGRGIFRVVPQTIVL mpcdh-21  
 359 GENQPQRFFELSMTEHPQGEILRGLKITVNDSDQGANAKFNLRVGPGRGIFRVVPQTIVL xpcdh-21  
 361 GENQPQRFFELSMTEHPQGEFLRGLKITVNDSDQGANAKFNLRVGPGRMLRVVPQTIVL zpcdh-21  
 GEeGPQRrFELsMyEHPpqGEiLRGLKITVNDSDQGaNAKFNLRrLVGPggifRVVPQTIVL consensus

415 NEAQVTIIIVENSAAIDFEKSKYLTFKLLAEVNTPEKFSSTADVIQLLDINDVVPKFTS hpcdh-21  
 416 NEAQVTIIIVENSAAIDFEKSKYLTFKLLAEVNTPEKFSSTADVIQLLDINDVVPKFTS ppcdh-21  
 418 NEAQVTIIIVENSAAIDFEKSKYLTFKLLAEVNTPEKFSSTADVIQLLDINDVVPKFTS mpcdh-21  
 419 NEAQVTIIIVENSAAIDFEKSKYLTFKLLAEVNTPEKFSSTADVIQLLDINDVVPKFTS xpcdh-21  
 421 NEAQVTIIIVENSAAIDFEKSKYLTFKLLAEVNTPEKFSSTADVIQLLDINDVVPKFTS zpcdh-21  
 NEAQVTiiVenSaaIdfEKskllTFKLLAieVnTPEkFSsTADivIqLLDINDVvPkFtS consensus

475 LYYARIPENAPGGSNVVAVTAVDPDTGPGVEVYYSITGIGADFLIHPSTGIITQPWA hpcdh-21  
 476 HYYARIPENAPGGSNVVAVTAVDPDTGPGVEVYYSITGIGADFLIHPSTGIITQPWA ppcdh-21  
 478 HYYARIPENAPGGSNVVAVTAVDPDTGPGVEVYYSITGIGADFLIHPSTGIITQPWA mpcdh-21  
 479 EYYARIPENAPGGSNVVAVTAVDPDTGPGVEVYYSITGIGADFLIHPSTGIITQPWA xpcdh-21  
 481 DYYARIPENAPGGSNVVAVTAVDPDTGPGVEVYYSITGIGADFLIHPSTGIITQPWA zpcdh-21  
 -yTiARIPENaPGGSnVVavTAvDpDtGpVGevkYsITGsGaDlFlIhpstGiITQPWA consensus

535 SLDAEATRYNFYKAEDEGKYSIAEVFVTLIDVNDHPQFGKSVQEKTKVLTGTPVKIE hpcdh-21  
 536 SLDAEATRYNFYKAEDEGKYSIAEVFVTLIDVNDHPQFGKSVQEKTKVLTGTPVKIE ppcdh-21  
 538 SLDAEATRYNFYKAEDEGKYSIAEVFVTLIDVNDHPQFGKSVQEKTKVLTGTPVKIE mpcdh-21  
 539 SLDAEVYSKYNFYKAEDEGKYSIAEVFVTLIDVNDHPQFGKSVQEKTKVLTGTPVKIE xpcdh-21  
 541 SLDAEVYSKYNFYKAEDEGKYSIAEVFVTLIDVNDHPQFGKSVQEKTKVLTGTPVKIE zpcdh-21  
 SLDAEAterYNFYKAEDEmGkYSIAEVFvTlIDvNDH-PqF---vqekTavlgTPvKIE consensus

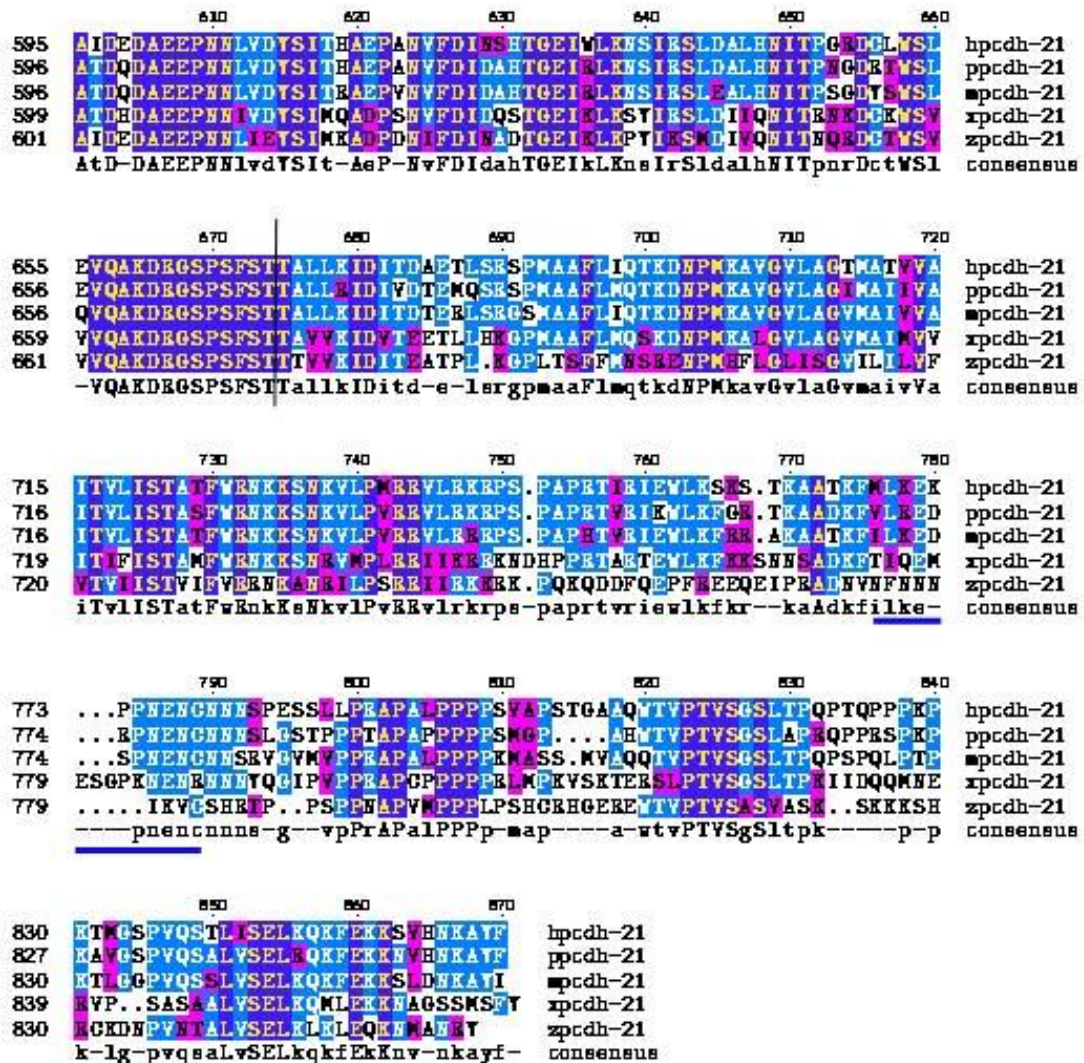


Fig.A-3. Protein sequence alignment of human (hpcdh-21), pig (ppcdh-21), mouse (mpcdh-21), *X.laevis* (xpcdh-21) and zebrafish (zpcdh-21). Two polyclonal antibodies were raised against the N- (red) and C-termini (blue) of xpcdh-21. Black vertical line indicates cleavage site predicted in mice.